METAL OCTACARBOXYPHTHALOCYANINE / MULTI-WALLED CARBON NANOTUBE HYBRID FOR THE DEVELOPMENT OF DYE SOLAR CELLS

by

KANYANE NONHLANHLA EUGENIA MPHAHLELE

Submitted in partial fulfilment of the requirements for the degree

MAGISTER TECHNOLOGIAE: CHEMISTRY

in the

Department of Chemistry

FACULTY OF NATURAL SCIENCE

TSHWANE UNIVERSITY OF TECHNOLOGY

Supervisor: Dr L M Cele

Co–supervisor: Prof K I Ozoemena

Co-supervisor: Dr L J le Roux

2013

DECLARATION

“I hereby declare that the dissertation/thesis submitted for the M Tech: Chemistry degree at Tshwane University of Technology is my own original work and has not previously been submitted to any other institution of higher education. I further declare that all sources cited or quoted are indicated and acknowledged by means of a comprehensive list of references.”

K.N.E. Mphahlele

DEDICATION

This thesis is dedicated to my parents

and my beautiful daughter Oletilwe

who endured this long process with me,

always offering support

and unconditional love

ACKNOWLEDGEMENTS

- Firstly and foremost, I would like to thank Almighty Father for His blessings and making all things possible, without you Lord I could not have done it, “Praise be to God”
- I would like to express my sincere gratitude to all my supervisors, Prof K. Ozoemena, Dr L. le Roux and Dr L. Cele for their generous support, for believing in me when nobody did and also for their intellectual guidance throughout my studies. I would have been lost without them.
- A special thanks to Prof. Tebello Nyokong, for her generosity and giving me the opportunity to visit Japan for 3 months.
- Thanks also to Prof. Nagao Kobayashi, Dr Soji Shimizu and the entire research team in Tohoku University (Japan) for their immense knowledge and support during my stay in their country.
- I also like to thank my big sister Dr. Mmalewane Modibedi for her encouragement and motivation during the course of my studies.
- I would like to extend my gratitude to the CSIR for funding this project.
- Thanks to the CSIR Nano centre materials, for allowing me to utilise their characterisation techniques throughout.
- I would also like to thank the rest of the Energy materials team, Nomthandazo and Thembelihle for their kind assistance throughout my thesis writing.
- I also like to thank all my friends, Mphahlele clan, my cousins and my love – Steve Ramashala who stood beside me and encouraged me constantly.
- Finally, I would like to thank my mother, my little brother, my daughter and my granny for their boundless love and moral support

ABSTRACT

This study reports the successful synthesis and integration of metallo-octacarboxyphthalocyanines–multi-walled carbon nanotubes (MOCPc-MWCNTs) (M = Zn, Ga(OH) and $Si(OH)_2$) hybrid system for the application of dye solar cells. The metallo-octacarboxyphthalocyanines–multi-walled carbon nanotubes hybrid was prepared through non- covalent π–π stacking. The metallo-octacarboxyphthalocyanines–multi-walled carbon nanotubes hybrid was later employed in dye solar cells as a photosensitiser of choice to enhance the performance and efficiency of this device. The dye solar cell devices were fabricated using metallo-octacarboxyphthalocyanines–multi-walled carbon nanotubes hybrid adsorbed on the TiO_2 semiconductor and further characterised with solar simulator.

The physical and electrochemical characterisations of metallo-octacarboxyphthalocyanines–multi-walled carbon nanotubes hybrid were investigated using spectroscopy (UV-Vis, FTIR, EDX, XRD), microscopy (TEM, SEM and AFM), TGA, and electrochemistry (Cyclic voltammetry, photo-chronoamperometry and electrochemical impedance spectroscopy). The effect of multi-walled carbon nanotubes on metallo-octacarboxyphthalocyanine was firstly verified by UV-Vis spectroscopy. The UV-Vis spectroscopy of metallo-octacarboxyphthalocyanines in DMF showed the characteristic Q-band at around 680 nm. Upon integration with multi-walled carbon nanotubes the Q-band was red-shifted.

The results obtained from the dye solar cell devices with metallo-octacarboxyphthalocyanines–multi-walled carbon nanotubes hybrid (photo-

chonoamperometric and photo-impedimetric data) showed an increase in the electron transport and poor recombination rate of electrons in the conduction band of TiO_2 semiconductor under illumination.

The photoelectrochemical studies of these hybrids gave promising overall efficiencies even though it was lower than unexpected. Nevertheless, the TiO_2/ZnOCPc/MWCNT performed better with the efficiency of about 0.1% than TiO_2/SiOCPc/MWCNT and TiO_2/GaOCPc/MWCNT. These findings open up avenues for improving the efficiency of dye solar cells with metallo-octacarboxyphthalocyanines–multi-walled carbon nanotubes hybrid.

CONTENTS

\

LIST OF FIGURES

LIST OF TABLES

LIST OF SCHEMES

LIST OF ABBREVIATIONS

AFM	Atomic force microscopy
Ag/AgCl	Silver/Silver chloride
CNT	Carbon nanotubes
PDT	Photodynamic therapy
DBU	1,8 – DIAZABICYCLO[5.4.0] UNDEC-7-ENE
DSCs	Dye solar cells
EDX	Energy dispersive x – ray spectroscopy
EIS	Electrochemical impedance spectroscopy
E_{pa}	Anodic potential peak
E_{pc}	Cathodic potential peak
FF	Fill Factor
FT-IR	Fourier transform infrared spectroscopy
Ga	Gallium (III)
GaOCPc	Gallium octacarboxyphthalocyanines
HOMO	Highest occupied molecular orbital
I^-	Iodide
I_3^-	Triiodide
I_{pc}	Cathodic current peak
I_{pa}	Anodic current peak
I_{sc}	Short circuit current
ITO	Indium Tin Oxide
I - V	Current v/s Potential
LMCT	Ligand-to-metal charge transfer
LUMO	Lowest unoccupied molecular orbital

MLCT	Metal-to-ligand charge transfer
MOCPc	Metal octacarboxyphthalocyanines
MTSP	Mobile Testing Station for Photovoltaics
MPc	Metal phthalocyanines
MPP	Maximum power point
MWCNT	Multi-walled carbon nanotubes
N3 dye	cis – bis-(4,4’ – dicarboxy- 2,2’-bipyridine)dithiocyanato ruthenium (II); $Ru(dcby)_2(NCS)_2$
N719	Bis(tetrabutylammonium)cis – bis(thiocyanato)bis(2,2’-bipyridine-4-carboxylic acid, 4’ – carboxylate)ruthenium(II)
Pc	Phthalocyanines
PDT	Photodynamic therapy
PVs	Photovoltaics
Ru	Ruthenium
Si (IV)	Silicon
SiOCPc	Silicon octacarboxyphthalocyanines
SEM	Scanning electron microscope
SWCNT	Single walled carbon nanotubes
TBA	Tetrabutyl ammonium
TBAP	Tetrabutylammonium perchlorite
TEM	Transmission emission microscope
TiO_2	Titanium dioxide
XRD	X – Ray diffraction
UV/Vis	Ultraviolet-visible spectroscopy
V_{oc}	Open circuit potential
Zn	Zinc (II)

ZnOCPc	Zinc octacarboxyphthalocyanines

CHAPTER ONE

1 INTRODUCTION

1.1 GENERAL OVERVIEW

A solar electricity-producing device known as a photovoltaic cell is one of the most promising inventions of its type in the last 50 years. This device is used to convert solar irradiation into electricity (Zhang & Cao, 2011) and this is an ideal way of utilising nature's renewable energy. Photovoltaic cells are known to be environmentally friendly and do not pollute the atmosphere.

Photovoltaic cells have the potential to benefit our world by spreading our energy supply and reducing our dependence on coal and imported fuels. The only challenge that remains is their high production cost and energy consumption during fabrication. Therefore, the new approaches towards stability, low cost and efficiency are of extreme importance. Dye solar cells are an attractive new type of photovoltaic cells that may provide a solution to these challenges.

Dye solar cells (DSCs) have become one of the most promising devices in solar cell technology (Zhang & Cao, 2011). This is because of the low cost, simple fabrication and potentially higher power output capabilities (Cheng *et al.,* 2010) as compared to the currently available solid state cells, such as crystalline silicon cells (Wu *et al*., 2010; Tan & Wu, 2006). However, the efficiency of these devices is much lower than that of solid state solar cells and more research is required to enhance efficiency and performance so that the true potential is realized.

Consequently, much research effort has been conducted to improve the performance of these devices by harvesting solar energy using metal phthalocyanines (MPcs) (Barea *et al.*, 2010). The use of MPc complexes in DSCs is regarded as promising as a result of their photo-electrochemical stability, absorption of light at a longer wavelength (Q-band at around 700nm) and high thermal stability (Idowu *et al*., 2010). The phthalocyanine dyes that have been investigated are mainly those containing diamagnetic metal centres (M = Ga(OH), $Si(OH)_2$ and Zn(II)) as they are known to exhibit excellent photosensitising properties in DSCs (Masilela *et al*., 2009).

This project describes the synthesis as well as the spectroscopic (UV/Vis and FTIR), microscopic (SEM) and thermal (TGA), properties of metal octacarboxyphthalocyanines (MOCPc, where M = Zn, $Si(OH)_2$ and Ga(OH)) integrated with MWCNT and investigates their suitability for potential application in DSCs. In addition, detailed electrochemical behaviour of MOCPc supported on amine MWCNT in DSCs is investigated.

1.2 PROBLEM STATEMENT

The relatively low efficiency of dye solar cells is the drive behind many research projects worldwide. Several methods and photosensitisers have been used but until now, no more than 11% efficiency has been achieved (Wu *et al*., 2009). In this project, we investigate the use of alternative photosensitisers that will enhance the long-term stability and efficiency of DSCs. Therefore, MOCPc, especially those containing the diamagnetic metals, were chosen as the best candidates in this project to replace the sensitisers that were utilised previously.

A significant effort has been made to enhance the photosensitisation in DSCs by modifying MPcs with carbon nanotubes (CNTs) (Umeyama & Imahori, 2008). It is well established that carbon nanotubes improve the electrochemical properties of MPc by increasing the rate of electron transfer in DSCs (Agboola et al, 2010; Umeyama & Imahori, 2008). MPc can be integrated with carbon nanotubes through covalent bonding or non-covalent bonding π–π stacking. It is expected that smart integration of the two π–electron species can tune the physico–chemical behaviour of CNTs or MPc complexes to specific potential applications in DSCs (Agboola *et al*., 2010).

1.3 OBJECTIVES

- To synthesise various metal octacarboxyphthalocyanine (MOCPc) complexes where M = Ga(OH), Zn and $Si(OH)_2$.
- To functionalise multiwalled carbon nanotubes with amine groups.
- To modify metal octacarboxyphthalocyanines with multi-walled carbon nanotubes through a chemical functionalisation process.
- To investigate the spectroscopic and microscopic properties as well as the electrochemical behaviour of metal octacarboxyphthalocyanines supported on carbon nanotubes.
- Fabrication, testing and electrochemical characterisation of dye solar cells incorporated with metal octacarboxyphthalocyanines supported on carbon nanotubes.

1.4 DISSERTATION LAYOUT

Chapter one gives a general overview of the project and describes the problems and how are they will be investigated. This chapter also gives the objectives of the study. Chapter two provides the background and theoretical content of the project: photovoltaics, DSCs, photosensitisers, support materials and characterisation techniques. Chapter three gives the methods and materials used in this project. In chapter four, the results are presented and discussed. This includes the microscopic, spectroscopic and electrochemical studies. Chapter five presents the conclusions and recommendations.

CHAPTER TWO

2 LITERATURE SURVEY

2.1 PHOTOVOLTAICS

2.1.1 Introduction

Photovoltaic cells is directly convert solar energy into electricity . In 1839, French physicist, Alexandre-Edmond Becquerel first observed the photovoltaic effect while experimenting the solid–liquid interface with a photoelectrode containing a liquid electrolyte in a photo electrochemical cell (Grätzel & McEvoy, 1994). Therefore, in 1954, a 4.5% efficiency was measured for the first photovoltaic module (practical cells) produced by Bell Laboratories (Grätzel & McEvoy, 1994). The demand for photovoltaic cells has continued to grow after the energy crisis in the 1970s when they gained recognition as a source of power for non-space applications (Knier, 2002). The photovoltaic power generator utilises solar panels which consist of a number of solar cells containing photovoltaic materials. In recent years, photovoltaic cells have become among the most promising devices for use as sustainable and renewable sources of clean energy (Chang *et al*., 2008). Two kinds of photovoltaic cells are recognised: Solid-state solar cells and dye solar cells (Zhang & Cao, 2011).

2.1.2 Solid-state solar cell

The most common kind of solid-state solar cell that is used worldwide is the silicon solar cell. Silicon solar cells are made out of semiconducting materials such as silicon and are composed of three active layers:

- a top junction layer made of N–type semiconductor.
- An absorber made of a P-N junction.
- A back junction layer made of a P-type semiconductor.

The P–type semiconductor is a semiconductor that is doped either with boron or aluminium and has an abundance of holes in the valence band. An N–type semiconductor is a semiconductor that is doped with phosphorus in silicon and is capable of creating excess negative charge carriers. The two semiconductors are separated into two bands, the valence band (E_V) and the conduction band (E_C). These two semiconductors are electrically neutral and sandwiching them together can cause a P-N junction at their interface to create an electric field. After being sandwiched, excess electrons move from the N–type to the P–type semicondoctor to fill up the valence band by a process called electron hole recombination (Backus, 1976).

2.1.3 Basic operation of a traditional solar cell

When incoming light strikes the cells, energy is absorbed as shown in figure 2.1. The absorbed energy releases electrons and causes them to move from a lower energy level to a higher energy level by a process called photo–excitation. Therefore, the excited electrons move freely into the conduction band of the semiconductor and flow through the material to produce electricity (Scout, 2005).

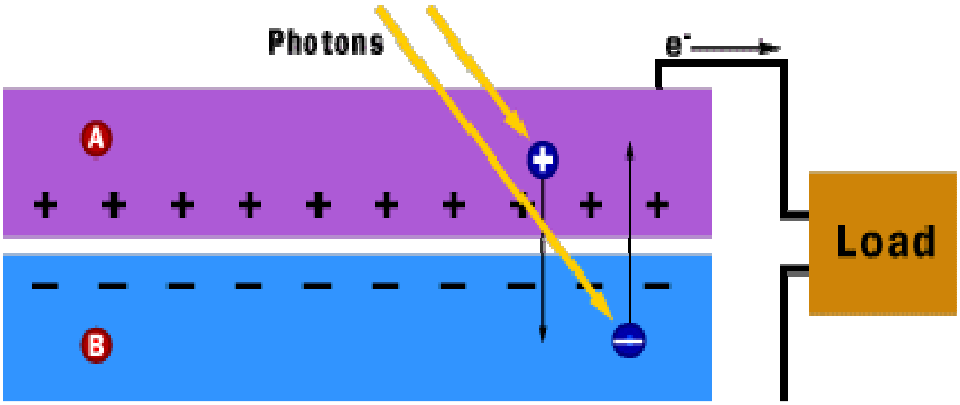

Figure 2.1: Schematic diagram of a photovoltaic cell (Scout, 2005)

Although silicon-based solar cells have been commercialised for the past 30 years, their disadvantages make them less attractive in this field and dye solar cells have showed more promise (Chang *et al*., 2008).

2.2 DYE SOLAR CELLS

2.2.1 Introduction

Dye solar cells were first established in 1991 by Michael Grätzel and Brian O'Regan (O'Regan & Grätzel, 1991) . What makes them attractive is their low cost fabrication and high energy conversion performance (Sawatsuk *et al.,* 2009). Since their discovery, an energy conversion efficiency of 11% (Chung *et al*, 2012) has been attained when utilising Ruthenium complexes as photosensitisers (Dhungel & Park, 2010). However, the efficiency of these devices is much lower (Zhang & Cao, 2011) when compared to solid-state solar cells. The advantages and disadvantages of silicon-based solar cells and dye solar cells are compared in Table 2.1.

Table 2.1: Advantages and disadvantages

Silicon-based solar cells	**Dye Solar Cells**
Fabrication process and raw matarials are costly	Low cost and easy fabrication
Toxic gases	Friendly to the environment and non-toxic
Heavy, big and rigid	Lightweight, semi-transparent and robust
Photovoltage is very sensitive to light intensity variation	Photovoltage is significantly less sensitive to light intensity variation

2.2.2 A brief description of DSCs

The structure and the operationg principles of DSCs are different from those of solid-state solar cells. The difference is that most solid state solar cells depend on a semiconductor (Silicon) for both light absorption and charge transfer (Brooks, 2006) whilst in DSCs the two processes require different materials. DSCs are photoelectrochemical solar cells composed of three main components (Kim *et al*., 2005): A dye monolayer is coated on the TiO_2 wide band gap semiconductor, platinum catalyst and a liquid electrolyte with the redox couple (I^- / I_3^-).

Typical dye solar cells are composed of two electrodes - working and counter electrodes as shown in figure 2.2 below. On the working electrode, a TiO_2 layer is coated on the surface of an Indium Tin Oxide (ITO) glass substrate. A monolayer of dye molecules is adsorbed on the surface of the TiO_2 layer. The counter electrode was prepared by coating a platinum catalyst paste on the other ITO glass substrate, to catalyse the triiodide reduction. The two electrodes are sandwiched together, filled with an electrolyte that contains an iodine/triiodide redox couple and properly sealed with a Surlyn gasket.

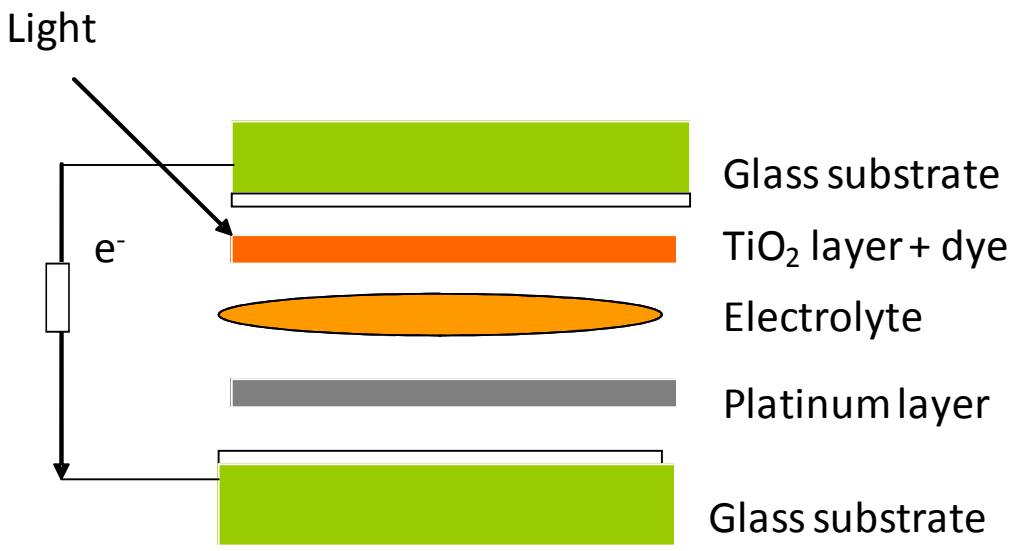

Figure 2.2: Schematic diagram of a typical dye solar cell

2.2.3 Operating principle of DSCs

By absorption of a photon, the dye molecule (S) (grafted on the surface of the TiO_2 layer) is excited. An excited electron (S^*) moves from the highest occupied molecular orbital (HOMO level) to the lowest unoccupied molecular orbital (LUMO level). During the photoexcitation of the latter, the photoexcited electrons are rapidly injected into the conduction band of the semiconductor. After a successful injection, a charge transport occurs in the conduction band of the semiconductor by diffusion of electrons to the ITO glass substrate. Upon reaching the ITO glass substrate, the electrons are conducted to the counter electrode via the external circuit. On the counter electrode, the electrons are received by the electrolyte and the electrons are transferred to triiodide (I_3^-) to produce Iodide (I^-). The reduced iodide will then regenerate the oxidised dye while the triiodide is formed and the electrical circuit is completed as shown in figure 2.3 (Zhang & Cao, 2011, Grätzel, 2003). The photocurrent flows as a results of this cycle. The operating system of

DSCs can be summarised in chemical reaction terminology as shown below (Nazeeruddin *et al*., 2003; Halme, 2002).

Working electrode

$TiO_2/S + hv \longrightarrow TiO_2/S^*$ **Absorption**

$TiO_2/S^* \longrightarrow TiO_2/S^+ + e^-$ **Electron injection**

$S^+ + 3I^- \longrightarrow S + I_3^-$ **Regeneration**

Counter electrode

$I_3^- + 2e^- \longrightarrow 3I^-$

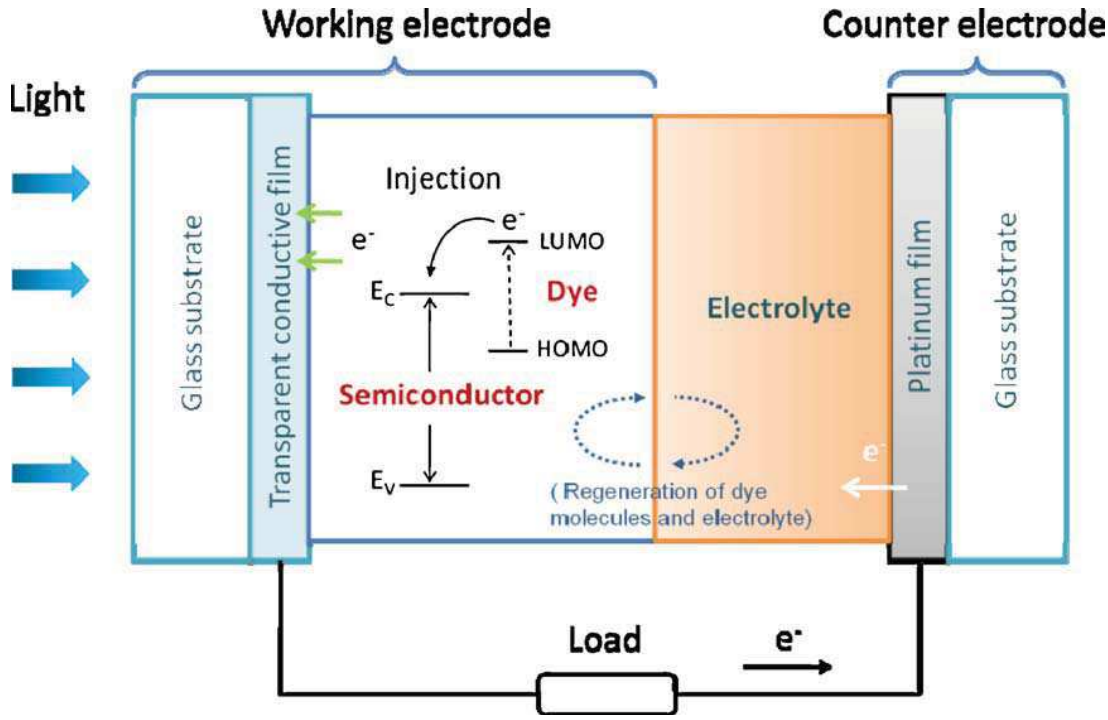

Figure 2.3: A typical diagram showing the operating principle of a dye solar cell (Zhang & Cao, 2011)

2.3 COMPOSITION OF DSCs

2.3.1 Titanium dioxide

Titanium dioxide (TiO_2) is a photostable and nontoxic oxide with a high refractive index of n= 2.4-2 (Hagfeldt *et al*, 2010). It is commonly used semiconductor as a white pigment in paint, toothpaste, sunscreen, self cleaning material and food (Hagfeldt *et al*, 2010). In renewable energy, nanoporous TiO_2 has great potential especially in DSCs as a result of its higher efficiency of over 10% compared to other metal semiconductors when adhered to the monolayer of dye molecule. Unique properties such as chemical stability, large surface area, opacity, and low cost make it more interesting in the application of DSCs (Kalyanasundaram & Grätzel, 1998). In addition to this, various metal oxide semiconductors such as ZnO, WO_3, Fe_2O_3, SnO_2, Nb_2O_5 and Ta_2O_5, have been used in DSCs. However, TiO_2 has become the semiconductor of choice in DSCs (Kalyanasundaram & Grätzel, 1998). One of the concerns is to utilise a large surface area semiconductor (such as TiO_2) with a large band gap of (> 3 eV) to supply sufficient light absorption even when utilised as a dye monolayer (Nguyen *et al.,* 2006). Moreover, nanoporous TiO_2 can also be used to combine high refractive index with a high degree of transparency in the visible region of the spectrum. It also serves as a mediator for the transport of electrons (Kalyanasundaram & Grätzel, 1998).

Two main crystalline phases that occur naturally on TiO_2: Rutile appears as needle like crystals formed at high temperatures with a density of 4.26 g/cm^3 (Halme, 2002). It is thermodynamically stable compared to Anatase (ca. 1.2–2.8 $kcalmol^{-1}$). The rutile-to-anatase transformation occurs in the temperature range 700–1000℃ depending on the crystallite size and impurity content. The band gap energies

have been estimated to be 3.2 and 3.0 eV for rutile and anatase respectively. Anatase, formed as pyramid like crystals, is stable at low temperatures with a density of 3.89 g/cm^3 (Halme, 2002).

2.3.2 General overview: Photo-sensitisers

Titanium dioxide is a white semiconductor that does not absorb visible light in the electromagnetic spectrum of DSCs. Therefore, it is necessary to enhance the absoptivity of visible light by sensitising TiO_2 with a photosensitiser that can absorb as much light as possible in the visible spectrum (Martineau, 2011). The dye molecule serves as a solar energy absorber in the DSC whose properties will have much effect on the light harvesting efficiency and the overall photoelectric conversion efficiency. Several dye molecules such as N3 dyes, N719 dyes, black dyes and organic dyes have been commonly employed in DSCs (Zhang & Cao, 2011).

2.3.3 Requirements for sensitisers

- A sensitiser should be panchromatic i.e. absorb all light below the threshold wavelength of about 920 nm.
- It must have functional groups such as carboxylate or phosphate to firmly attach to the TiO_2 semiconductor oxide.
- It should have suitable ground and excited states for redox properties.
- The energy level of the excited dye molecule should be about 0.2–0.3 eV above the conduction band of the TiO_2 to allow efficient electron transfer.
- It should be stable to sustain about 10^8 turnover cycles for about 20 years when exposed to light.

- It should show thermal and photochemical stability.

2.3.4 Types of Photosensitisers

2.3.5 Ruthenium complexes

Grätzel and his co-workers reported low cost ruthenium dyes such as N3 dye (cis – bis-(4,4' – dicarboxy- 2,2'-bipyridine) dithiocyanato ruthenium (II); $Ru(dcby)_2(NCS)_2$ in 1993 and N719 Bis(tetrabutylammonium)cis – bis(thiocyanato)bis(2,2'-bipyridine-4-carboxylic acid, 4' – carboxylate)ruthenium(II) in 1993 (Horiuchi *et al*., 2004) after exceeding the high conversion efficiency of 7%. The structures of the two dyes are shown in figure 2.4. Their performance and excellent properties (long term stability, absorb light in the wide range of the solar spectrum, reduce recombination between the photoinjected electrons at TiO_2 and the oxidise electrolyte) render them to be more attractive in the application of DSCs (Reynal & Palomares, 2011). In addition, ruthenium dyes in DSCs were found attractive because they possess the chemical structure $ML_2(X)_2$, where L is 2,2'-bipyridyl-4,4'-dicarboxylic acid M is Ru or Os and X stands for a halide, cyanide, thiocyanate, acetyl acetonate, thiocarbamate or water substituent (Grätzel, 2004). The main drawback of these dyes is that they lack the absorption of light in the red region of the electromagnetic spectrum whereas the ideal dye should harvest the near IR region of the solar spectrum (Grätzel, 2000).

More research needs to be conducted on how to improve the performance of these devices and organic dyes are considered possibly to be among the best candidates (Grätzel, 2003).

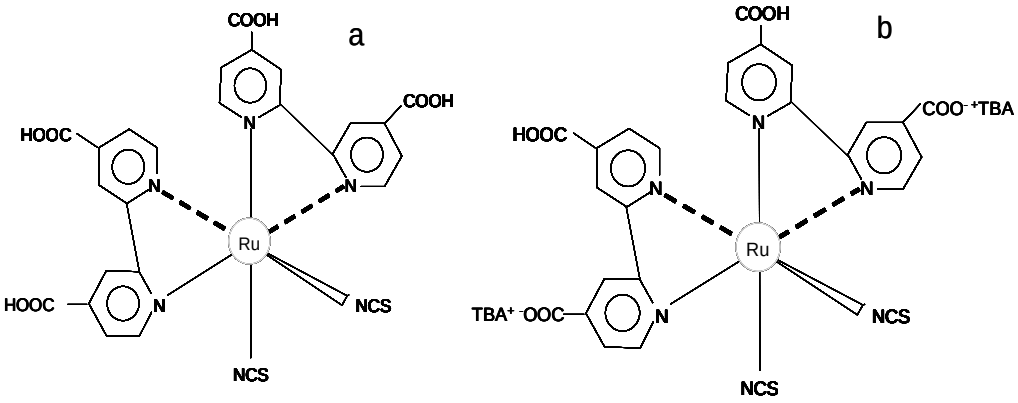

Figure 2.4: Chemical structure of: **(a)** N3 ruthenium complex and **(b)** N719 ruthenium complex (Le Roux, 2009)

2.3.5.1 Mechanism: Light absorption via Ligand-to-Metal ChargeTransfer (LMCT) excitation

At the heart of the DSC system, the excited dye molecules transfer electrons from the metal to the π^* orbital of the ligand species (carboxylated bipyridyl) where electrons are transferred into the conduction band of the semiconductor (Grätzel 2003). The linkage of carboxylate groups to the TiO_2 surface occurs in various ways i.e. unidentate, bidentate, chelating and bridging (Nazeeruddin *et al*., 2003; Hagfeldt & Grätzel, 2000). The dye is attached to four carboxylate groups via their two bipyridyl groups. Only two carboxylate groups are be attached to the Ti-ions through their bidentate coordination. The Ti-ions interact with the hydroxyl groups through their hydrogen bonds on the carboxylic acid (Hagfeldt *&* Grätzel, 2000). Of the two remaining carboxylate groups, one carboxylic acid will ionise while the other will remain in the protonated state. The bipyridyl rings share their LUMO with the $COOH^-$ groups, so that the electrons can migrate into the conduction band of the TiO_2. The anchoring carboxylic groups do not have to be conjugated to the π–electron system of the chromophore for electron transfer to take place. Ancillary ligands are not attached to the semiconductor but are used to tune the overall

properties of the complexes. The main idea behind these complexes is to have a good anchoring ligand to allow an efficient adsorption onto the semiconductor surface while its properties can be tuned by using different ancillary ligands (Hagfeldt & Grätzel, 2000).

2.3.5.2 Organic dyes

Several dyes have been examined but the efficiency has generally been low. It was reported that the efficiency of DSCs can be improved by using dyes that absorb light at the red end and near infrared region of the visible spectrum (O'Regan *et al*., 2008), such as indolines, coumarins, squaraines, porphyrins and phthalocyanines.

Phthalocyanine dyes were chosen for investigation in this project, especially those containing diamagnetic metal centres (M = Ga(OH), $Si(OH)_2$, Zn(II)) as they are known to exhibit excellent photosensitising properties in DSCs (Masilela *et al*., 2009). These molecules generally have larger absorption co-efficiencies ($E>10^5 M^{1} cm^{-1}$), high thermal and chemical stability and also absorb light at the red end and the near infrared region of the spectrum. A strong Q-band at the longest wavelength of 650–800 nm and a weaker B-band at 330 nm are usually observed (Wiederkehr, 1996). These properties make phthalocyanines more interesting in this field. However, phthalocyanines also have their own disadvantages in the application of DSCs such as their propensity to aggregate and the unsuitable energetic position of the LUMO level (Grätzel, 2003). Therefore, in this context, effort has been made to enhance the cell performance by modifying phthalocyanine dye molecules with carbon nanotubes.

2.3.6 Platinum electrode

As a result of its strong catalytic activity, platinum has been used as one of the essential components in DSCs (Khelashvili *et al.*, 2006). The main role of the Pt is to transfer the electrons arriving from the external circuit back to the redox reaction and ensuring that the overvoltage is low (Li *et al.*, 2008). While showing excellent properties, its high cost and degradation in the electrolyte make it less attractive in application of DSCs. Various methods have been employed to deposit platinum on the ITO glass surface. These include sputtering, spin coating and the pyrolytic method (Halme, 2002). However, these methods require high platinum loading whereas DSCs use low cost materials. Several procedures can be followed to minimise this problem and these include:

- The use of carbon-based counter electrodes with enough conductivity as inexpensive substitutes for the platinum electrode. This, however, resulted in reduced efficiency.
- Saito *et al*., utilised chemically polymerised poly (3,4–ethylenedioxythiophene) as a counter electrode.
- Platinum electrode was electrodeposited on the ITO glass sheet.
- The use of the doctor blading method. This method has been shown to be simple and feasible. The electrode is generally transparent and has low platinum loading and high catalytical performance (Li *et al*., 2008).

2.3.7 Electrolytes

The electrolyte plays a key role in DSCs and its properties have much effect on the conversion efficiency and stability of DSCs. Most of the electrolytes generally used in DSCs have the redox couple (I^-/I^-_3) with counter ions (Li^+, K^+, Na^+, Mg^{2+} or

tetrabutylammonium (TBA^+)) (Reynal & Palomares, 2011) and additives (4- tert – butylpyridine 4TBP, 1- methylbenzimidazole) in an organic solvent (Acetonitrile, propylene carbonate, methoxyacetonitrile). The redox couple is used to reduce the photo-oxidised dye molecule (Reynal & Palomares, 2011). Up to now, the most efficient DSCs are based on organic solvent electrolytes owing to their low viscosity, fast ion diffusion and high percolation into the pores of the semiconductor (Martineau, 2011).

2.3.8 Sealing

The two electrodes (working and counter) need to be properly sealed to avoid moisture absorption. Different kinds of sealing materials can be used such as a polymer hot melt seal foil known as Surlyn 1702, epoxy glues, and silicon and UV adhesives. Up to now, the results obtained from using these various kinds of sealing are not promising and do not guarantee long term stability. When sealing the glass, certain precautions need to be taken:

- Materials used must be chemically inert towards the electrolytes and other components in the cell, well attached to the glass substrate and avoid contact with the coated area (Halme, 2002).
- The material must be UV stable and thermally stable at 85℃ (Sastrawan, 2006).

2.3.9 Solar cell performance

A solar simulator (shown in figure 2.5) is an instrument which acts as the light source for the characterisation of DSCs when determining efficiency and performance. The technique involves the measurement of the relationship of

between current and voltage. There are four factors that should be considered when performing I-V curves in DSCs:

- Open circuit potential (V_{oc},V) - is the maximum potential measured at an open voltage.
- Short circuit current (I_{sc}/A) – is the current measured at the short circuit.
- Efficiency (η) – is used to compare different solar cells and is defined as the percentage of the solar irradiation that is converted into power. It is calculated as the ratio between the maximum power output (MPP) and the power of incoming irradiation (Grätzel, 2003). P_{input} is the input radiation power of the solar simulator (100 mWm^{-2}) (Chang *et al.*, 2008).

$$\eta = \frac{V_{OC} I_{SC} FF}{P_{input}} \qquad \text{(Eq. 2.1)}$$

- Fill Factor (FF) – measures the squareness of the curve and is calculated from the maximum power, the product of the short circuit current and the open circuit potential as shown in equation 2.3. The fill factor is a number between 0 and 1.

$$FF = \frac{I_{\max} V_{\max}}{I_{sc} V_{oc}} \qquad \text{(Eq. 2.1)}$$

Figure 2.5: A photograph of a solar simulator system used to test cell efficiency

2.4 BACKGROUND: PHTHALOCYANINES

Phthalocyanines (Pcs) are aromatic planar analogues of tetraazoporphyrins with four additional isoindole subunits. Phthalocyanine is a Greek word derived from naphtha (rock oil) and cyanine (dark blue). The structure is shown in figure 2.6. They were first discovered in 1907 by Braun and Teherniac by chance during a study of the properties of 1,2-cyano benzamide (Braun *et al* 1907; Nyokong, 2007). In the 1930s, Professor Linstead and his students continued with the study of the structure of Pcs. The X-ray crystallography of Pcs and its derivatives, such as those of nickel, copper and platinum, were studied by Professor Robertson and his co-workers in the 1940s (Nyokong, 2007). Since then, Pc-complexes have been used as pigments and dyes for over 70 years as a result of their intense green-blue colour (de la Torre *et al.*, 2010).

These molecules have large absorption coefficients ($E>10^5\ M^{-1}\ cm^{-1}$), high thermal and chemical stability and absorb light at the red end and the near infrared region of the electromagnetic spectrum (Wiederkehr, 1996). Their absorption spectra

exhibit an intense Q-band in the visible region usually ranging from 620–700 nm and a B-band in the ultraviolet region usually centred at 350 nm (de la Torre *et al.*, 2010). They are macrocyclic complexes with an 18 π-conjugated system, consisting of 16 carbon atoms associated together by 8 Nitrogen atoms (Torres, 2006). The diagonal N-N distance between the rings is smaller (396 pm) than that of porphyrins (402 pm) as shown in figure 2.8 (Stillman & Nyokong, 1989). Phthalocyanines are versatile complexes as they can accommodate more than 70 metals and non-metals in the centre (dianion (Pc^{2-}) and can integrate different substituents at the peripheral and non-peripheral end of the ring, thus allowing fine turning of the physical properties (de la Torre *et al.,* 2010; Agboola, 2007).

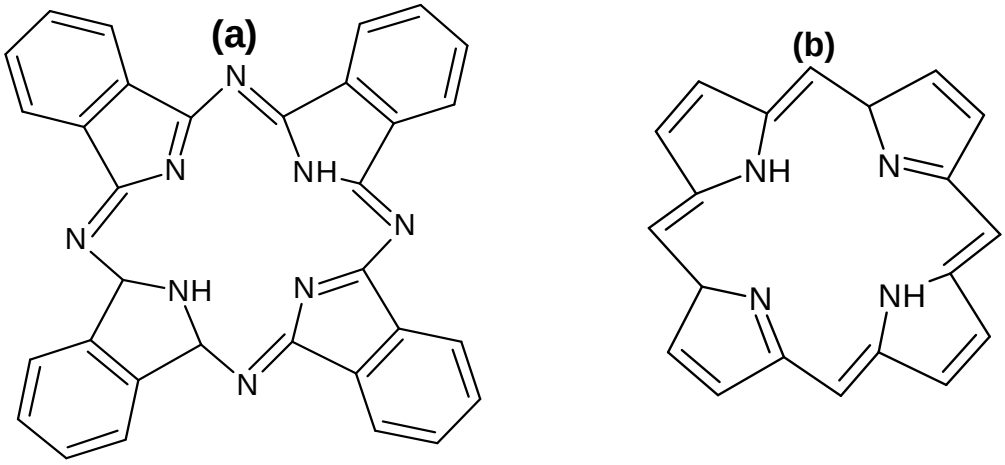

Figure 2.6: Geometric structure of **(a)** unmetallated phthalocyanines and **(b)** porphrins

2.4.1 Metallophthalocyanines

Since metal phthalocyanines (MPcs) and their derivatives were discovered, more attractive properties have been studied and applied in different fields and applications such as inorganic conductors, photoconductors in xerography, catalysis, gas sensing, photosensitisers, non-linear optics, (Bayir, 2005),

electrochromic devices, dyes and pigments. These MPcs and their derivatives have become more attractive and promising as photosensitisers especially in the photodynamic therapy of cancer (PDT) (Durmus & Nyokong, 2007), photovoltaic cells, fuel cells, Liquid Crystal Display (LCD) devices, dyes in the recording layers for CD-R and DVD-R storage discs, diverse catalytic systems, Light Emitting Diodes (LEDs), electrochemical sensors, molecular electronics, semiconductor devices and photocopying and laser printing although more research is still going on this field and commercialisation is expected in the near future (Cong et al., 2008).

2.4.2 General methods of synthesis

Phthalocyanines are synthesised in various ways and different starting materials have been developed and used. The starting materials are generally phthalonitrile, phthalic acid, O-Cyanobenzaimide, diiminoisoindoline and phthalic acid anhydride as shown in figure 2.7 (Torres, 2006; Stillman & Nyokong, 1989). In this regard, different kinds of phthalocyanines can be obtained using the listed precursors depending on the intended phthalocyanine. The most commonly synthesised phthalocyanines are metal free phthalocyanines and symmetrical or asymmetrical metallophthalocyanines**.**

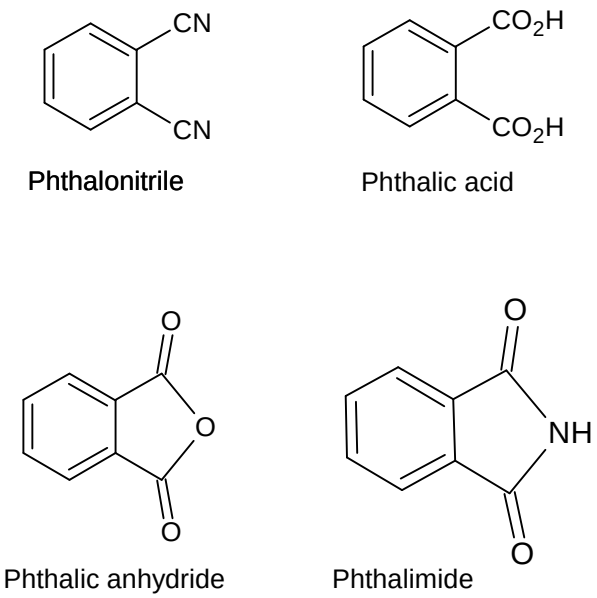

Figure 2.7: The structure of the common starting materials for MPc synthesis

2.4.3 Synthesis of Metal-free phthalocyanines

Synthesis of metal-free phthalocyanines can be achieved in various methods but the common method involves the use of phthalonitrile as a precursor. The first synthesis of unsubstituted metal-free phthalocyanines was achieved from the reaction of phthalonitrile by firstly bubbling gaseous ammonia as a base and refluxing into a solution of sodium methoxide in methanol solution at room temperature to yield 1,3 diiminoisoindoline. The treatment of 1,3 diiminoisoindoline in a high boiling alcohol produced the H_2Pc (metal-free) which condenses under mild conditions (Wohrle *et al.*,1992).

Similarly, phthalonitrile can be readily converted to the H_2Pc ring by refluxing lithium metal, dissolved in a solution of pentanol (lithium pentyloxide), to give Li_2Pc, followed by heating with the non-nucleophillic hindered base 1,8-diazabicyclo[4.3.0]non-5-ene (DBN) in a solution of pentanol to finally produce H_2Pc (metal free). The synthesis of H_2Pc can also be achieved by using co-

reactants such as hydroquinone, 1,2,3,6-tetrahydropyridine or 4,4' – dihydroxybiphenyl to provide two electrons and two protons for the cyclotetramerisation of phthalonitrile (Vollman, 1971).

2.4.4 Synthesis of Metallophthalocyanines

The unsubstituted metallated phthalocyanines were synthesised by heating the various starting materials (Phthalic anhydride, O-Cyanobenzimide and Phthalimide) at high temperature in the presence of metals salts, urea and DBU or ammonium molybdate acting as catalyst as shown in scheme 2.1 (Vollman, 1997). Phthalonitrile can also be used to synthesise unsubstituted metallophthalocyanines in the presence of metal salts as shown in scheme 2.2 (Agboola, 2007).

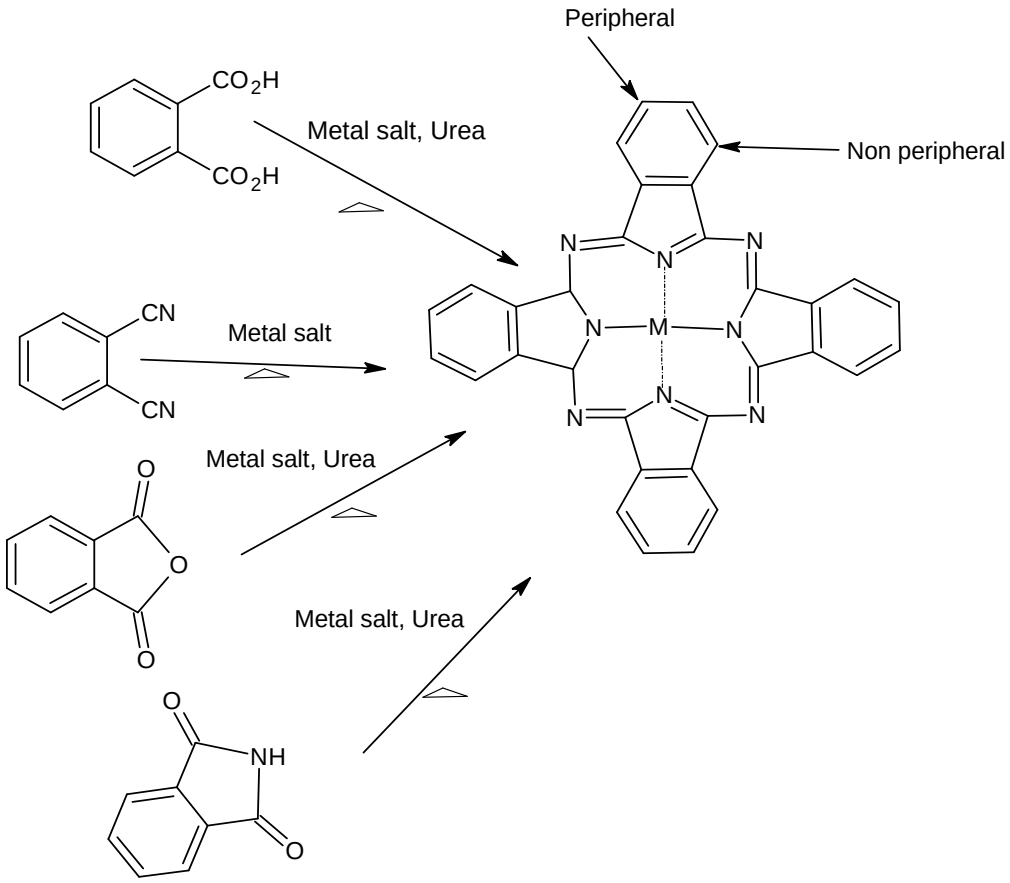

Scheme 2.1: Synthesis of unsubstituted metal phthalocyanines

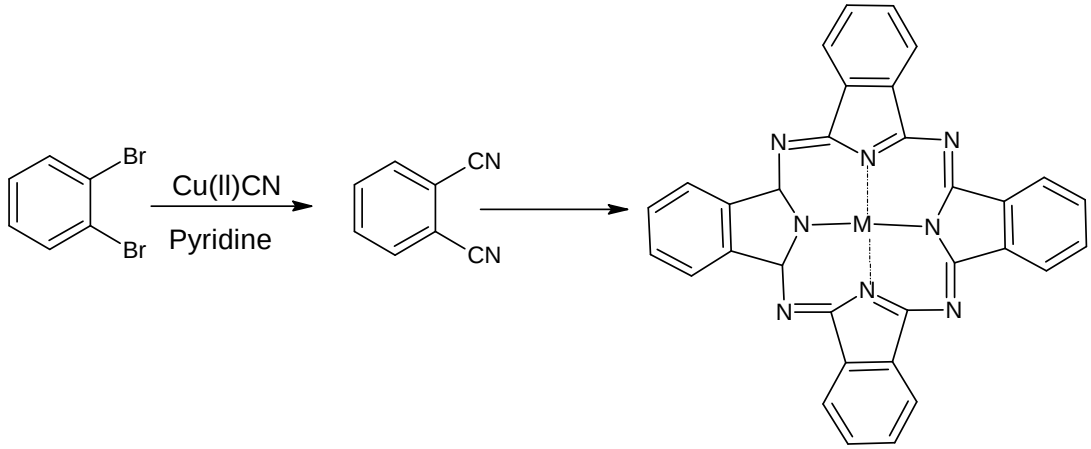

Scheme 2.2: Synthesis of unsubstituted metal phthalocyanines

2.4.5 Axially substituted phthalocyanine

The central cavity of the macrocycle phthalocyanine ring can accommodate central metal ions that are attached with axial ligands. These axial ligands are coordinated with central metal ions having oxidation states of +3 or +4, such as in SnPc, SiPc, GePc and O-TiPc. The existence of the axial ligand contributes to enhancing the solubility and also reducing the face-to-face intermolecular interaction within the MPc ring (Leznoff & Lever, 1989).

In the industrial production process, the synthesis of oxo-titanium phthalocyanines is achieved from the reaction of phthalonitrile, diimiisoindoline and titanium trichloride ($TiCl_4$). The mixture is hydrolysed to yield the product i.e Cl-TiPc. The Cl-TiPc product has been used in the field of photoconductors and photoreceptors in electrophotographic printing. Another method of synthesising 87% oxo-titanium phthalocyanines is by heating a mixture of phthalonitrile and titanium (IV) butoxide, urea and 1-octanol at 150℃ (Winter *et al.*, 1998).

The Cl_2-SiPc was synthesised from the cyclomerisation of phthalonitrile or diimiisoindoline by heating in the presence of a high boiling solvent such as quinoline with silicon tetrachloride. The product - Cl_2-SiPc - is readily hydrolysed to yield $(OH)_2$-SiPc in acidic or basic conditions. The O-TiPc is obtained from the synthesis of phthalonitrile in the presence of titanium (IV) butoxide and urea. In this case, the use of titanium (IV) butoxide makes the synthesis much easier due to its stability against moisture compared to the use of titanium tetrachloride (Kim, 2006). A similar method may be utilised when synthesising GePC and SnPc. $(OH)_2$-SiPc and Cl_2-SiPc are commercially available and soluble in common solvents when coordinated with alcohols, alkyl halides, thio-ethers, sulfonyl, carboxyl, amino and chlorosilanes (Leznoff and Lever,1989).

2.4.6 Tetrasubstituted metallophthalocyanines

Tetra- and octa-substituted phthalocyanine derivatives are of interest as a result of their excellent solubility in common organic solvents. The solubility is mainly caused by the bulky ligand around the peripheral end of the macrocycle ring. In addition, the presence of the bulky ligands has a good influence on the properties of the Pc ring especially on improving the visible absorption spectrum of the ring and also improving its thermal and chemical stability (Sanchez *et al.*, 2001).

Generally, tetra-substituted phthalocyanines produce a mixture of four structural regioisomers such as D_{2h}, C_{4h}, C_{2v} and C_s (Torres, 2006). These isomers are synthesised from the asymmetrical starting material 4-tert butyl phthalonitrile with the product ratio of C_{4h}: D_{2h}: C_{2v}: C_s = 1:1:2:4 (Schmid *et al.,* 1996). Therefore, during the cyclotetramerisation of the symmetrical starting material, 3,6 and 4,5 di-substituted phthalonitrile, octa-substituted phthalocyanines were produced instead

of tetra-substituted phthalocyanines (McKeown, 1998). Sanchez and co-workers reported that tetra-substituted phthalocyanines exhibit higher solubility compared to the octa-substituted derivatives due to their mixture of isomers and also the asymmetric arrangement of the substituents (Sanchez *et al.*, 2001).

2.4.7 Water soluble metal phthalocyanines

Metal phthalocyanines containing carboxy- and sulpho- groups at the peripheral end of the ring were investigated and are known to be soluble in water. Methods of synthesising metallo–tetrasulphophthalocyanine ($MPcS_4$) were established by Weber and Bush (Weber & Bush, 1965). The methods include refluxing (at a temperature about 180℃) a mixture of the monosodium salt of the 4-sulphonic acid, urea and metal salt in nitrobenzene in the presence of ammonium molybdate as catalyst as shown in scheme 2.3. The synthesis of metallo–tetrasulphophthalocyanine can also be achieved by direct sulphonation of unsubstituted MPcs with oleum (Agboola, 2007).

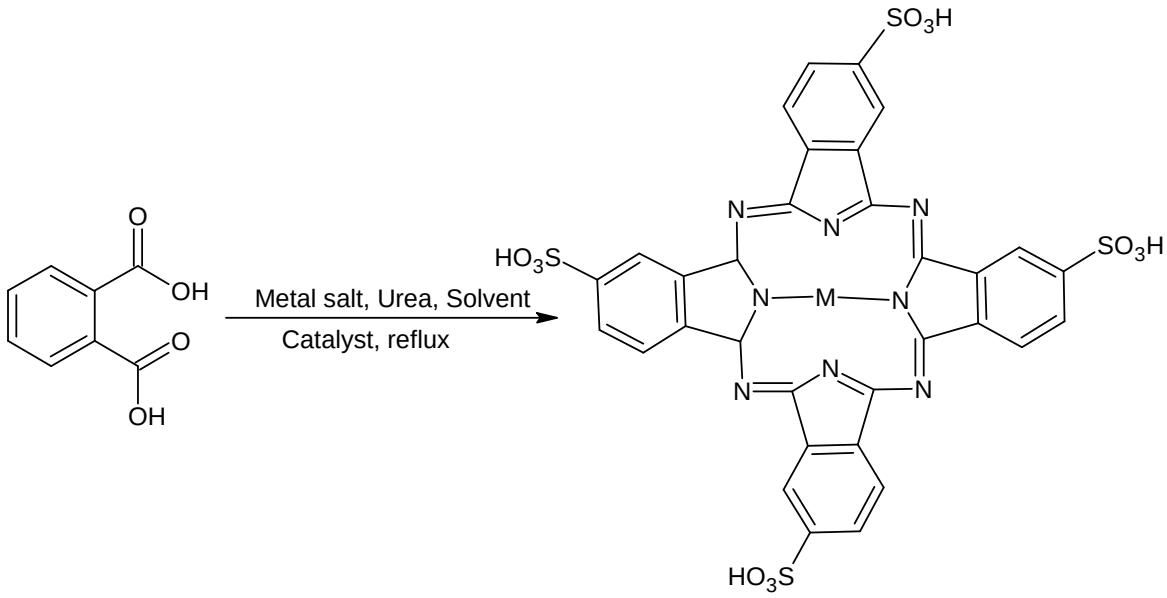

Scheme 2.3: General route for synthesis of metallo–tetrasulphophthalocyanines ($MPcS_4$)

The method of synthesising carboxy-substituted MPcs was first reported by Keiichi Sakamoto and his co-worker (Sakamoto & Ohno, 1997). The products can be obtained from benzene–1,2,4,5–tetracarboxylic dianhydride (pyromellitic dianhydride) in the presence of urea, metal salt and DBU as a catalyst as shown in scheme 2.4. Firstly, tetraimido metallophthalocyanines are formed as intermediates and are easily converted to octacarboxylic acids via acid or base hydrolysis (Sakamoto & Ohno, 1997).

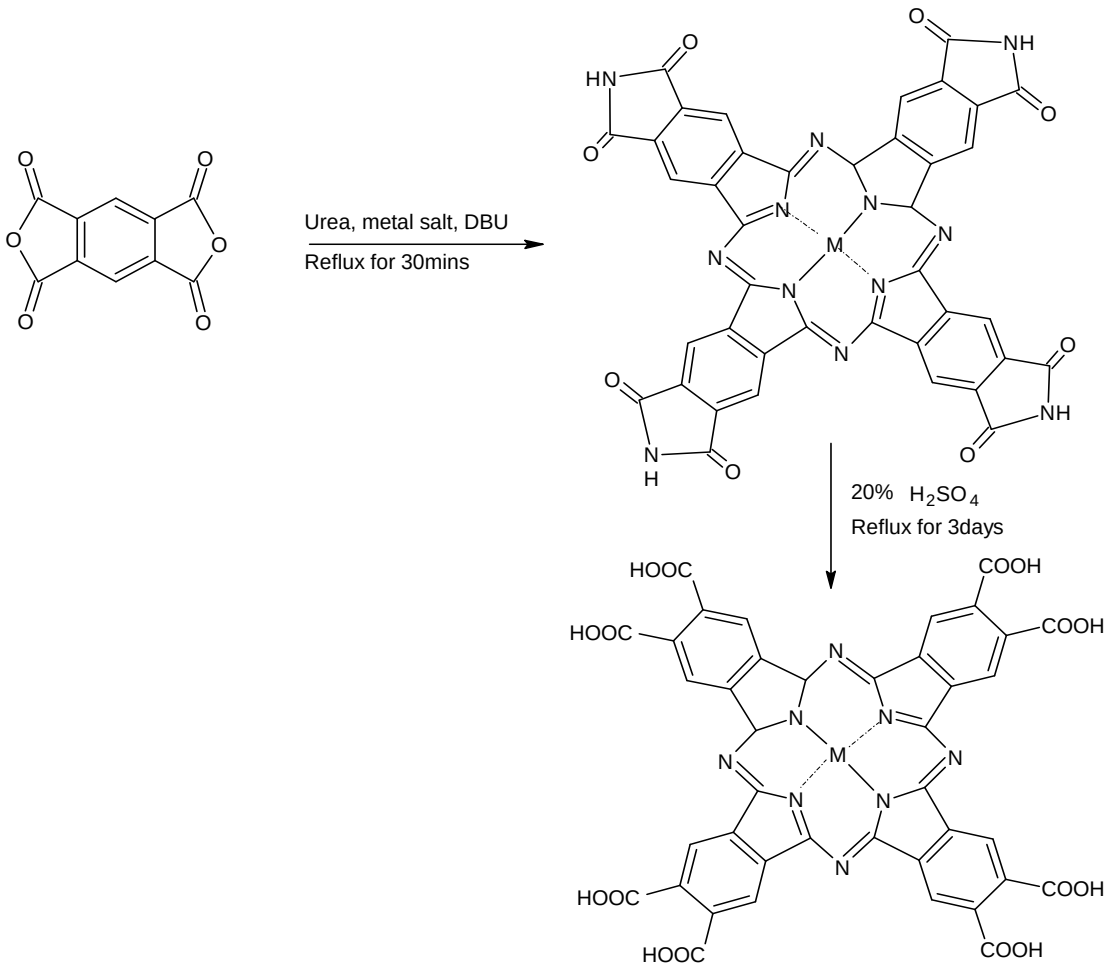

Scheme 2.4: Synthetic route for water soluble metal octacarboxyphthalocyanines (MOCPc).

2.5 SPECTRAL PROPERTIES OF MPc COMPLEXES

2.5.1 UV-visible spectra

The metallated phthalocyanines exhibit the two intense isolated absorption peaks in the UV/Vis absorption spectrum, which are the Q–band and B-band as shown in figure 2.8. The Q-band is in the visible region (600 nm) of the spectrum with the molar absorptivity of more than 10^5 dm^3 mol^{-1} cm^{-1} whereas the B-band or the Soret band is in the ultraviolet region of the electromagnetic spectrum (Stillman & Nyokong, 1989; Wiederkehr, 1996).

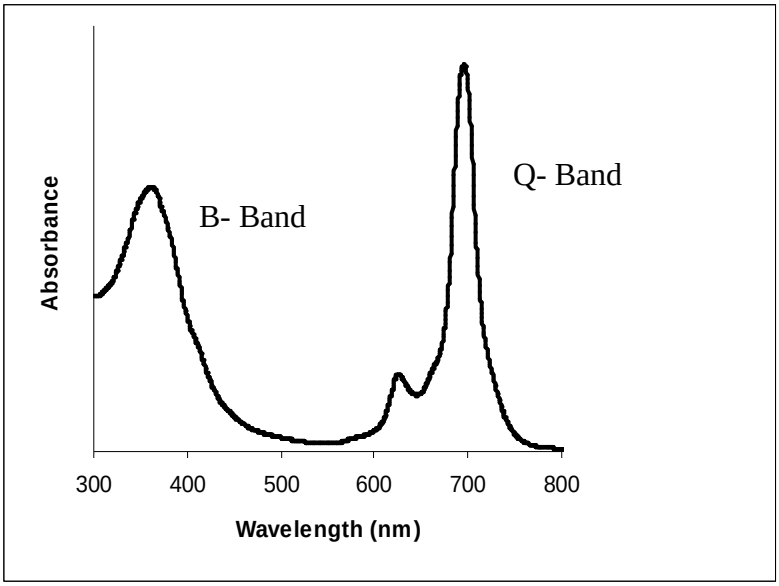

Figure 2.8: Typical electronic absorption spectra of metal phthalocyanines

Generally, the UV-Vis spectrum of an MPc ring is described by Gouterman's four models. The optical spectrum of an MPc complex is defined by the transition energies from the highest occupied molecular orbital (HOMO - a_{2U} and a_{1U}) to the lowest unoccupied molecular orbital (LUMO - e_g). Compared to the porphyrins, the transition levels of the HOMOs (a_{2U} and a_{1U}) in phthalocyanines, are widely separated from each other as a result of the presence of aza–bridges and the benzene groups around the ring. Furthermore, the Q-and the B-band (B_1 and B_2)

lie from the $a_{1U,}$ a_{2U} and b_{2U} to the e_g of the energy transition respectively as explained in figure 2.9 (Stillman & Nyokong, 1989).

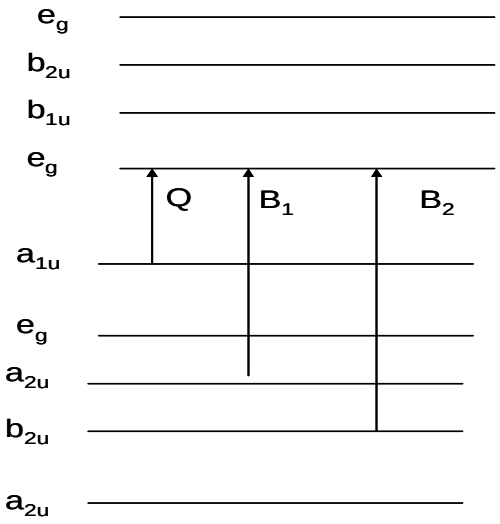

Figure 2.9: Energy transition level diagram for Metal phthalocyanines

In fact, the Q-band of the phthalocyanines in the absorption spectrum can be red shifted or blue shifted and this depends on several factors such as the increase or the decrease of the atomic number of the central metal used, axial ligands, peripheral and non-peripheral substituents, effect of aggregation and the effect of solvent used to dissolve the materials. Possibly, the most significant use of phthalocyanines complexes results from their exclusive spectral properties (Q-band) in the region of 600–750 nm in the visible spectrum. These properties make MPc more attractive photosensitiser complexes (Leznoff & Lever, 1989).

Gouterman's four models had elucidated other transition bands for MPc with higher energy states (below 300 nm) such as N, L and C showing band energies of 4.4, 5.0 and 5.9 eV respectively (Leznoff & Lever, 1989). These bands occur in the ground state of the electronic absorption spectra of some diamagnetic MPcs (ZnPc, MgPc etc). In this regard, some of the MPc complexes do not exhibit any absorption intensity in these bands (Agboola, 2007). In addition, MPcs have a

tendency of undergoing charge transfer transitions which may be either metal-to-ligand (MLCT) or ligand-to-metal (LMCT). This transition can be expected in the spectral region from 200 nm to 1000 nm.

2.5.2 Aggregation of metal phthalocyanines

MPcs have the propensity to aggregate in solution and this is not desired for PDT and photovoltaic cell applications. During aggregation, phthalocyanines dimerise or polymerise readily in solution and, according to Leznoff and Lever (1989), this can result from:

- The direct linkages or bridges between two or more phthalocyanines (due to the intramolecular bonding).
- Covalent bonding between the metals as μ OXO links (especially MPc complexes of Fe and Si).
- Sandwich type complexes – two MPc rings sharing one central metal

  ($Sn(pc)_2$, $Lu(pc)_2$).

- A weak association whereby the peripheral substituents hold two rings in space.

Therefore, the aggregation of the symmetrical MPcs in solution (dimerisation) can also be identified by the blue shift in the Q-band as well as splitting and broadening of the Q-band. In addition to these features, the spectral effects can also depend on the closeness of rings, the overlap position, the tilt angle, the bulkiness of the peripheral groups and the extinction coefficients of the electronic

bands involved. Solvent effects can also result in an increase in aggregation, depending on solvent polarities (Leznoff & Lever, 1989).

This might also change the chemical properties of the MPc complexes which will result in the co-planar association of the aromatic rings. For polar solvents, monomeric species are expected because of the strong interaction between the water molecules and the Pc substituents (electron withdrawing groups) as compared to non-polar solvents. However, aggregation can be reduced by utilising central metal enclosing axial ligands which will act as spacers between the rings (Leznoff & Lever, 1989).

2.5.3 Infrared spectroscopy

The infrared spectra of MPc complexes, especially the water soluble ones, are complex but similar (Agboola *et al*., 2010). The main bands in the aromatic MPc ring that are crucial and visible are the C-H stretching vibration at 3030 cm^{-1}, the C-C benzene ring stretching vibrations at 1600 and 1475 cm^{-1} and the C-H out-of-plane vibrations at 750–790 cm^{-1} (Agboola *et al*., 2010). Metal sensitive bands appear at about 1490 and 1410 cm^{-1}. The spectra for this result is included in the Appendix.

2.6 INTRODUCTION TO CARBON NANOTUBES

The synthesis of nanofilaments was first patented by Hughes and Chambers in 1889. This catalytic synthesis of carbon filaments made use of iron catalyst and carbon source gas (Colbert & Smalley, 2002). Conclusive evidence that the nanofilaments are carbon nanotubes with an inner cavity (approximately 50 nm in diameter) was established by two Russian scientists in 1952 (Radushkevich &

Lukyanovich, 1952). In 1991, Sumio Iijima discovered microtubules of graphitic carbon with outer diameters of 4–30 nm and a length of up to 1 μm (Iijima, 2002). Since then, the number of publications on carbon nanotubes has grown exponentially (Wildgoose *et al*., 2006).

The images confirming the tubular nature of the nanometric-sized carbon filaments/carbon nanotubes were determined by transmission electron microscopy (TEM). In 1978, Wiles and Abrahamson also reported the successful synthesis of carbon fibres on a graphite anode and these carbon fibres came to be known as carbon nanotubes (Wildgoose *et al*., 2006).

Carbon nanotubes have been the subject of worldwide research as a result of their unique properties such as mechanical strength, good electrical conductivity, high thermal stability and large surface areas (Sahoo *et al.*, 2010). Even, in the application of DSCs, CNTs have shown promise for use as support materials even though more research is still required. For efficient performance of this support material, functionalisation needs to be conducted in order to enhance the hydrophilicity of the CNTs. The functionalisation involves harsh treatment with acids and amines at their edge plane sites (Fei *et al*., 2006 ; Agboola *et al.,* 2010).

Carbon nanotubes (CNTs) are tubular nanocrystalline carbon clusters structurally built from rolled graphene sheets closed at the ends by fullerene caps (Khabashesku *et al*., 2006). CNTs consist of two main types with high structural perfection: Single walled carbon nanotubes (SWCNTs) and Multi-walled carbon nanotubes (MWCNTs) (Sun *et al*. 2002). Single-walled carbon nanotubes are characterised as one dimensional nanowires that are either metallic or semiconducting depending on their diameters and helicity (Campidelli *et al.,* 2008).

The MWCNTs are made of two or more concentric graphitic layers surrounding the central tubule as shown in figure 2.10 (Sun *et al*., 2002).

The diameter of SWCNTs can range from 0.2–2 nm and for MWCNTs can be from 2–100 nm (Valcarcel *et al*., 2005). MWCNTs have also been shown to have relatively higher conductivities and larger outer shells when compared to SWCNTs (Kasumov *et al*., 1998). In this work, MWCNTs were used because their large diameter to length ratio properties are more significantly different from that of SWCNTs. Therefore, it is generally believe that the interactions between the MPc with MWCNT can enhance the electrochemical properties such as electon transport in DSCs. The MPcs are 2-D 18 π-electron aromatic porphyrin synthetic analogues, which can be integrated with CNTs through covalent bonding (i.e., upon appropriate functionalisation) or through non-covalent π–π stacking

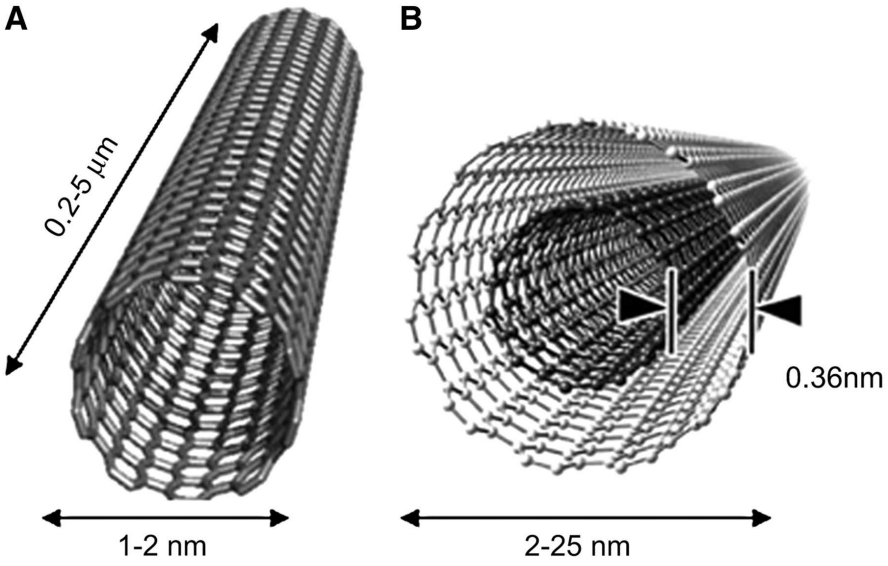

Figure 2.10: Schematic diagram of Single-walled carbon nanotube (SWCNTs) **(a)** and Multi-walled carbon nanotubes (MWCNTs) **(b),** illustrating a typical dimension of length, width and separation distance between graphene layers (Hirsch, 2002)

2.7 CHARACTERISATION TECHNIQUES

The synthesised materials (MPc-MWCNT hybrid) were analysed using various techniques: Physical and Electrochemical characterisations. Therefore, this chapter describe the background of microscopic, spectroscopic and electrochemical techniques used to analyse MOCPc-MWCNT.

2.7.1 Scanning Electron Microscopy

Scanning electron microscopy (SEM) is a technique that utilises a beam of energetic electrons instead of light to examine the materials (carbon nanotubes and MPcs) on a very small scale ranging from nanometers to micrometers. This technique is essential in the field of nanotechnology and phthalocyanine studies. A larger depth of field focuses on a large amount of the sample at one time resulting in a three dimensional image. The images produced are utilised to investigate the samples characteristics such as topography, morphology, composition and crystallographic information (Dunlap & Adaskaveg, 1997).

The beam of electrons is produced at the top of the microscope by an electron gun. The beam travels through electromagnetic fields and lenses, and is then focused on the sample. Once the beam enters the sample, the backscattered and secondary electrons as well as x-rays emitted from the sample are collected by the detectors as shown in figure 2.11 (Hafner, 2007). This results in the formation of an image. In this work, SEM technique was used to determine the morphology of the MPc-MWCNT hybrid.

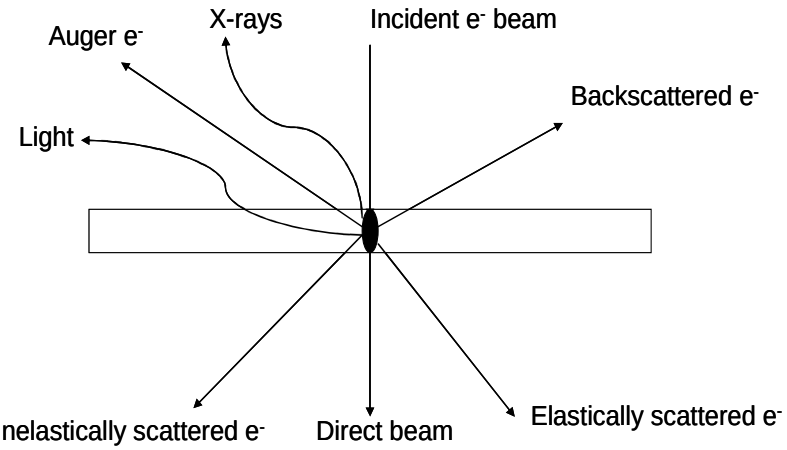

Figure 2.11: Types of Interaction between electrons and materials

2.7.2 Transmission Electron Microscopy

Transmission electron microscopy (TEM) is a technique that reveals the crystallographic information of the material in the form of an image. During TEM analysis, the electron beam strikes an ultra thin specimen and the electrons interact to produce an image. The image is recorded on an imaging device such as fluorescent screen (Palisaitis, 2008). The operation of TEM is similar to that of a light microscope except that it uses an electron beam, generated from an electron gun, instead of light. In addition, TEM produces quality images possessing higher resolution compared to light microscopy due to the small Broglie wavelength of electrons (Fuitz & Howe, 2007). In this work, TEM technique was used to study the structure of the MPc-MWCNT hybrid.

2.7.3 Atomic Force Microscopy

Atomic force microscopy (AFM) is the analogue of scanning probe microscopy used to “view” details at the atomic and molecular level (Vilalta-Clemente & Gloystein, 2008). AFM provides extremely high resolution images by employing an

ultra-small probe tip at the end of a cantilever. It measures the forces acting between the sharp cantilever tip and sample. AFM does not utilise electron beams, but produces information on surface morphologies by running a very small and sharp cantilever tip over the sample (Raposo, 2007).

2.7.4 X-Ray Diffraction

X-Ray Diffraction (XRD) is a rapid technique used for phase identification of the crystalline materials. It is used to identify the crystalline phases powders, crystals and thin film samples with high resolution and good signal to noise ratio. The interaction of the crystalline material causes the x-ray to diffract uniformy in all directions. Therefore, the diffracted beams obeys the Bragg's law as shown in equation 2.3.

$$n\lambda = 2d \sin \theta \qquad \text{(Eq 2.3)}$$

Where n is the diffraction order , λ is the wavelength of the X-rays, d is the distance between two lattice and θ is the Bragg angle between the surface and the X-ray beam where a maximum in the diffracted intensity occurs. In this work, XRDs technique was used to determine the crystalline structure of the MPc-MWCNT hybrid.

2.7.5 Themorgravimetric analysis

Thermogravimetric analysis (TGA) is an analytical technique primarily used to determine the composition and the thermal stability of the material as a function of temperature (Widmann, 2001). It is commonly used in research and testing to determine the weight loss or gain of materials such as carbon nanotubes. The

TGA is composed of several components such as the balance, furnace, temperature programmer and the recorder.

During the analysis, the sample is placed in a sample pan that is supported by a balance in a furnace. Then, the sample temperature is varied at a constant rate during the experiment while purging with a gas (inert or reactive). The gas flows over the sample and is released through an exhaust. Then the results are recorded in the form of a plot of mass change against temperature (Mansfield, 2010). The TGA curves reveal the change in the mass of the sample as the temperature increases. In this work, TGA analysis was used to study the thermal stability of the MPc-MWCNT.

2.7.6 UV/Visible Spectroscopy

UV/Vis spectroscopy is a commonly used analytical technique with applications in both quantitative and qualitative analysis. The absorption of the material in different wavelength ranging from 190 (Ultraviolet region) – 900nm (Visible region) (Lam, 2012) is measured and plotted against. The wavelength of light that a compound will absorb is a characteristic of its chemical structure. The specific region of the electromagnetic spectrum is absorbed by exciting molecules. All molecules will undergo electronic excitation following absorption of light, but for most molecules very high energy radiation (200 nm) is required (Skoog & West, 1980).

The amount of light, I, transmitted through a solution of an absorbing substance in a transparent solvent can be related to its concentration by the Beer-Lambert law as shown in equation 2.4:

$$A = \log 10(I_0 / I) = Ebc \qquad \text{(Eq. 2.4)}$$

where A is the measured absorbance, I_0 the intensity of incident light, I the transmitted intensity, E the molar absorptivity, c the concentration and b the path length of the sample. The Beer-Lamber law is fully described by Strong theory (Greenlief, 2004). In this work, UV/Vis was used frequently in order to observe the purity of MPc after filtration and also to identify the two absoption bands presence in the phthalocyanine structure.

2.7.7 Fourier-Transform Infrared Spectroscopy

Fourier Transform Infrared Spectroscopy (FTIR) is a commonly used technique for the identification of the chemical functional groups in a compound. The IR radiation passed through a sample and some of the radiation is absorbed by the sample while the rest is transmitted (Settle, 1997; Kalsis, 1993) Then a signal is sent to the detector creating a molecular fingerprint of the sample i.e. IR spectrum. Each functional group within a molecule will have various bond energies resulting in infrared absorption at different wavelengths (Coates, 2000). The total bond energy is defined in equation 2.5.

$$E_{total} = E_{electronic} + E_{vibrational} + E_{rotational} + E_{translational} \qquad \text{(Eq. 2.5)}$$

When a molecule vibrates, the atoms move towards and away from each other at a certain frequency. Therefore, the number of vibrational modes in a molecule is given by 3N – 6 (non linear) and 3N - 5 (linear) where N is the number of component atoms in the molecule (Settle, 1997; Kalsis, 1993). In this work, FTIR was used to confirm the functional groups presence in MPc-MWCNT hybrid.

2.8 ELECTROCHEMISTRY: CHARACTERISATION OF MOCPcs

In this work, electrochemistry is used routinely to describe electron transport properties of the MPc–CNT hybrids in DSCs when the device is exposed in the dark and under illumination (Sakamoto & Ohno, 1997). The Autolab potentiostat PGSTAT is generally used with a solar simulator and a two electrode compartment i.e. Reference electrode (RE) connected to a counter electrode (CE) and working electrode (WE). Therefore, the charge transfer within the cell is determined by using different electrochemical techniques such as cyclic voltammetry, chronoamperometry, square waves and electrochemical impedance spectroscopy (EIS).

2.8.1 Cyclic Voltammetry

Cyclic voltammetry is the most popular technique that is used to provide qualitative and quantitative information about the electrochemical reaction. During cyclic voltammetry analysis, the potential of the electrochemical cell is applied and the response of the cell is measured at the end of each step (as shown in figure 2.12) and the resulting current is recorded, producing a cyclic voltammogram. A cyclic voltammogram was obtained by measuring the current at the surface of the working electrode where the reaction is occurring and the plot measures the current against potential (Shippy & Lu, 2007).

During the scan, one or more peak currents of the redox active species at the electrode surface is observed. Moreover, when the applied potential of the redox species becomes positive, oxidation occurs i.e. anodic current (I_{Pa}) whereas when the applied potential becomes negative reduction occurs i.e cathodic current (I_{Pc}).

In this case, there are significant parameters in cyclic voltammetry that are used and these include the magnitude of the peak currents, (both anodic and cathodic) and the potential at which the peak current occurs, anodic peak potential (E_{Pa}) and cathodic peak potential (E_{Pc}) as presented in figure 2.13. In addition, a cyclic voltammogram process can either be reversible or irreversible depending on the material used (Shippy & Lu, 2007).

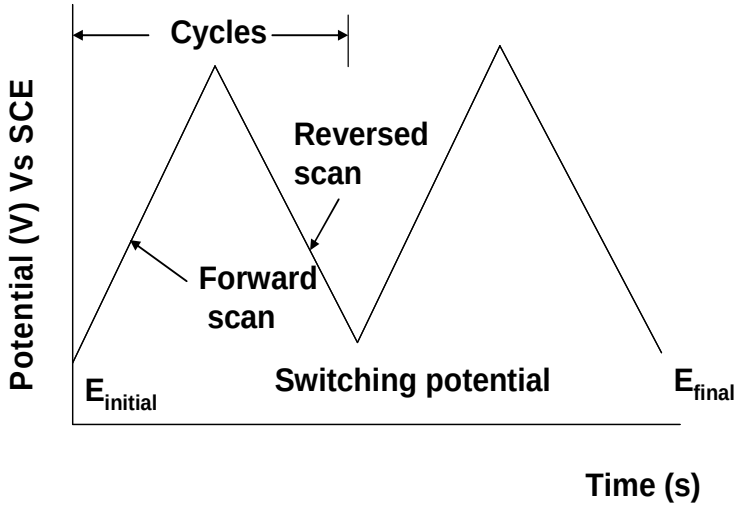

Figure 2.12: Typical excitation signal for cyclic voltammetry (Shippy & Lu, 2007)

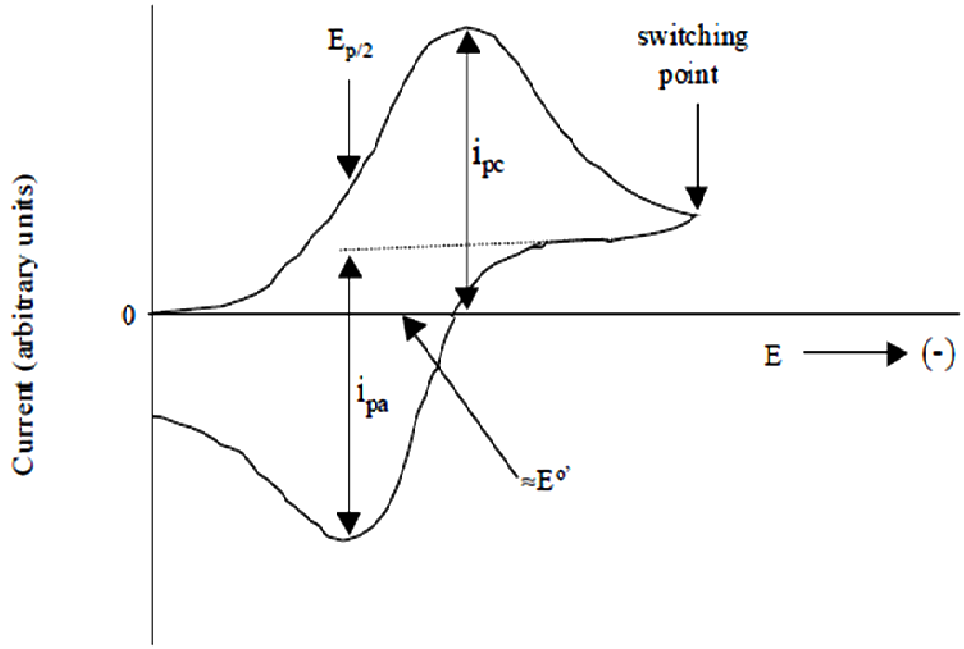

Figure 2.13: Typical cyclic voltammogram for reversible reaction (Shippy & Lu, 2007)

2.8.2 Chronoamperometry

Chronoamperometry is the electrochemical technique in which the step potential of the working electrode is applied while the current is recorded as a function of time (Ventures, 2008). This technique is mostly performed while the solution is not stirred to enable mass transport by diffusion. During the analysis, the starting potential is applied to the electrochemical cell for a brief period of time where there is no current and the cell is allowed to equilibrate at this stage. Therefore, after the induction period, the potential of the working electrode is accelerated and the resulting current measured for a period of time. Then the potential of the working electrode is held constant (at initial potential) for a brief period of time and rapidly decreased as the analyte near the electrode is completely oxidised or reduced as shown in figure 2.14 (Ventures, 2008).

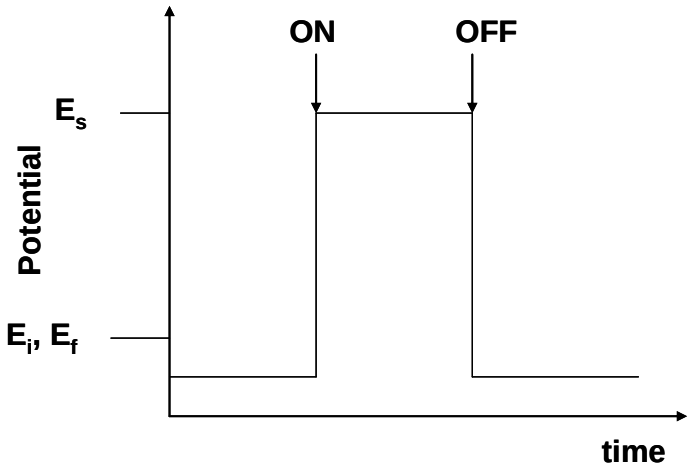

Figure 2.14: A potential wave form for chronoamperometry

The relationship between the current plotted against time is describe as the Cottrel (see quation 2. 6):

$$i = nFACD^{1/2}\pi^{-1/2}t^{-1/2} \qquad \text{(Eq. 2.6)}$$

where F is Faraday's constant (96500 C/mole), A is the electrode area (cm^2), C is the Ionic concentration (mol/cm^3), n the number of electrons per molecule, D the diffusion coefficient (cm^2/s) and t the measurement time in seconds (Ventures, 2008).

2.8.3 Electrochemical Impedance spectroscopy (EIS)

Electrochemical impedance spectroscopy (sometimes known as ac impedance) is a very well known and powerful technique that is used for analysing the charge transport process occurring on the electrode surface of the electrochemical cell (Wang *et al.,* 2005). EIS has been shown to be a very useful technique in the study of the kinetics of electrochemical and photoelectrochemical processes as well as the elucidation of salient electronic and ionic processes in dye solar cells (Wang *et al.,* 2005). This technique reveals that when a tiny AC voltage amplitude

(Sinusoidal) excitation signal is applied on a potential, a current or a voltage is measured (Amirudin & Thierry, 1995).

The sinusoidal excitation signals are described by equation 2.7:

$$E_t = E_0 \sin(\omega t) \qquad \text{(Eq. 2.7)}$$

where, E_t is the potential at time, E_0 is the amplitude of the signal, ω is the radial frequency. The relationship between the radial frequency (ω) and frequency (f) is expressed by given equation 2.8:

$$\omega = 2\pi f \qquad \text{(Eq. 2.8)}$$

In a linear system, the response signal, I_t, is shifted in phase $|\phi|$ and has a different amplitude and I_0 is expressed by equation 2.9 (Gramry instruments, 2012)

$$I_t = I_0 \sin(\omega t + \phi) \qquad \text{(Eq. 2.9)}$$

This steady state technique measures the impedance over a range of frequencies and the frequency response to the system as a result of two plots i.e. the Bode plot and the Nyquist plot as shown in figure 2.15. The Bode plot is a plot of log of magnitude of impedance and phase angle against frequency whereas Nyquist plot is a plot of the imaginary impedance against real impedance. The Nyquist plot is obtained when the real impedance is plotted on the x - axis and the imaginary plot is on the y - axis. Therefore, the impedance can also be calculated using Ohm's law as shown in equation 2.10 (Lasia, 1999):

$$Z = \frac{E}{I} = Z' + jZ'' = Z_{real} + jZ_{imaginary} \qquad \text{(Eq. 2.10)}$$

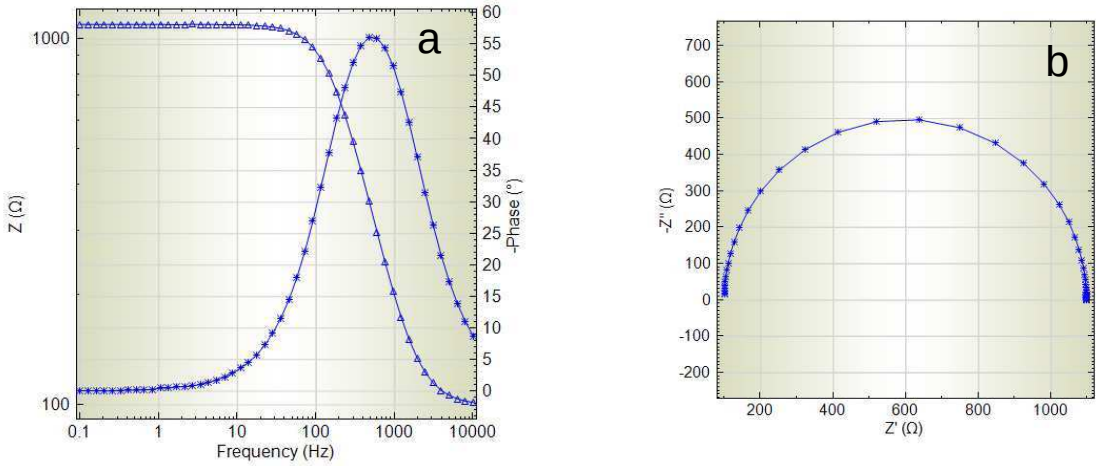

Figure 2.15: Typical **(a)** Bode plot and **(b)** Typical Nyquist plot (Lasia,1999)

The use of this technique in DSCs results in the formation of three semicircles in the Nyquist plot and three characteristic frequency peaks in the bode plot as shown in figure 2.16 (Wang *et al*, 2005). The equivalent circuit as shown in figure 2.17 was employed for fitting the EIS plots which resulted in three semicircles. The fitting parameters observed in the Nyquist plot after fitting include the series resistance (Rs) which occurs as a result of the sheet resistance of ITO, the electron transfer resistance R_{TiO2} at the ITO/TiO_2 film interface, the electron transfer resistance (R_{Rec}) arising due to the recombination reaction (Back reaction) at the TiO_2/electrolyte interface and the charge transfer resistance (R_{pt}) at the Pt/electrolyte interface (Lee *et al*., 2008); Sawatsuk *et al*., 2009).

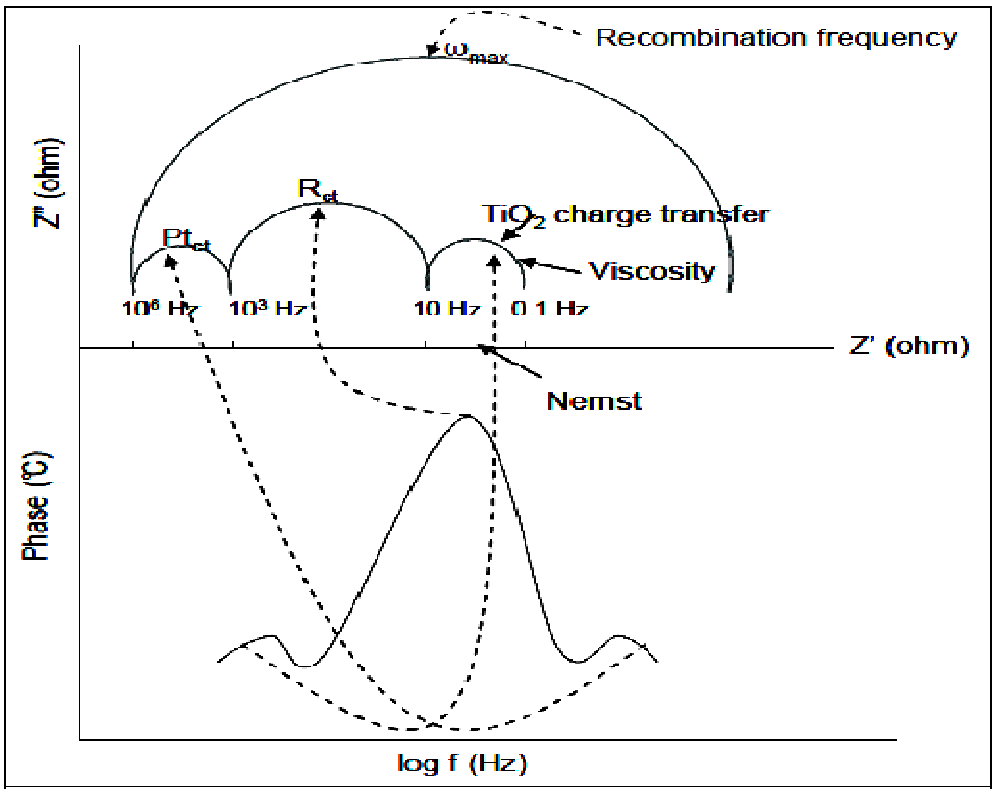

Figure 2.16: Diagram presenting the bode and Nyquist plots for DSCs

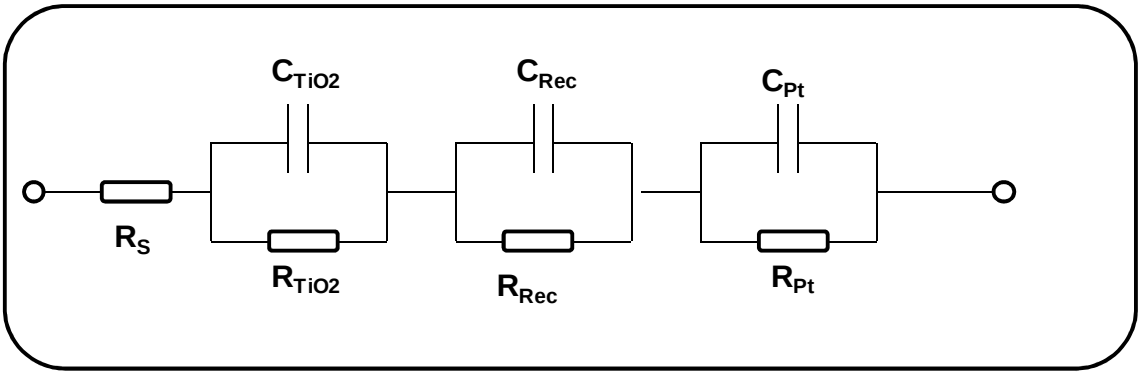

Figure 2.17: Equivalent circuits for impedance spectra

CHAPTER THREE

3 METHODS AND MATERIALS

The initial part of this chapter described the materials and reagents and the characterisation parameters used during the course of the study. Functionalisation of amine-MWCNTs, synthesis of ZnOCPc, $(OH)_2$SiOCPc and (OH)GaOCPc complexes and incorporation of MWCNT with MOCPc are described later. The final part of this chapter explains each component used for the preparation of the dye solar cells i.e. TiO_2 semiconductor pastes, deposition of dye molecule, injection of electrolyte and platinum catalyst paste as well as their assembly to form the whole device.

3.1 MATERIALS AND REAGENTS

The materials and reagents utilised for the synthesise of metal octacarboxyphalocyanines/multiwalled carbon hybrid are listed in table 3.1.

Table 3.1: List of used materials and reagents

Chemicals and materials	**Specification**	**Supplier**
Carbon nanotubes, multiwalled	Bundles >95% (length 7-15 nm x 3–6 nm in diameter 0.5–20 μm)	Sigma Aldrich
Diazabicyclo[5,4,0] – 7-undecene (DBU)	Min 99%	Nacalai Tesque
Dimethyl sulfoxide (DMSO)	Min 99%	Merck
Ethylenediamine	Min 99% Density = 0.896–0.898	Merck
Electrolyte (Iodolyte PN-50)		Solaronix
Gallium (III)Chloride ($GaCl_3$) anhydrous beads	Min 99% Density = 2.47 g/ml at 25℃	Sigma Aldrich
Hydrochloric acid (HCl)	37 %	Sigma Aldrich
Hydrogen peroxide (H_2O_2)	30% by weight	Sigma Aldrich
Nitric acid (HNO_3)	65%	Sigma Aldrich
N,N-dimethylformamide (DMF)	Min 99%	Merck
Platinium catalyst paste		Solaronix SA, Switzerland
Pyromellitic dianhydride (Benzene – 1,2,4,5 – tetracarboxylic anhydride)	Min 97%	Sigma Aldrich
Potassium hydroxide (KOH)	Min 85%	Sigma Aldrich
Sodium hydroxide (NaOH)	Min 97%	Sigma Aldrich
Sulphuric acid (H_2SO_4)	98%	Merck
Surlyn 1702 (DuPont)		Solaronix SA, Switzerland
Silver paste (SPS 1248)		Solaronix SA,

		Switzerland
TiO_2 paste (DSL 18NR-T)	15–20 nm 18% wt	Solaronix SA, Switzerland
Trichlorosilane (HCl_3Si)	99%	TCI (Japan)
Thionyl chloride	99%	Merck
Zinc acetate dehydrate ($Zn(CH_3COO)_2.2H_2O$)	99–102%	Sigma Aldrich
Urea crystals $(NH_2)_2CO$	Min 99%	Merck

3.2 CHARACTERISATION CONDITIONS

3.2.1 UV/Vis spectroscopy

Ultra-violet–Visible absorption spectra were obtained by using a Perkin Elmer, Lambda 750 s. The wavelength ranges from 190 nm to 800 nm. A scan rate of 267 nm/min was used. Resolution: 1 nm. The UV/Vis method was used to investigate absorption spectra of MPc with and without MWCNTs in the wavelength region of 650 –700 nm (visible region) and at 350 nm (ultraviolet region). The sample for analysis were prepared by dissolving a 0.1 mg of MOCPc and MOCPc-MWCNT respectively in 5 mL DMF solution until it desperse. The solution and a blank solvent of DMF were transferred in a two separate curvettes for analysis.

3.2.2 Fourier-Transform Infrared Spectroscopy

FTIR spectra were recorded on a Perkin Elmer, Spectrum 100, in the range 4000-400 cm^{-1} with the resolution of 4.00 cm^{-1}. The analysis was carried out using a diamond crystal probe and air was used as the background. The FTIR method was used to identify the chemical structure of the raw MWCNTs, acid-treated MWCNTs, aminated MWCNT, MOCPc and MOCPc-MWCNTs.

3.2.3 Scanning Electron Microscopy/ Energy Dispersive X-Ray

The morphology and chemical composition of the functionalised CNTs and MOCPc were studied using a LEO 1525 FE-SEM with the acceleration voltage of 2.00 kV. The SEM was also utilised to reveal the morphology and composition of MPcs and MPc-MWCNTs. The sample was prepared by putting approximately 0.1 mg of the sample on a carbon tape and coated to prevent charging for few minutes.

3.2.4 Transmission Electron Microscopy

The TEM analysis was performed by using a Philips CM 200 electon microscope with beam energies of 120 kV. TEM was used to determine the particle size of the functionalised MWCNTs and MOCPc-MWCNTs. The samples for analysis were prepared by sonicating about 0.5 mg of the materials in 5 ml DMF for 5 min. One drop of the resulting suspension was dropped on a copper grid.

3.2.5 X-Ray Diffraction

The crystallinity of the MOCPc-MWCNT hybrids were determine using and X-ray diffraction spectrometer using a PANanalytical X'Pert pro diffractometer with CuKα radiation, with a wavelength of λ = 1.5046 Å as a radiation source operating at 45 kV and 40 mA. The XRDs diffractograms were obtained in a scan range between 0 and 90°.

3.2.6 Atomic Force Microscopy

AFM images were obtained under ambient conditions with an Agilent 5500 microscope (Agilent Technologies, USA) in acoustic mode (tapping mode) at a

scanning frequency of 1 Hz. Silicon cantilevers with a nominal resonant frequency and force constant of ~ 330 kHz and 40 N/m, respectively, were used for imaging. Approxiamately 0.1 mg of the samples were dissolved in a 5 mL DMF and sonicated for 15 minutes until dispersed. One drop of the resulting suspension was dropped on a freshly cleaved Mica.

3.2.7 Thermogravimetric Analysis

Thermal analyses were performed using a TGA Q500 instrument (TA Instrument). Approximately 0.1-20 mg CNT samples were analysed in platinum pans at a heating rate of 10℃/min up to 1000℃ in nitrogen a t a flow rate of 30 ml/min. TGA was used to determine the thermal stability of MPc and MPc-MWCNT.

3.2.8 Ultrasonic Bath Treatment

Dispersion of the materials in a solvent were carried out using a Mechanical Ultrasonic Cleaner AC-200H. The sample in DMF solution was dispersed by immersing the sample holder in a bath containing water for 15 min.

3.2.9 Electrochemical characterisation conditions

All the electrochemical analyses were conducted using an Autolab potentiostat PGSTAT 302 (Eco Chemie, Utrecht, Netherlands driven by the General purpose electrochemical systems data processing software (GPES and FRA software version 4.9) shown in figure 3.1. The photoelectrochemical characterisation data for DSCs were collected using two electrodes set up with ITO/Pt catalyst as a counter electrode and the ITO/TiO_2/dye molecule as a working electrode. EIS measurements (Nyquist and Bode plot) were recorded using an Autolab Frequency Response Analyser (FRA). The cyclic voltammograms were carried out

with an Autolab GPES using the three-electrodes system with a glassy carbon as a working electrode, silver wire as a reference electrode and Pt wire as a counter electrode.

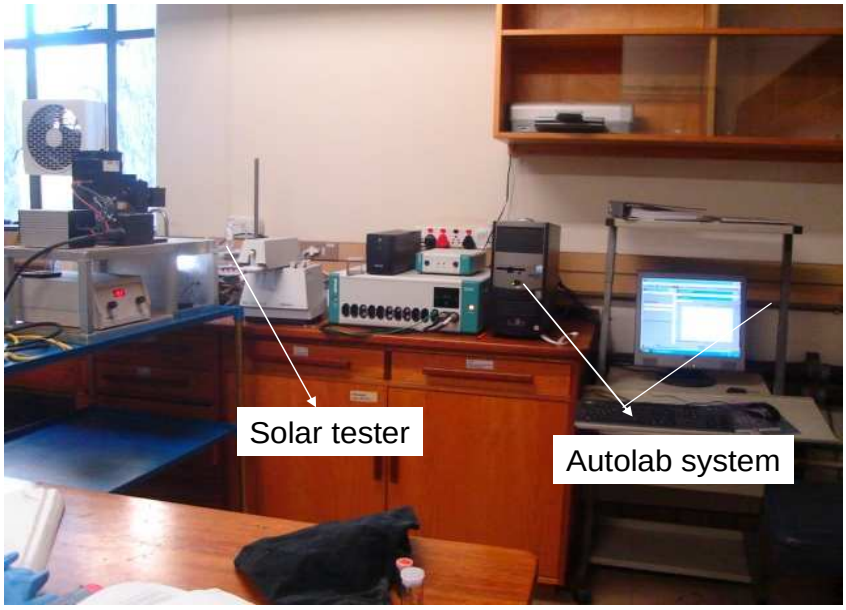

Figure 3.1: A photograph of the Auto lab system connected to the solar tester

3.3 FUNCTIONALISATION OF MULTI-WALLED CARBON NANOTUBES

3.4 Purification and oxidation of MWCNT

The multi-walled carbon nanotubes (MWCNTs) were purified and acid-functionalised as discussed by Siswana *et al.,* (2006). Approximately 1.0 g of MWCNTs was added to 140 mL of 2.6 M HNO_3 and the mixture was refluxed open to air for 24 hours. The carbon nanotube sediment was separated from the solution through filtration, continuously washed with water and dried overnight. It was then sonicated in a 3:1 (v/v %) mixture of H_2SO_4 and HNO_3 for 28 hours. Thereafter, the sediment was washed with distilled water through filtration and stirred for 30 min in a 4:1 (v/v %) H_2SO_4/H_2O_2 mixture at 70℃. The mixture was

then washed again with distilled water and the acid-treated MWCNTs (abbreviated as a-MWCNTs) were air dried for 48 hours.

3.4.1 Amine-functionalised MWCNT

The amine-functionalisation of MWCNTs was carried out by the method described by Jang *et al., (*2004). Approximately 0.05 g of a-MWCNTs was sonicated in 1.25 mL DMF for 10 s and then 25 mL of thionyl chloride was added. The mixture was refluxed for 24 hours, filtered and washed with THF to remove any unreacted $SOCl_2$. The filtrate was stirred in 25 mL of ethylenediamine for 5 days and filtered. The amine MWCNTs were air-dried for 2 days.

3.5 SYTHESIS OF METAL 2,3,9,10,16,17,23,24 OCTACARBOXYPHTHALOCYANINES

3.5.1 Synthesis of Zinc 2,3,9,10,16,17,23,24 octacarboxyphthalocyanines (ZnOCPc)

ZnOCPC was prepared, purified and characterised according to the method described by Sakamoto & Ohno (2008), (scheme 3.1). benzene-1,2,4,5-tetracarboxylic dianhydride (Pyromellitic dianhydride) (0.25 g, 1.15 mmol), urea (1.30 g, 0.022 mol), zinc acetate (0.5158 g, 0.0024 mol) and DBU (10 µl) were transferred into a 30 mL three necked round bottom flask, then heated to 250℃ until the mixture was fused. The reaction product was washed with water, acetone and 6 M hydrochloric acid (HCl) and dried for 3 hours in a vacuum oven. After being dried, 5 g of the crude product was base-hydrolysed with a solution of 5 g KOH in 15 mL deionised water, then heated for 8 hours at 120℃. The reaction mixture was diluted with water and filtered. The filtrate was acidified with

concentrated HCl to pH 2. The precipitated green product was collected by filtration and repeatedly washed with water and dried.

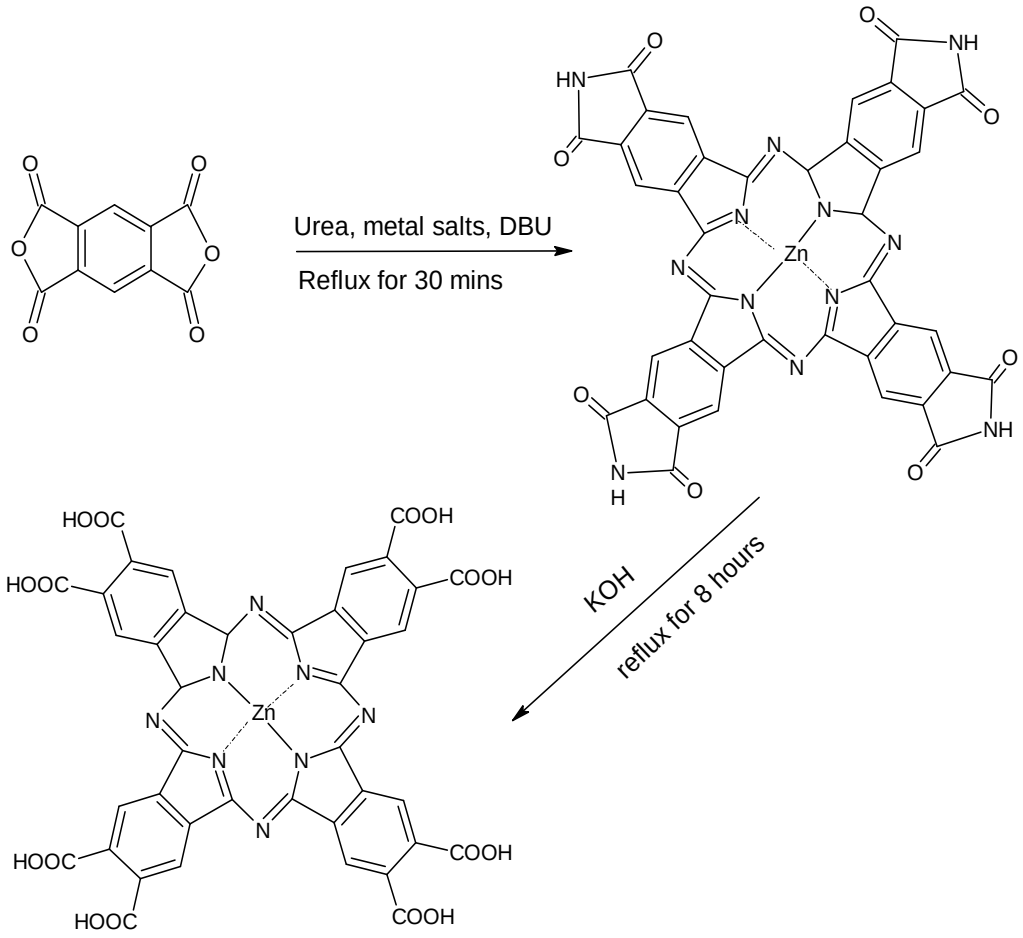

Scheme 3.1: Schematic of the synthesis route for Zinc octacarboxyphthalocyanines (ZnOCPc)

3.5.2 Synthesis of Silicon 2,3,9,10,16,17,23,24-octacarboxyphthalocyanines ($(OH)_2$SiOCPc)

$(OH)_2$SiOCPc was prepared, purified and characterised according to the method discussed by Masilela *et al.* (2009) and Sakamoto & Ohno (2008): scheme 3.2. Benzene-1,2,4,5-tetracarboxylic dianhydride (Pyromellitic dianhydride) (0.25 g, 1.15 mmol), urea (1.3 g, 0.022 mol), trichlorosilane (0.237 mL, 0.00235 mol) and

DBU (10 µl) were transferred into a 30 ml three-necked round-bottom flask and heated to 250℃ until the mixture was fused. The re action product was washed with water, acetone and 6 M hydrochloric acid and dried for 3 hrs in a vacuum oven. After being dried, the product was acid hydrolysed with 20% H_2SO_4 for 3 days at 120℃. The blue product was collected by fi ltration and washed with 2% H_2SO_4 and water. The blue product was further purified with water several times and dried.

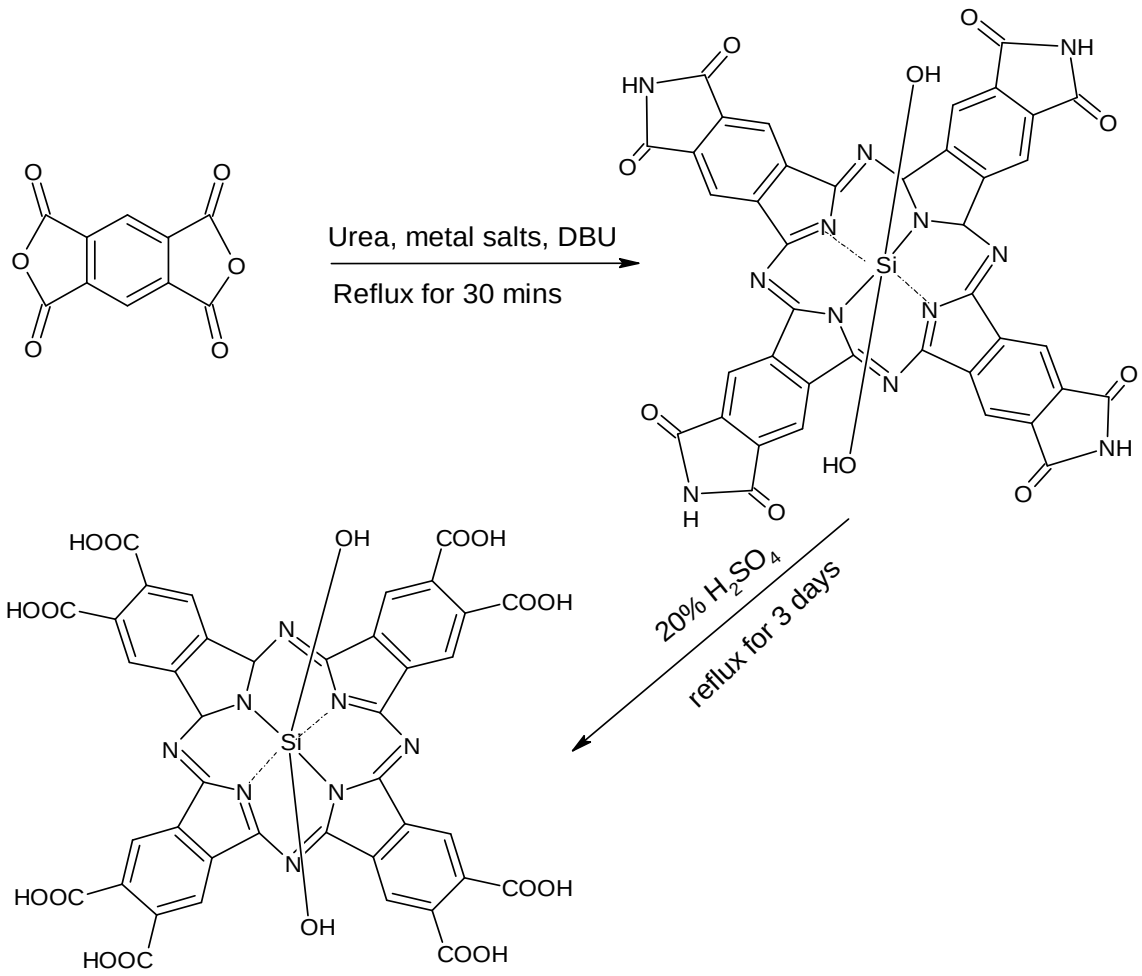

Scheme 3.2: Schematic of the synthesis route of Silicon octacarboxyphthalocyanines $(OH)_2SiOCPc$

3.5.3 Synthesis of Gallium (III) 2,3,9,10,16,17,23,24 octacarboxyphthalocynines ((OH)GaOCPc)

(OH)GaOCPc was prepared, purified and characterised according to the method described by Masilela *et al.,* (2009); Sakamoto & Ohno, (1998), scheme 3.3. Benzene-1,2,4,5-tetracarboxylic dianhydride (pyromellitic dianhydride) (0.25 g, 1.15 mmol), urea (1.30 g, 0.022 mol), (0.237 mL, 0.00235 mol) of gallium(III)chloride (moisture sensitive) and DBU (10 µl) were transferred into a 30 ml three necked round bottom flask, then heated to 250℃ until the mixture is fused. The reaction product was washed with water, acetone and 6 M hydrochloric acid and dried for 3 hours in a vacuum oven. After being dried, the product was acid hydrolysed with 20% H_2SO_4 for 3 days at 120℃. The blue product was collected by filtration and washed with 2% H_2SO_4 and water. The blue product was further purified with water several times and was dried.

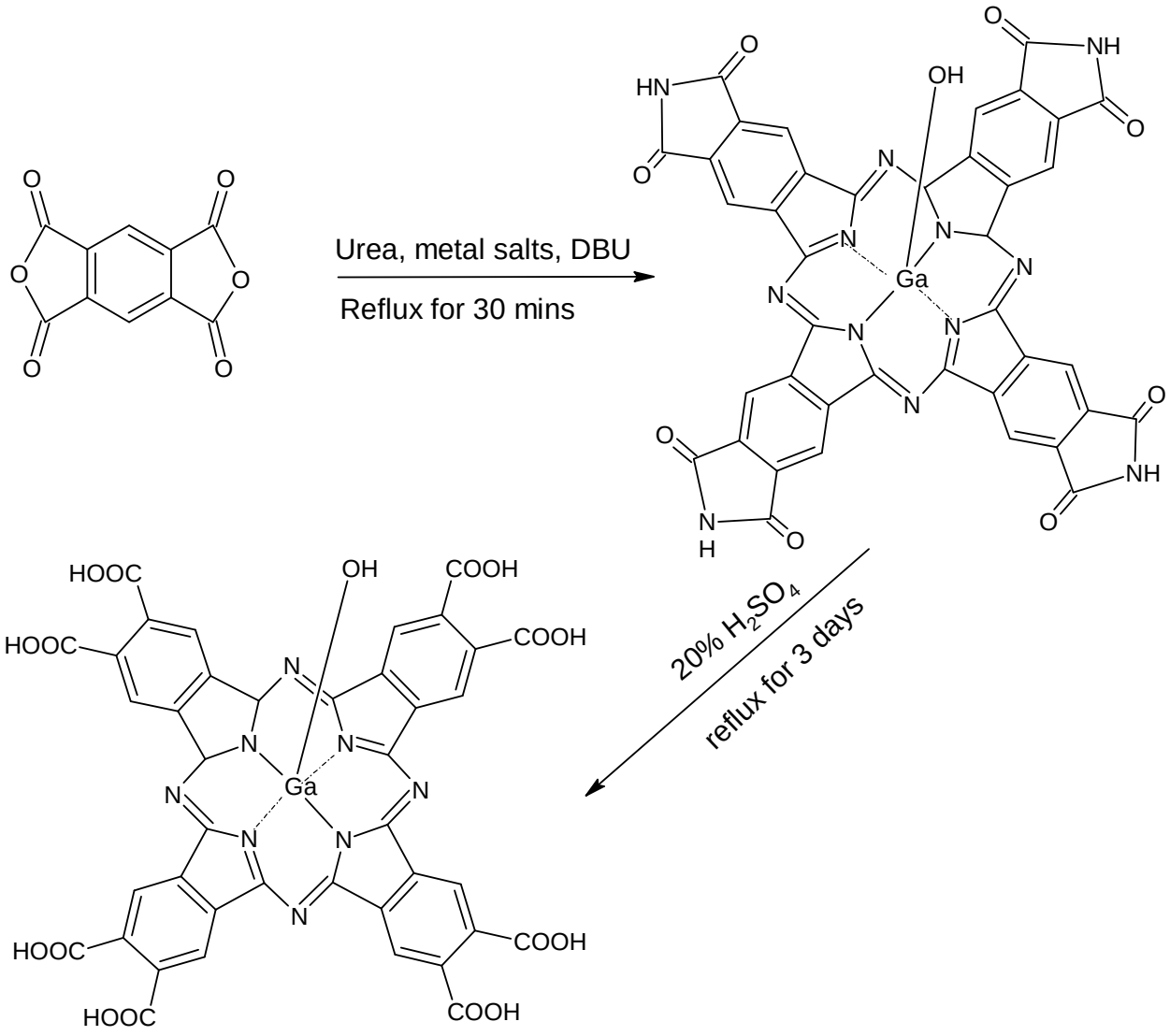

Scheme 3.3: Schematic of the synthesis route of Gallium (III) octacarboxyphthalocyanines ((OH)GaOCPc)

3.6 SYNTHESIS OF MOCPc-MWCNT

MOCPc-MWCNT was obtained using the method described by Chidawanyika & Nyokong, (2010). Approximately 0.30 g of amine-MWCNTs were sonicated for 15 min in 10 ml DMF. MOCPc was added to the mixture (resulting in a green-coloured suspension) and the mixture was stirred for 3 days. The solid product was separated through filtration and washed several times with DMF (to remove excess unreacted MOCPc) to give MOCPc- MWCNT.

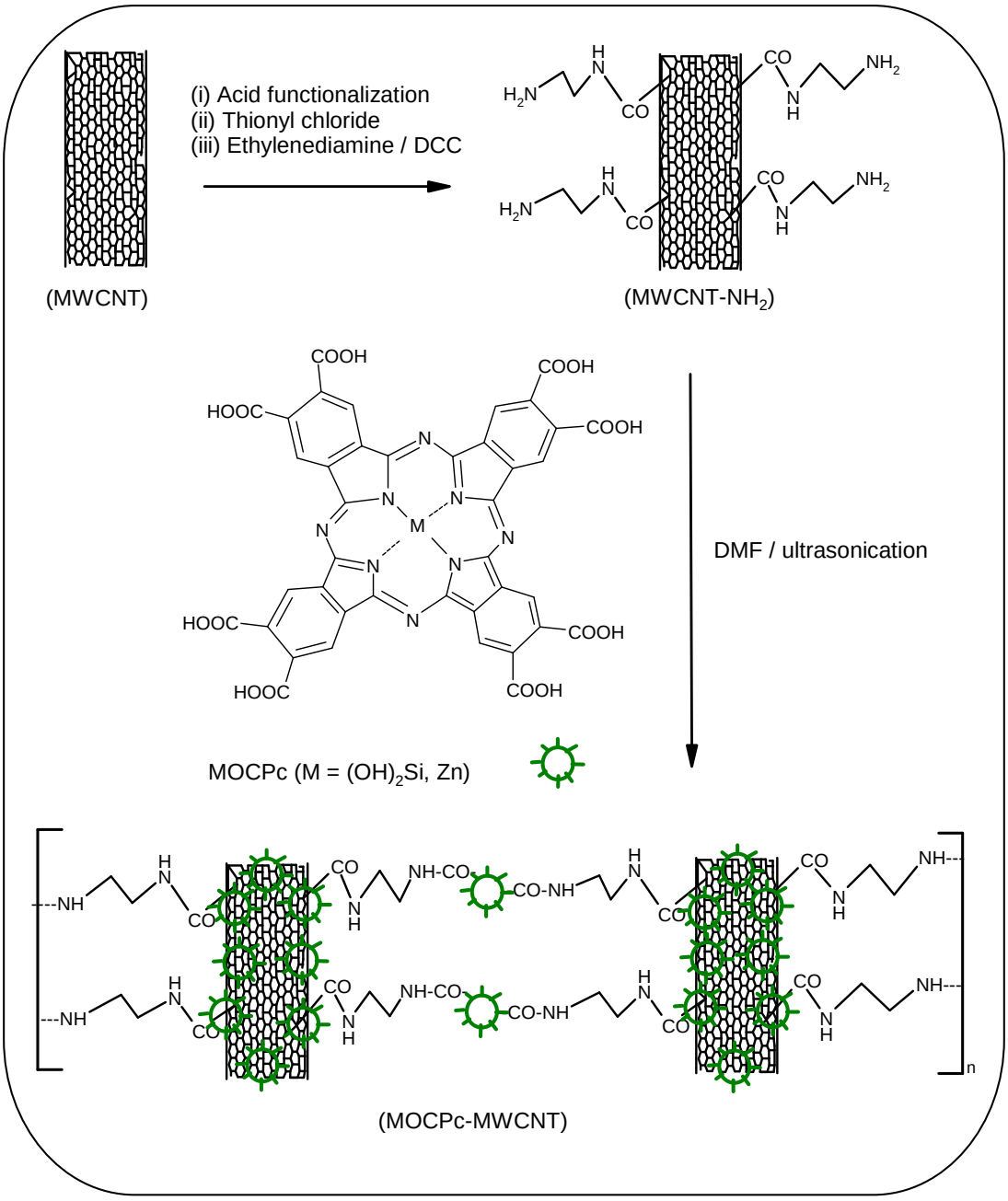

Scheme 3.4: Schematic of the synthesis route for the MOCPc-MWCNT hybrid

3.7 FABRICATION PROCEDURE OF DYE SOLAR CELLS

3.7.1 Doctor blading on the working electrode

The simplest and most widely used method for depositing TiO_2 paste on the ITO glass substrate is the so-called doctor blading method (Martineau, 2011). With the conductive side of the ITO glass facing up, the two parallel strips of tape were

applied on the edges of the glass plate. A portion of TiO_2 paste was applied near the top edge of the ITO glass between the two strips. The paste was spread using a glass rod on the glass surface supported by the tapes on both sides. The gap between the two tapes was filled with TiO_2 paste and this was repeated until the desired homogenous layer was obtained as shown in figure 3.2. The tapes were removed and the TiO_2 electrode was sintered for 35 min at 450℃. MOCPc-MWCNTs were then attached to the TiO_2 surface by immersing TiO_2 films in 3.5 ml of DMF solutions containing both 0.3 mM MOCPc and 0.1 mg of MOCPc-MWCNTs for 24 hours at room temperature.

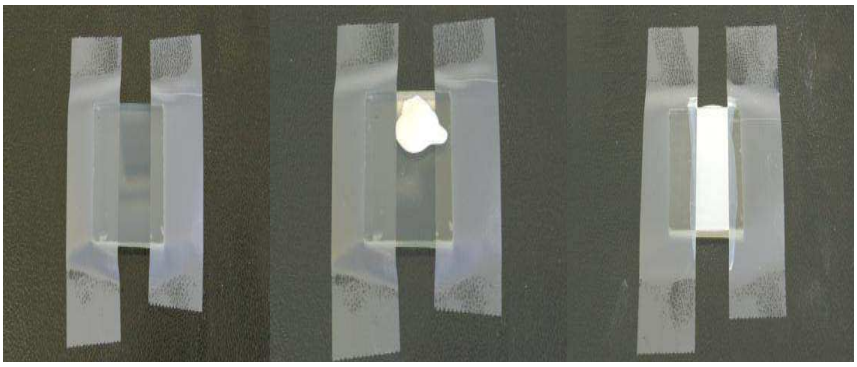

Figure 3.2: Coating of TiO_2 nanocrystalline on a glass substrate

3.7.2 Doctor blading on the counter electrode

With the conductive side of the ITO glass facing up, two parallel strips of tape were applied on the edges of the glass. A portion of platinum catalyst paste was applied near the top edge of the ITO glass between the two tape as shown in figure 3.3. The paste was flattened using a glass rod on the glass surface supported by both tapes on both sides. The gap between the two tapes was filled with platinum catalyst paste until a homogenous layer was obtined. The tape was removed and the glass slide treated for 15 min at 450℃.

Figure 3.3: Coating of platinium catalyst paste on a glass substrate.

3.7.3 Device Fabrication

The Surlyn 1702 template was placed on the side of the working electrode. The counter electrode was placed on top of the working electrode and sandwiched together with an alligator clip and heated for 15 min. After the heat treatment, the two electrodes were peeled off to remove the plastic and the glue remained on the working electrode. Thereafter, the two electrodes were sandwiched together and heated for 15 min at 100℃. The complete cell was f illed with electrolyte through the drilled hole on the counter electrode side using a 100 µl syringe as shown in figure 3.4. Measurements of the performance and the efficiency of the DSCs were performed using a solar tester.

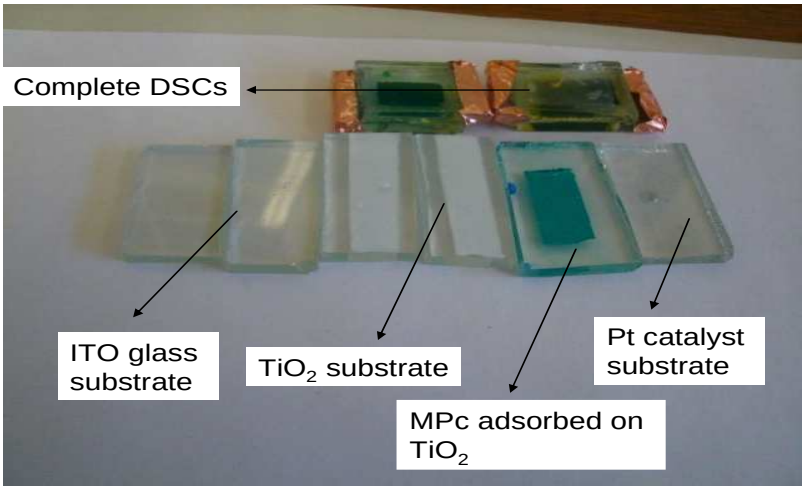

Figure 3.4: The fabrication of DSCs using MOCPc-MWCNT composites as a photosensitiser.

3.8 SOLUTION ELECTROCHEMISTRY

3.8.1 Preparation of Ag/AgCl wire Reference electrode

Silver wires were immersed in 0.1 M HNO_3 for few seconds to remove any oxide from the metal surface and were thoroughly rinsed with distilled water before coating.

Coating of Ag wire with AgCl

The AgCl layer was formed by immersing the silver wire (working electrode), Ag/AgCl (reference electrode) and a Pt wire (counter electrode) in a 0.05 M KCl solution and the chronopotentiometric technique was used to determine the coating performance (Potential: 1 V and Time: 1800 s).

The MOCPc complexes were dissolved in dry DMF and a small amount of tetrabutylammonium perchlorite (TBAP) was added to the solution. Nitrogen was bubbled vigorously through the solution. The Ag/AgCl wire (reference electrode), glassy carbon (working electrode) and a Pt wire (counter electrode) were immersed in the solution and the cyclic voltammograms and square waves were measured using an Autolab PGSTAT 302.

CHAPTER FOUR*

4 RESULTS AND DISCUSSIONS

This chapter describes the detailed spectroscopic and microscopic characterisation of the MOCPc complexes and the effect of incorporation of MWCNTs by UV/Vis spectroscopy, FTIR spectroscopy, SEM, TGA and XRD. The electrochemical and current-voltage curve characterisations of DSCs fabricated with MOCPc and their corresponding MWCNT-integrated hybrids are presented and described in this chapter.

* A part of this chapter has been submitted for publication as:

Nonhlanhla E. Mphahlele, Kenneth I. Ozoemena, Lukas J. Le Roux, Charl J. Jafta, Leskey Cele, Mkhulu K. Mathe, Tebello Nyokong, and Nagao Kobayashi, "Carbon Nanotube-Enhanced Photoelectrochemical Properties of Metallo-octacarboxyphthalocyanines for the Development of Dye-Sensitised Solar Cells", (submitted 2012)

4.1 CHARACTERISATION

4.1.1 UV-Visible spectroscopy

Figure 4.1 shows the UV/Vis spectra of ZnOCPc, $(OH)_2$SiOCPc and (OH)GaOCPc. The spectra of all three complexes exhibit two absoption bands (B-band and Q-band) assigned to phthalocyanines structure. All complexes exhibited the B-band absoption spectra ranges from 300-350 nm is attributed to charge transfer band between metal and ligands. The spectra of the three MOCPc complexes in DMF show the presence of two main bands one at 680–700 nm assigned to the monomeric species and the absorption peak appearing at 620 nm is attributed to the dimeric species of phthalocyanine complexes (Masilela *et al.*, 2009). The dimeric species around 620 nm of the three complexes may be due to the co-planar association of phthalocyanine ring in a solid state (Masilela *et al*., 2010). The monomeric species in the Q-band region represents the $\pi - \pi$ electron transition of the phthalocyanine macroring (Shaposhnikov *et al.,* 2005). These MOCPc complexes showed excellent solubility in DMF and no aggregation occurred (Chidawanyika & Nyokong 2010).

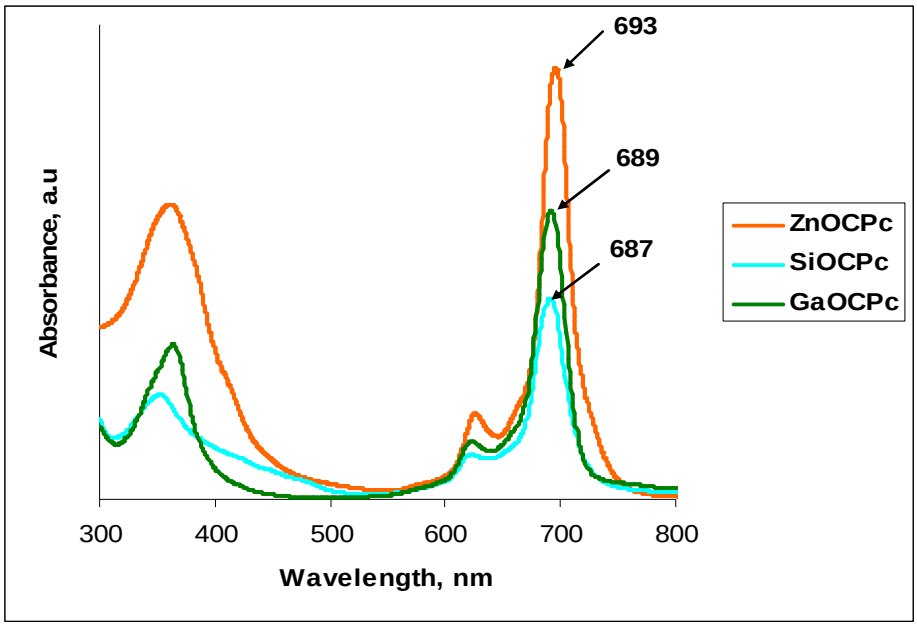

Figure 4.1: UV/Vis spectra of ZnOCPc, $(OH)_2$SiOCPc and (OH)GaOCPc in DMF.

Figure 4.2, presents the UV/Vis spectra of (OH)GaOCPc-MWCNT, ZnOCPc-MWCNT, $(OH)_2$SiOCPc-MWCNT hybrid and MWCNT–NH_2 in DMF. The three MOCPc-MWCNT hybrids show a slight red shift at the Q-band region as compared to the one without MWCNT. A slight shift may be ascribed to the successful introduction of the electron-withdrawing species (amine MWCNTs) on the phthalocyanine backbone (Chidawanyika & Nyokong, 2010). The SiOCPc-MWCNT showed a Q-band split at around 709 nm which may be ascribed to aggregation of the SiOCPc-MWCNT hybrid in solution. Upon intergration with MWCNT-NH_2 the intensity of the B-band decreased and slightly blue shifted as compared to the one without MWCNT-NH_2. This is specify an electron withdrawing species on the phthalocyanines complexes.

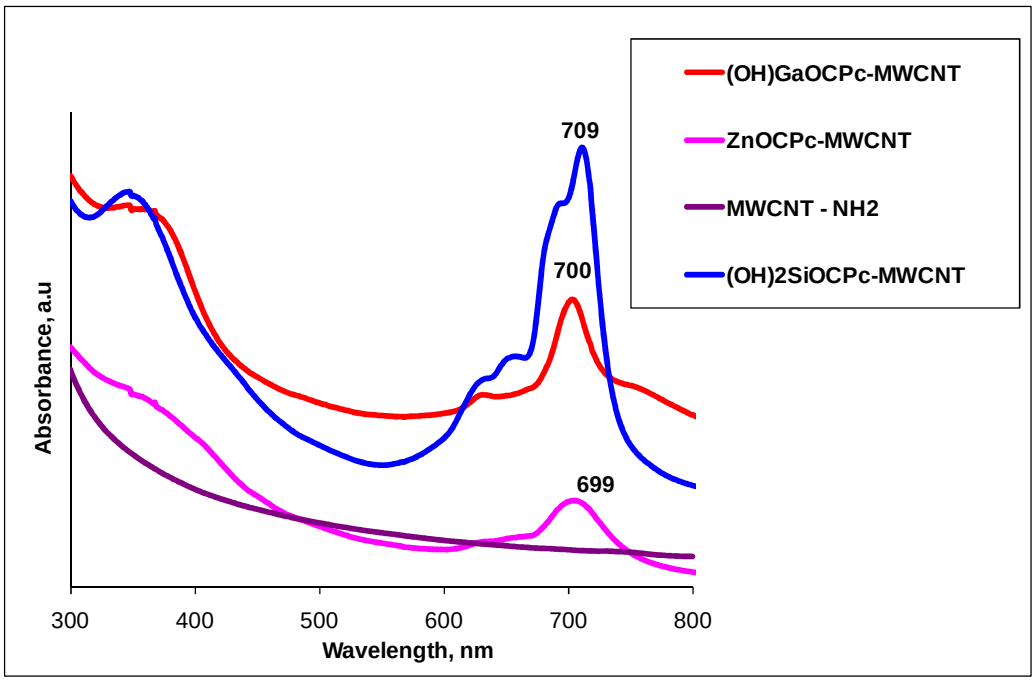

Figure 4.2: The UV/Vis spectra of ZnOCPc-MWCNT, $(OH)_2$SiOCPc-MWCNT, (OH)GaOCPc-MWCNT and MWCNT–NH_2 in DMF

4.1.2 Fourier Transform Infrared spectroscopy analysis

The FTIR spectra of the synthesised ZnOCPc, $(OH)_2$SiOCPc and (OH)GaOCPc confirm the existence of the characteristic pattern of carboxylic acid group on the MPc ring complexes (Shaposhinikov *et al*, 2005). The C=O stretching peak of the carboxylic acid group appears at 1700–1730 cm^{-1} while the peak at 1620–1650 cm^{-1} indicates the appearance of C=O stretching of the conjugated aromatic ring (Shaposhinikov *et al*, 2005). The FTIR spectra of ZnOCPc, $(OH)_2$SiOCPc and (OH)GaOCPc are attached in appendix A.

Figure 4.3 shows the FTIR spectra of raw MWCNTs, acid-MWCNTs (acid functionalised MWCNTs), MWCNT–NH_2 and ZnOCPc-MWCNT. FTIR spectroscopy was used to verify the chemical functionalisation of the MWCNTs. Prior to the purification of the MWCNTs, no peaks were observed on the higher frequency region as described by Ramanathan *et al*. (2005). After oxidation

treatment, the FT-IR spectrum of acid-MWCNT shows the C=O peak of carboxylic acid group at 1719 cm^{-1}, which is formed by hydrogen peroxide treatment.

The carboxylic acid groups were converted to acid chlorides by reacting with thionyl chloride. Then, the chloride terminated MWCNTs were reacted with ethylenediamine to yield amine-MWCNT as described by Lee and Yoo (2005). The disappearance of the 1719 cm^{-1} peak was observed and additional bands appeared at 1674 and 1498 cm^{-1} indicating the presence of C=O and C–N bonds of the amine functional group (Ramanathan *et al*., 2005; Shen *et al.*, 2007). In addition, the peak at 3276 cm^{-1} is assigned to the NH_2 symmetric stretch of the amine group (Ramanathan *et al*., 2005). The multiple peaks appearing around 2200 cm^{-1} on all the spectra attribute the presence of the carbon-carbon double bond of the MWCNTs (Yasuda *et al.,* 1999). The FTIR spectra for all the complexes were the same, hence only one has been shown in this report.

The ZnOCPc-MWCNT spectra show the chemical shift after the integration with amine-MWCNTs (Lee & Yoo, 2005). The peak due to the C=O stretching at 1722 cm^{-1} in the ZnOCPc-MWCNT spectrum has shifted to the lower frequency compared to the one without electron withdrawing species, (Chidawanyika & Nyokong, 2010). This indicates that successful integration occurred between the amine-MWCNTs and MOCPc. In addition, the peaks appearing at 1800 – 2200 cm^{-1} on all spectra attribute the presence of the carbon-carbon double bond of the MWCNTs (Yasuda *et al.,* 1999). The Spectra for $(OH)_2$SiOCPc-MWCNT and (OH)GaOCPc-MWCNT are attached on the Appendix A.4. The discussion is similar to that of ZnOCPc-MWCNT.

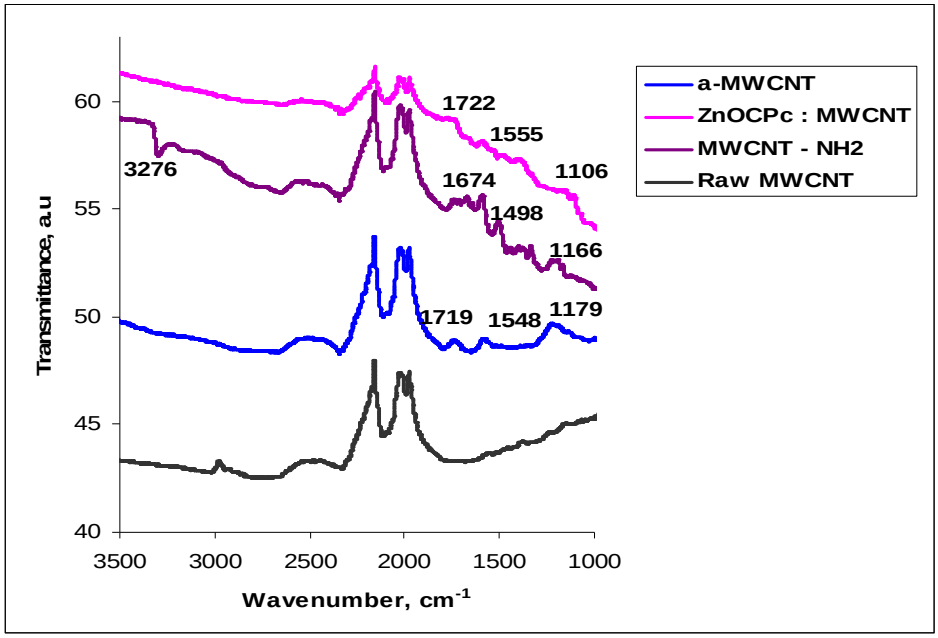

Figure 4.3: FTIR spectra of raw MWCNTs, a-MWCNT, MWCNT–NH_2 and ZnOCPc-MWCNT

4.1.3 Themogravimetric analysis

TGA was used to determine the structural difference between the MWCNT–NH_2 and the ZnOCPc-MWCNT as shown in figure 4.4. The analysis was performed under a steady flow of N_2, at a heating rate of 10℃ min^{-1}. The thermogravimetric results presented an initial weight loss of about 17.82% for MWCNT-NH_2, 15.13% for ZnOCPc and 10.65% for ZnOCPc-MWCNT were observed in 100 – 250℃ temperature. The weight loss is an indication of the removal of moisture or solvent in the sample and also is due to the removal of the carboxyl group from the macrocycle ring of the phthalocyanines (Chidawanyika & Nyokong, 2010 ; Giribabu *et al*., 2013).

The weight loss occurred about 28.99% for MWCNT-NH_2 between 200℃ and 600℃ is attributed to the destruction of the resid ual amorphous carbon present in the MWCNT and their decarboxylation of the oxidised species (Campidelli *et al*., 2008). The weight loss observed about 44% for ZnOCPc and 38% for ZnOCPc-

MWCNT between 400℃ and 600℃ may be ascribed to ph thalocyanine ring and functional groups decomposition (Giribabu *et al*., 2013). Therefore, TGA revealed the chemical functionalisation of MWCNT enhances the stability of the ZnOCPc as shown from the weight loss observed in 600℃ (Campi delli *et al.*, 2008; Chidawanyika & Nyokong, 2010).

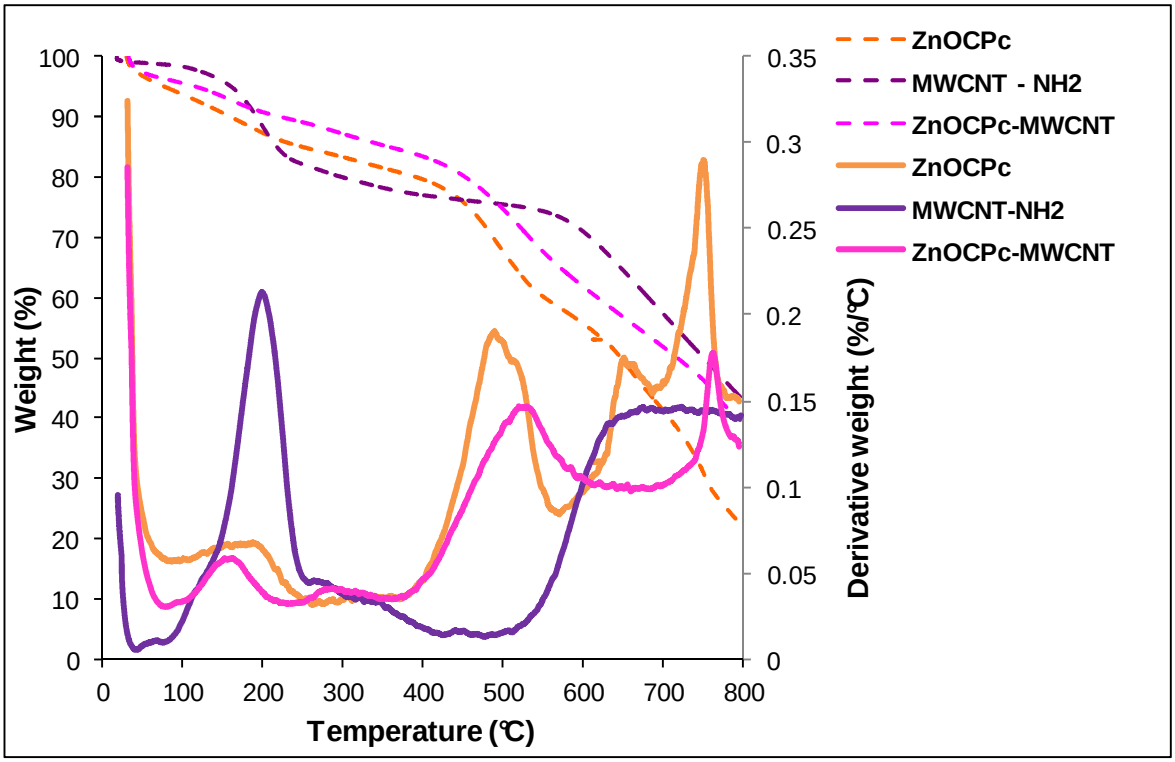

Figure 4.4: TGA analysis of MWCNT–NH_2, ZnOCPc, ZnOCPc -MWCNT (10℃ min^{-1} under N_2)

4.1.4 Transmission Electron Microscopy

Figure 4.5, presents the comparative TEM images of raw-MWCNT, MWCNT-NH_2 and ZnOCPc-MWCNT. The MWCNT-NH_2 appears to be spaghetti-like and the features shows that they were chemically "cut" and functionalised during amine functionalisation treatment. The ZnOCPc-MWCNT aggregated on the surface of the MWCNT-NH_2 confirming the integration of the ZnOCPc on MWCNT-NH_2 (Campidelli *et al*, 2008).

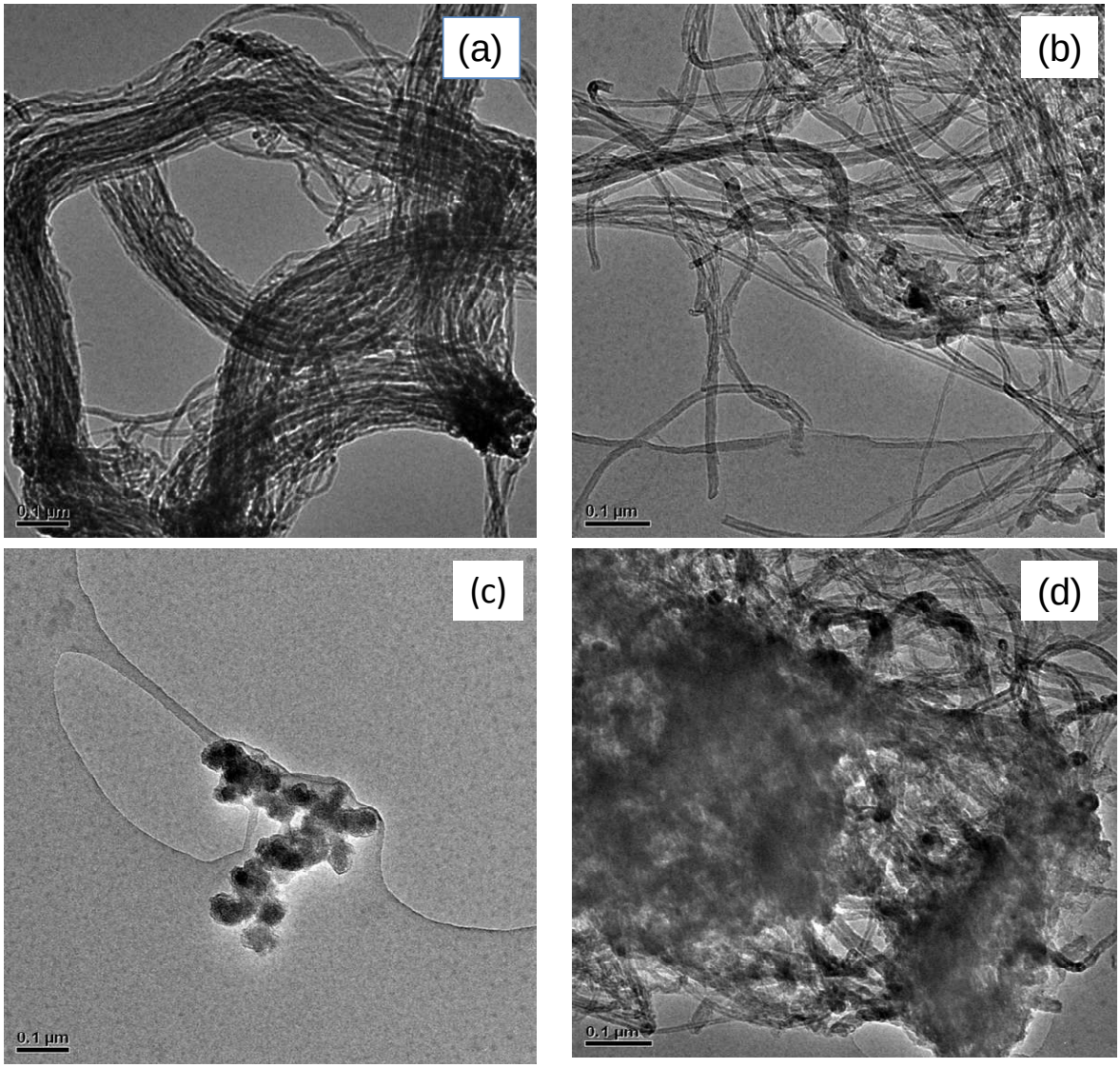

Figure 4.5: TEM images for **(a)** raw-MWCNT **(b)** MWCNT-NH_2 **(c)** ZnOCPc and **(d)** ZnOCPc-MWCNT

4.1.5 X–ray diffraction analysis

Figure 4.6 compares the XRD patterns of raw MWCNT, a–MWCNT, MWCNT–NH_2 and SiOCPc-MWCNT. The XRD patterns of all the spectra show the diffraction peaks around 26.3° and 43.3° indicating the graphit e structure (C 002) and (C 100) of the MWCNT (Zhang *et al*., 2005). The diffraction peaks obtained are similar to the standard one (26.5 ° and 42.5) acq uired from JCPDS card No. 88 – 8487. The XRDs patterns observed are not giving more information on the hybrid

but the position changes for different spectra might indicate the change in the interplanar spacing of the C lattices. The peak appearing at for raw MWCNT 2θ = 40° is due to the impurities hence it disappear aft er treatment.

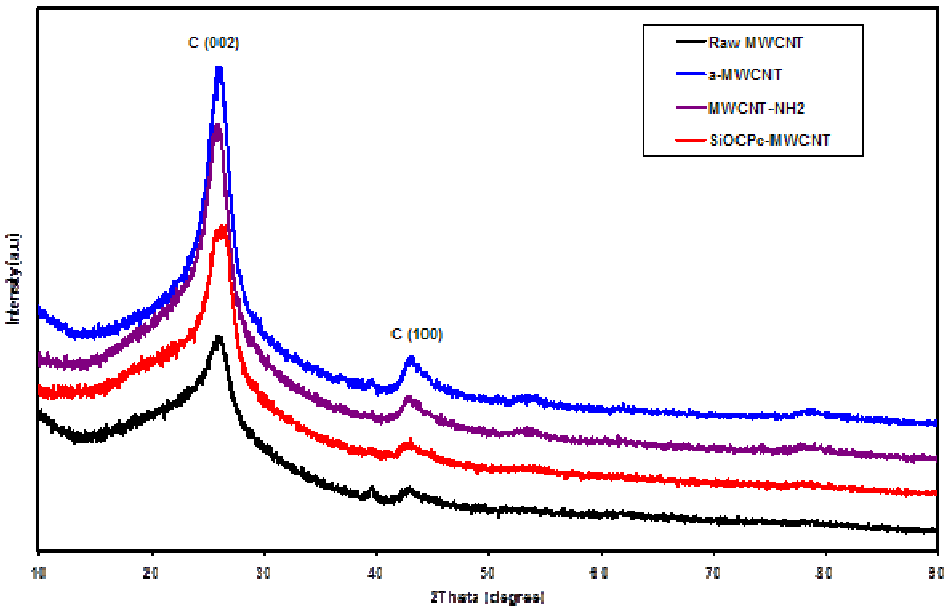

Figure 4.6: XRD patterns of raw MWCNT, a–MWCNT, MWCNT–NH2 and (OH)2SiOCPc-MWCNT composites

4.1.6 Atomic Force Microscopy

Figure 4.7 presents typical AFM images of the ZnOCPc-MWCNTs hybrid, clearly showing the attachment of ZnOCPc aggregates on the MWCNTs. The ZnOCPc is larger (20 – 500 nm) than expexted for a single molecule of the phthalocyanine (ca. 2 nm). This high concentration of the ZnOCPc aggregates on the MWCNTs is a clear indication of the cofacial interaction or aggregation between the ZnOCPc molecules.

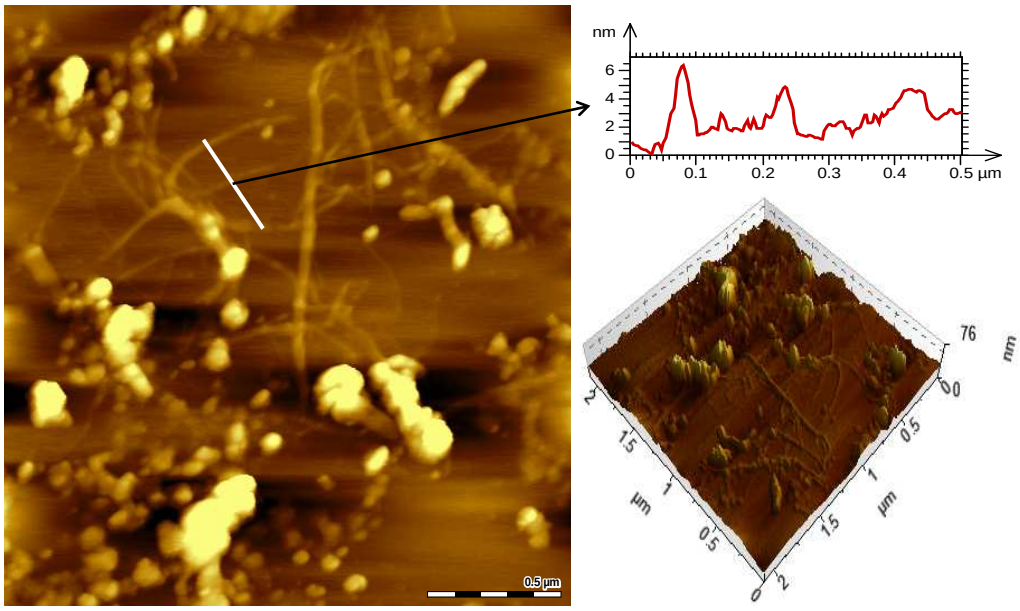

Figure 4.7: Typical AFM image of ZnOCPc-MWCNTs with the scale of 0.5 µm

4.1.7 Scanning Electron Microscopy

Figure 4.8 shows the comparative SEM micrographs of the MWCNT–NH_2, $(OH)_2$SiOCPc and $(OH)_2$SiOCPc-MWCNT. The SEM micrographs show the distinct surface morphology between $(OH)_2$SiOCPc without MWCNT and $(OH)_2$SiOCPc-MWCNT. The $(OH)_2$SiOCPc is homogenously enclosed by the MWCNTs, forming spaghetti like aggregates compared to the one without MWCNTs as discussed by Agboola *et al.*(2010). The activated carbon nanotube with large surface areas can offer more active sites for SiOCPc to enhance its conductivity in the application of DSCs.

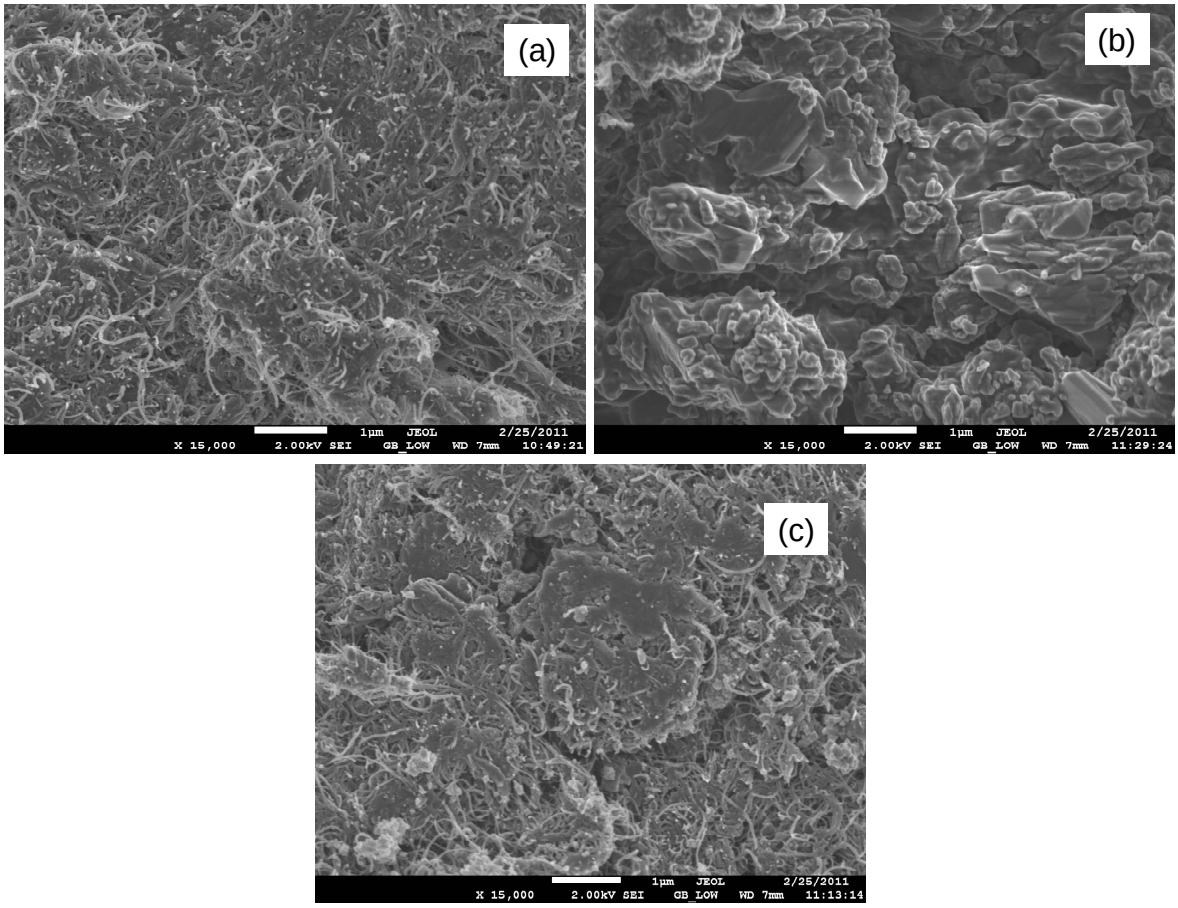

Figure 4.8: SEM micrographs of **(a)** MWCNT–NH_2, **(b)** (OH)2SiOCPc and **(c)** $(OH)_2$SiOCPc-MWCNT

4.1.8 Energy dispersive X-ray analysis

Figure 4.9 shows the EDX profile of ZnOCPc-MWCNT, GaOCPc-MWCNT and SiOCPc-MWCNT. The presence of carbon and oxygen peaks on all the EDX profiles are an indication of the successful modification of MWCNT in MOCPc. The Zn, Si and Ga peaks also confirm the presence of the MOCPc in MWCNT.

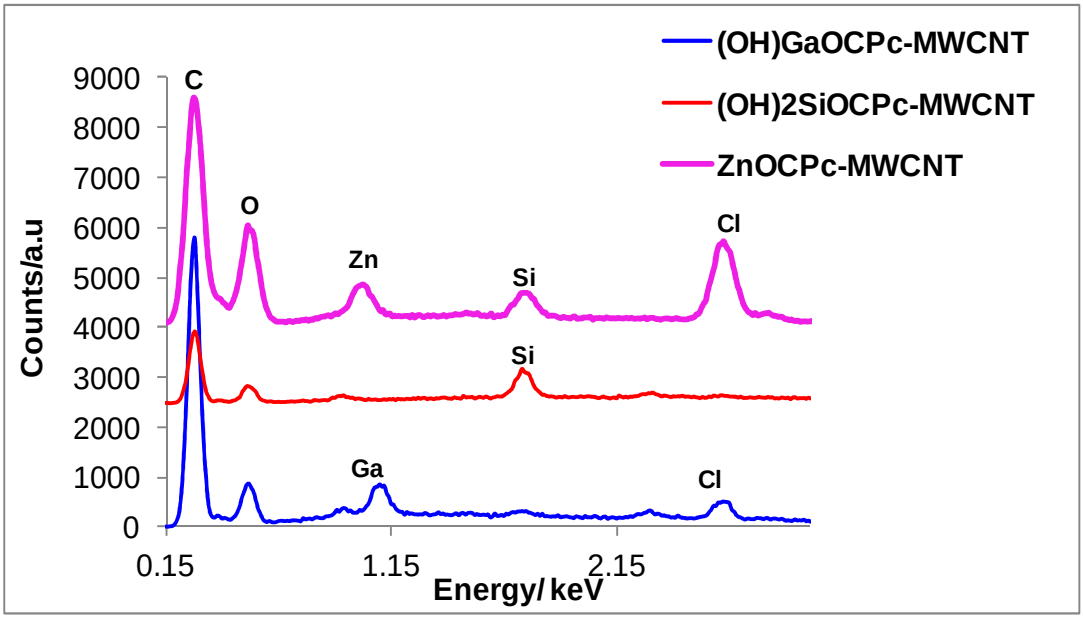

Figure 4.9: EDX profiles of ZnOCPc-MWCNT, GaOCPc-MWCNT and SiOCPc-MWCNT composites

4.2 ELECTROCHEMICAL CHARACTERISATION

4.2.1 Cyclic Voltammetry

The cyclic voltammograms and the square waves of all the phthalocyanine complexes showed the anodic and the cathodic peaks. The phthalocyanines usually undergo up to six reduction and two oxidation processes. SiOCPc shows one anodic peak and four cathodic peaks in figure 4.10. Thus, GaOCPc shows one anodic peak and five cathodic peaks in figure 4.11 whereas ZnOCPc shows five cathodic peaks in figure 4.12 in agreement with Sakamoto & Ohno (1998) and Masilela *et al.* (2009). Both the anodic and the cathodic peaks that are shown in the complexes are associated with the phthalocyanine ring-based processes since diamagnetic metals especially Zn, Al, Ga, Si metals are electro-inactive (Ozoemena & Nyokong, 2003). The redox couples and the potential values of all the complexes are described in table 4.1 below. The cyclic voltammograms correlate with the square waves of all the complexes shown in figure 4.13.

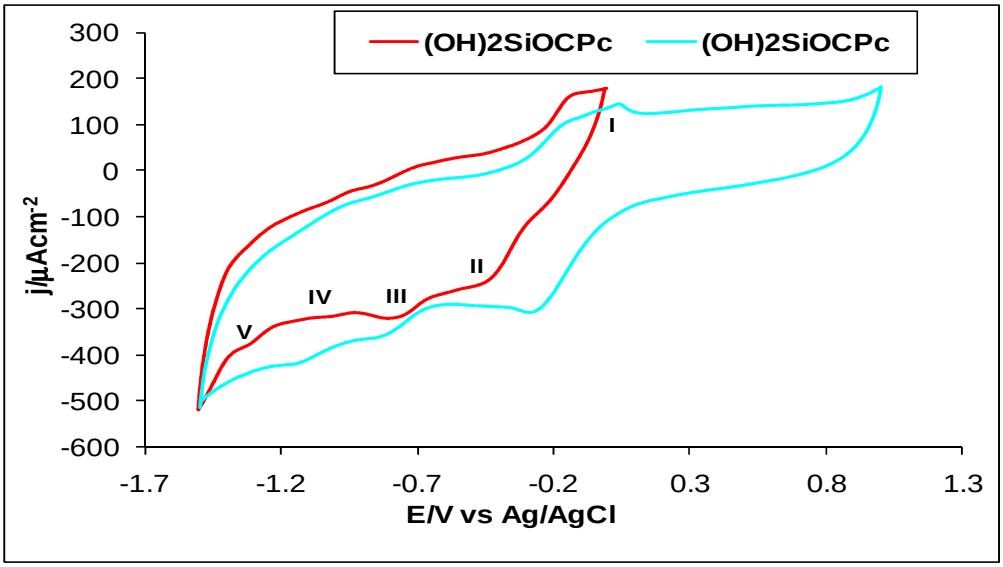

Figure 4.10: Cyclic voltammograms of SiOCPc **(a)** - 1.6 - -0.1V vs Ag/AgCl **(b)** -1.6 - +1.4V vs Ag/AgCl in DMF with 0.1M TBAP, scan rate = 50 mV s^{-1}

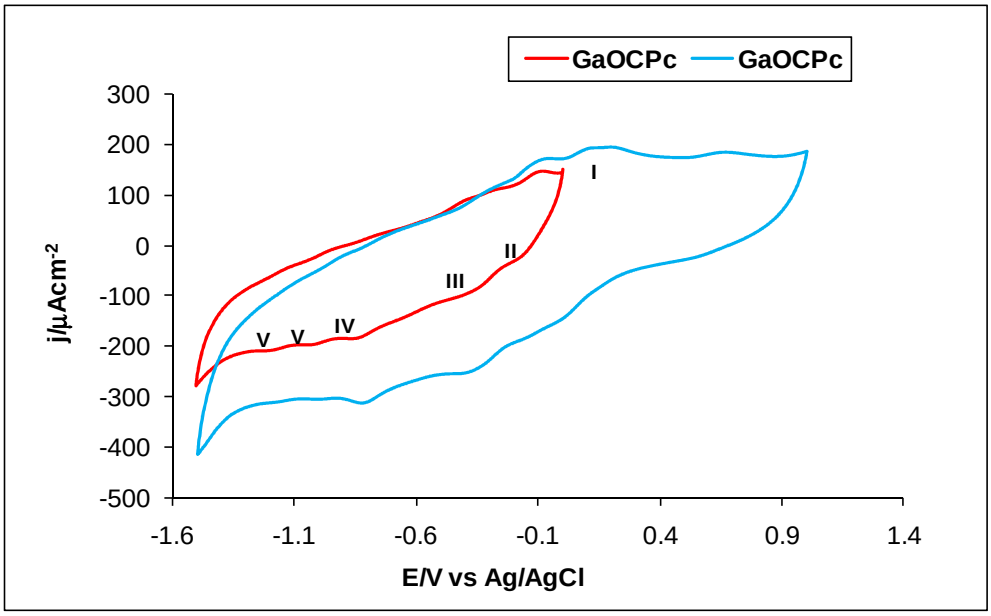

Figure 4.11: Cyclic voltammograms of GaOCPc **(a)** -1.5 – 0V vs Ag/AgCl **(b)** -1.6 - + 1.4V vs Ag/AgCl in DMF with 0.1M TBAP, scan rate = 50 mV s^{-1}

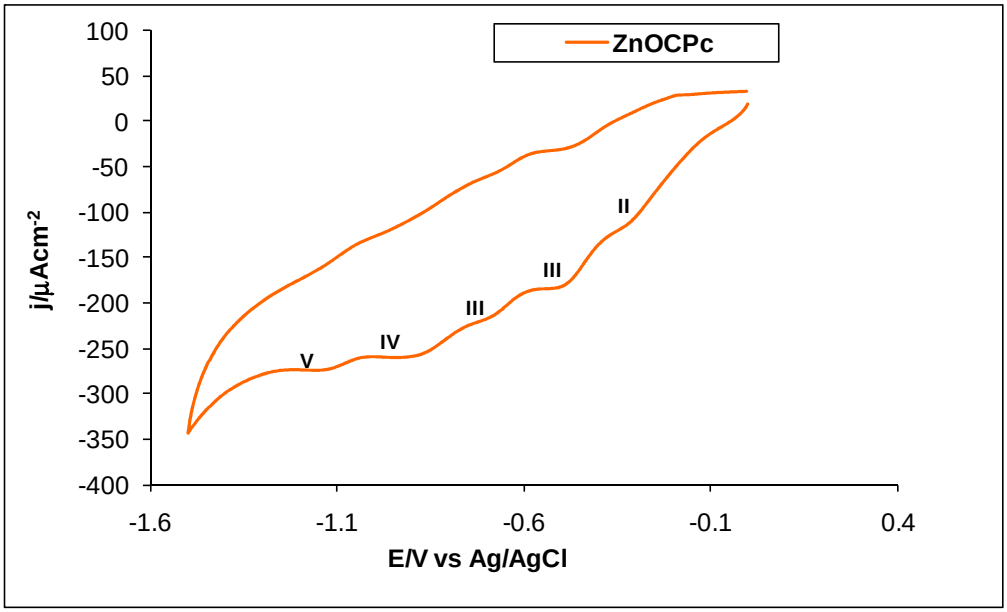

Figure 4.12: Cyclic voltammograms of ZnOCPc -1.6 – 0V Ag/AgCl in DMF with 0.1M TBAP, scan rate = 50 mV s^{-1}

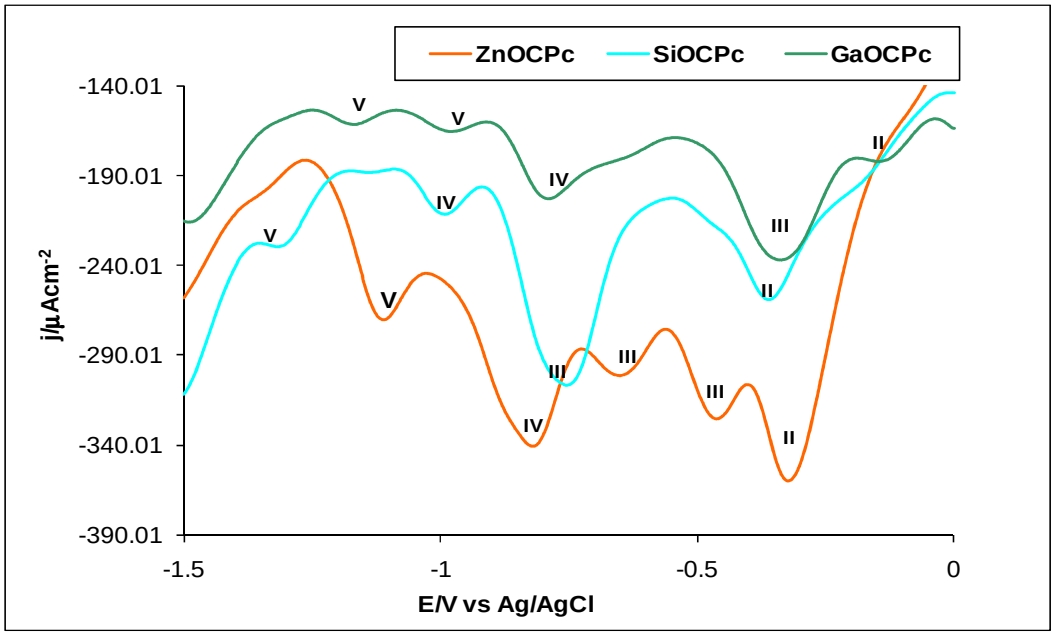

Figure 4.13: Square waves voltammograms of $(OH)_2$SiOCPc, ZnOCPc and (OH)GaOCPc in DMF with 0.1M TBAP, scan rate = 50 mV s^{-1}.

Figure 4.14 shows the cyclic voltammograms of SiOCPc, GaOCPc and ZnOCPc with MWCNTs. All the complexes show two reduction processes and one oxidation process. Their redox couples are described in table 4.1. Similarly from the one without MWCNT, their reduction and oxidation peaks are associated with

the phthalocyanine ring as discussed previously. However, the MWCNTs have played a role in this instant causing the first cathodic peak of SiOCPc to shift to the oxidation side by 0.06 V. Thus, the other redox couples such as Pc^{-4}/Pc^{-5} and Pc^{-5}/Pc^{-6} disappeared after the addition of MWCNT in the SiOCPc complexes. The anodic peak of SiOCPc is more intense as compared to the one without MWCNT, indicating that MWCNT reduces the intensity of the peaks. All the complexes with MWCNT showed the more enhanced cathodic peaks compared to the ones without MWCNT.

The ZnOCPc-MWCNT shows two reduction couples as compared to the ZnOCPc. The first cathodic peak of ZnOCPc-MWCNT has shifted towards the reduction side by 0.12 V whereas for GaOCPc-MWCNT the first cathodic peak has shifted towards the reduction side by 0.26 V. Both complexes also showed the disappearance of Pc^{-4}/Pc^{-5} and Pc^{-5}/Pc^{-6} redox couples after the addition of MWCNT.

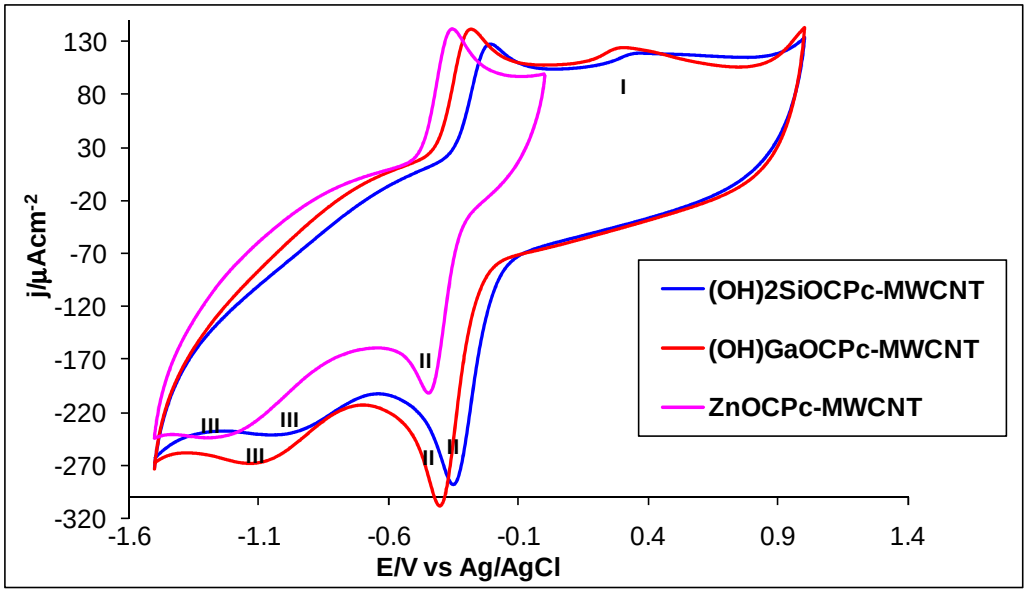

Figure 4.14: Cyclic voltammograms of SiOCPc-MWCNT, ZnOCPc-MWCNT, GaOCPc-MWCNT composites in DMF with 0.1M TBAP, scan rate = 50 mV s^{-1}.

Table 4.1: Redox potentials of $(OH)_2$SiOCPc, ZnOCPc, (OH)GaOCPc, $(OH)_2$SiOCPc - MWCNT, ZnOCPc -MWCNT and (OH)GaOCPc – MWCNT

Compounds	**Oxidation / V (vs Ag/AgCl wire)**	**Reduction/ V (vs Ag/AgCl wire)**			
	I	II	III	IV	V
	Pc^{-1}/Pc^{-2}	Pc^{-2}/Pc^{-3}	Pc^{-3}/Pc^{-4}	Pc^{-4}/Pc^{-5}	Pc^{-5}/Pc^{-6}
$(OH)_2$ SiOCPc	0.60	-0.43	-0.45	-0.80	-1.34
(OH)GaOCPc	0.18	-0.17	-0.36	-0.87	-1.03 -1.20
ZnOCPc		-0.34	-0.50 -0.68	-0.90	-1.16
$(OH)_2$SiOCPc - MWCNT	0.40	-0.37	-1.05		
(OH)GaOCPc - MWCNT	0.32	-0.43	-1.12		
ZnOCPc - MWCNT		-0.46	-1.25		

4.2.2 Cyclic voltammetry for DSC in light

Figure 4.15 shows the linear sweep voltammograms of ZnOCPc, ZnOCPc-MWCNT, SiOCPc, SiOCPc-MWCNT and GaOCPc, GaOCPc-MWCNT at 10 mV under illumination. The measurements without MWCNTs show the same maximum current peaks and onset potential even though there was a slight shift on the current of GaOCPc. Therefore, the incorporation of the MWCNTs resulted in an increase in the maximum current peaks, with about 40% improvement in the ZnOCPc response as discussed by Colucci *et al.* (1999). The onset potential for all the measurements are similar, however, the current of SiOCPc has increased. A significant increase of the maximum current peak of ZnOCPc-MWCNT indicates that the electron injection of ZnOCPc-MWCNT to the conduction band of the TiO_2 semiconductor was fast.

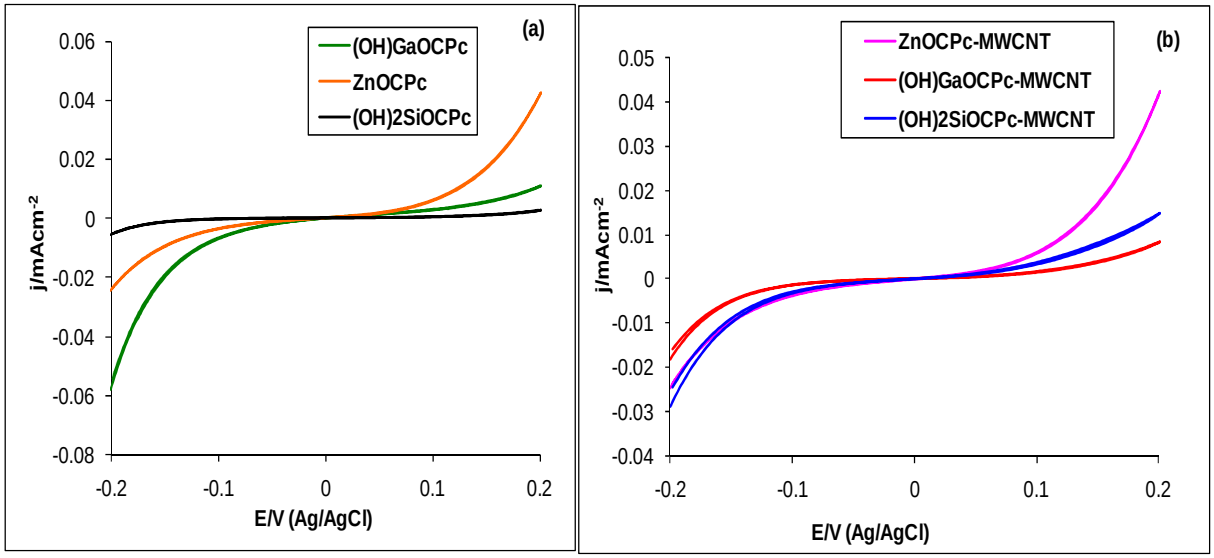

Figure 4.15: The linear sweep voltammograms of DSCs with ZnOCPc, ZnOCPc-MWCNT, $(OH)_2$SiOCPc, $(OH)_2$SiOCPc-MWCNT and (OH)GaOCPc, (OH)GaOCPc-MWCNT at 10mV under illumination.

4.2.3 Cyclic voltammetry for DSC in dark

Figure 4.16 shows the linear sweep voltammograms of DSCs with ZnOCPc, ZnOCPc-MWCNT, $(OH)_2$SiOCPc, $(OH)_2$SiOCPc-MWCNT and (OH)GaOCPc, (OH)GaOCPc-MWCNT at 10mV in the dark. The onset potential for both DSCs of MOCPc and MOCPc with MWCNT in the dark are almost the same, however, there is a slight difference in the peak currents. The maximum peak current of ZnOCPc and ZnOCPc-MWCNT increased by about 40% compared to other materials. This probably related to the fast electron injection of ZnOCPc-MWCNT to the conduction band of TiO_2 semiconductor.

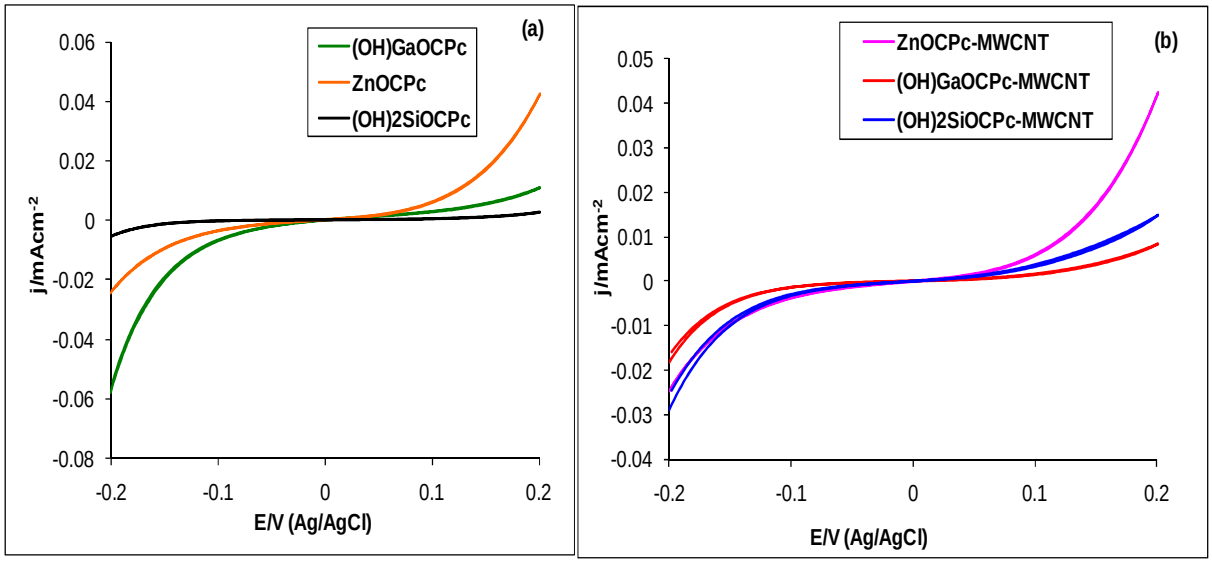

Figure 4.16: Linear sweep voltammograms of DSCs with TiO_2/ZnOCPc, TiO_2/ZnOCPc-MWCNT, TiO_2/SiOCPc, TiO_2/SiOCPc-MWCNT and TiO_2/GaOCPc, TiO_2/GaOCPc-MWCNT electrodes at 10mV in the dark.

4.2.4 Chronoamperometry

Figure 4.15 presents the chronoamperometric evolution of the fabricated DSC cells using the TiO_2/ZnOCPc, TiO_2/ZnOCPc-MWCNT, TiO_2/$(OH)_2$SiOCPc, TiO_2/$(OH)_2$SiOCPc-MWCNT and TiO_2/(OH)GaOCPc, TiO_2/(OH)GaOCPc-MWCNT

electrodes recorded at 50 second intervals for 600 s. The time resolved photocurrent measurements were carried out for the DSCs to give a comparison between MOCPc-MWCNT and MOCPc without MWCNT. Both the MOCPc and MOCPc-MWCNT hybrids on the ITO glass substrate show photocurrent response under visible light illumination as well as a reversible rise/decay of the photocurrent in response to the on/off illumination.

The photocurrent measurement of all the complexes in DSCs depicts an almost rectangular photocurrent response when switching on and off the illumination. These indicate that the dye molecules (MOCPc) are in contact with the electrolyte in the DSCs device (Masilelaa *et al.,* 2010; Nonomura *et al.*, 2007). The measurement showed no overshoots for all the complexes at a steady state level and almost a rectangular photocurrent response was observed when switching the illumination on and off (Nonomura *et al.,* 2007).

A significant increase of the photocurrent density occurred when MWCNTs were incorporated into the MOCPc, with about 36% improvement in the ZnOCPc response. This indicates that the injection of electrons to the conduction band of the TiO_2 in the MOCPc-MWCNT complex is faster than in the one without MWCNT (Idowu *et al.,* 2010).

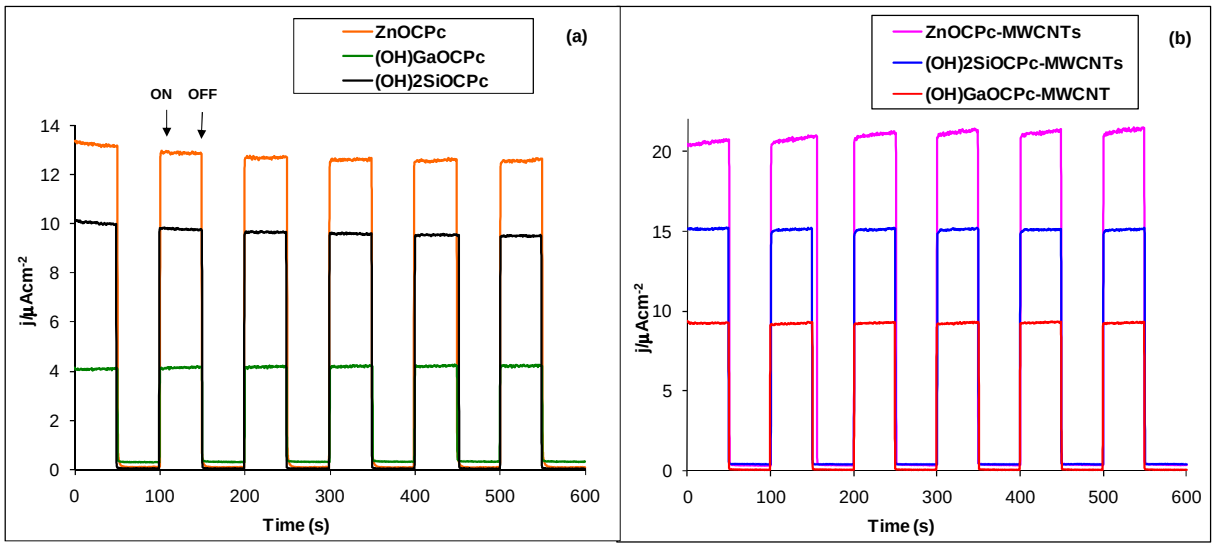

Figure 4.17: Chronoamperometry of DSCs with TiO_2/ZnOCPc, TiO_2/ZnOCPc-MWCNT, TiO_2/$(OH)_2$SiOCPc, TiO_2/$(OH)_2$SiOCPc-MWCNT and TiO_2/(OH)GaOCPc, TiO_2/(OH)GaOCPc-MWCNT electrodes at an applied potential of 10mV, recorded at 50 second intervals for 600 s.

4.2.5 Electrochemical Impedance Measurement

Electrochemical impedance spectroscopy (EIS) is an important technique for investigating the electron transport and recombination mechanisms of DSCs (Wang *et al.*, 2005). In this work, the EIS experiments were performed to provide some insight into the origins and differences of the photocurrent responses at the MOCPc complexes and MOCPc-MWCNTs dyes.

4.2.6 Nyquist plot measurement

Figure 4.18 presents the comparative Nyquist plots obtained from the DSCs fabricated from the MOCPc complexes before (a) and after incorporation of the MWCNTs (b). The EIS spectra were easily fitted with Voigt circuit comprising three RC elements in series (Figure 4.19). The fitting parameters involve the series resistance (R_s) arising from the sheet resistance of the ITO and the contact resistance of the cell, electron transfer resistance at the ITO/TiO_2 film interface

(R_{TiO2}), electron transfer resistance due to back reaction (recombination reaction) at the TiO_2/electrolyte interface (R_{Rec}), and charge transfer at Pt-ITO/electrolyte interface (R_{Pt}). The C_{TiO2}, C_{Rec} and C_{Pt} are the double layer capacitances due to the ITO/TiO_2 interface, TiO_2/electrolyte interface, and Pt-ITO/electrolyte interface, respectively.

The EIS parameters are summarised in table 4.2. Thus, from the EIS data, the high performance of the ZnOCPc-based cells is related to the excellent electron transport and poor recombination rate of electrons in the TiO_2. The reverse is true for the poorly-behaved $(OH)_2$SiOCPc-based DSCs and (OH)GaOCPc-based cell that showed slow electron transport coupled with easy recombination rate of electrons. The nyquist plot in the dark are presented in the appendix (A.5).

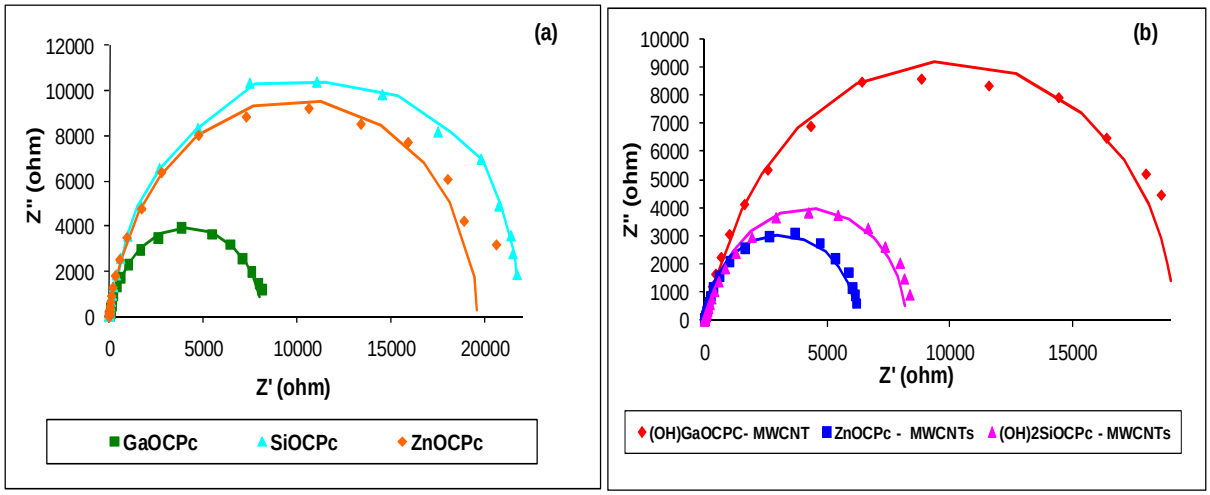

Figure 4.18: Nyquist plots of DSCs fabricated with **(a)** TiO_2/ZnOCPc, TiO_2/GaOCPc and TiO_2/$(OH)_2$SiOCPc **(b)** their corresponding MWCNT-integrated hybrid.

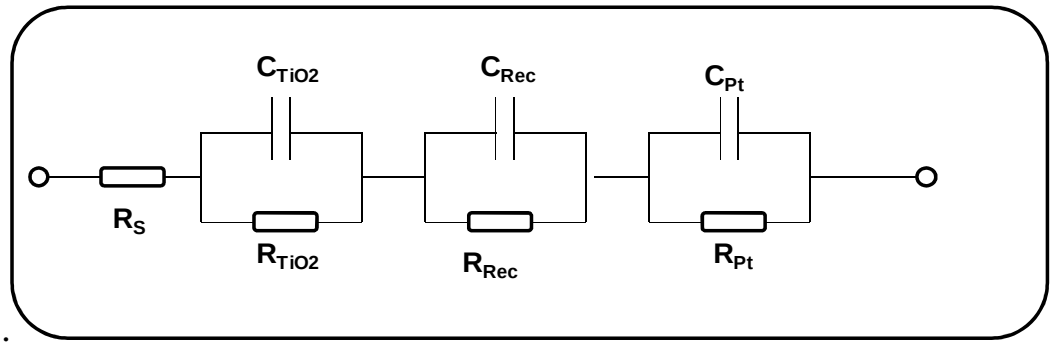

Figure 4.19: Equivalent circuit used to fit the Nyquist plots

Table 4.2: Electrochemical impedance measurement data of the DSCs

MOCPc	EIS Parameters (light)								
	R_s/Ω	R_{TiO2}/Ω	C_{TiO2}/μ f	R_{Rec}/Ω	C_{Rec}/μ f	R_{Pt}/k Ω	C_{Pt}/μ f	Slope	-phase angle
ZnOCPc	20.8 ±0.4	12.6 ±2.2	12.4±2.1	414±151	35.7±5. 22	19.2 ±0.5	11.7 ±0.5	-0.8754 R^2 = 0.9988	79.7
SiOCPc	17.5±0.2	17 ±1.4	7.8±0.5	215±59	21.3±1.4	21.3±0.3	7.8±0.14	-0.8193 R^2 = 0.9996	80.56
GaOCPc	20.7±0.3	14.59±2.4	10.10±1.3	135.7± 23.2	27.1±3.2	7.8±0.2	10.8±0.4	-0.8529 R^2 = 0.9991	76.2
Light (MWCNT)									
ZnOCPc	15.21±0.3	21.8±2.9	6.07±0.5	648±68.7	12.5±0. 9	8±0.2	8±0.2	-0.7694 R^2 = 0.9999	68.94
SiOCPc	19.3± 0.3	22.3±2.5	5.4± 0.5	413±63.6	19.86±2 .12	6.10± 0.13	11.06± 0.31	-0.8193 R^2 = 0.9929	76.9
GaOCPc	38.3 ±0.47	801±140	17.4±3.0	34.9± 4.17	8.14± 0.8	18.23 ±0.36	10.20±0.36	-0.8123 R^2 = 0.9968	80.2

MOCPc	X^2	X^2_{Real}	$X^2_{Imaginary}$
Light			
ZnOCPc	3.9065×10^{1}	4.0327×10^{-10}	3.9065×10^{1}
SiOCPc	1.2839×10^{-1}	2.0376×10^{-7}	1.2839×10^{-1}
GaOCPc	2.6081×10^{1}	7.9681×10^{-8}	2.6081×10^{1}
Light (MWCNT)			
ZnOCPc	5.3694×10^{-4}	4.5701×10^{-20}	1.2605×10^{1}
SiOCPc	1.2605×10^{1}	1.6391×10^{-7}	1.4063×10^{2}
GaOCPc	1.4063×10^{2}	3.446×10^{-6}	1.4063×10^{2}

4.2.7 Bode Plot measurement

Figures 4.20 – 4.22 show the Bode plots of TiO_2/ZnOCPc, TiO_2/SiOCPc, TiO_2/GaoCPc and TiO_2/ZnOCPc-MWCNT, TiO_2/SiOCPc-MWCNT, TiO_2/GaOCPc-MWCNT in DSCs. From the Bode plots, the slopes of the log Z vs log f plots at the mid frequency region are less than the ideal -1.0 for a pure capacitor, which is an indication of pseudocapacitive behaviour. Also, the phase angles lie between 69^o and 85^o, which are less than the 90^o expected of an ideal capacitor, further confirming the pseudocapacitive behaviour of the DSCs studied here. Fast electron propagation (R_{TiO2}) and the slow rate of electron recombination (R_{Rec}) are of critical importance for achieving high performance in DSCs.

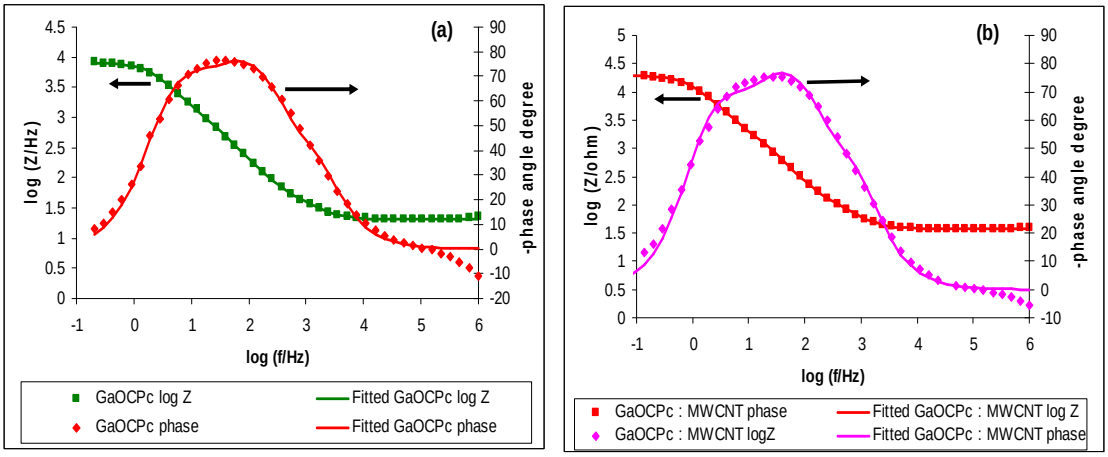

Figure 4.20: Bode plot of DSC with **(a)** TiO_2/GaOCPc **(b)** TiO_2/GaOCPc-MWCNT composites under illumination.

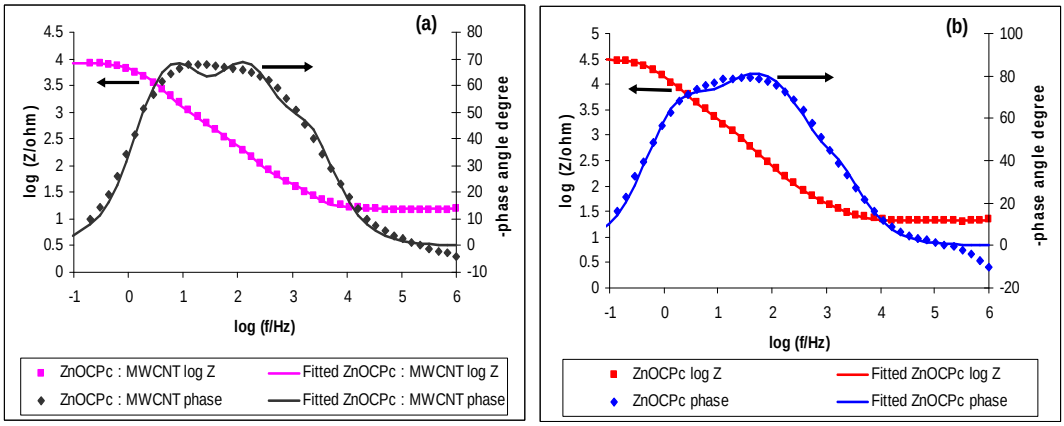

Figure 4.21: Bode plot of DSC with **(a)** TiO_2/ZnOCPc-MWCNT composite **(b)** TiO_2/ZnOCPc under illumination.

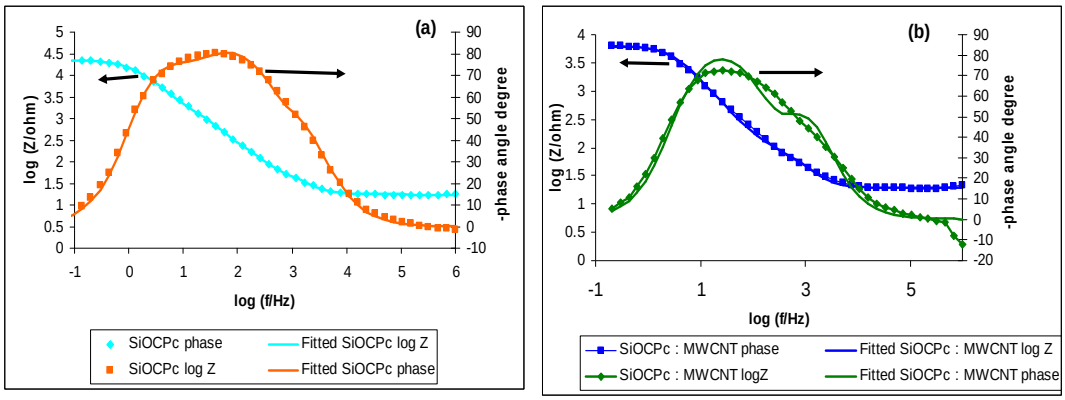

Figure 4.22: Bode plot of DSC with **(a)** TiO_2/SiOCPc **(b)** TiO_2/SiOCPc-MWCNT composites under illumination.

4.3 CURRENT–VOLTAGE CURVES

Figure 4.23 presents the current–voltage characteristics of the DSCs with TiO_2 /ZnOCPc, TiO_2/$(OH)_2$SiOCPc ,TiO_2/(OH)GaOCPc without MWCNT and TiO_2/ZnOCPc-MWCNT, TiO_2/$(OH)_2$SiOCPc-MWCNT and TiO_2/(OH)GaOCPc-MWCNT. The corresponding cell performance is shown in table 4.3. The cell without MWCNT showed an inferior performance with a low short circuit current density (j_{sc}) of 0.008 (mA/cm^{-2}) and a conversion efficiency of 0.01%. However, the cell with MWCNT resulted in a great improvement of j_{sc}, which was increased to 0.016 mA/cm^{-2} and a slight increase in the conversion efficiency to 0.1%. Even though the efficiency is small, the effect of MWCNT on DSCs is demonstrated.

Table 4.3: Photovoltaic performance parameters of DSCs using TiO_2/MOCPc and TiO_2/MOCPC-MWCNT under AM 1.5 illumination (Power 100 mWcm^{-2}) and active area of 1.125 cm^2

	Jsc/mAcm^{-2}	**Voc (V)**	**FF(%)**	**Efficiency (%)**
ZnOCPc	0.0075	0.1	30	0.011
SiOCPc	0.0066	0.1	20	0.007
(OH)GaOCPc	0.0048	0.084	12	0.002
ZnOCPc-MWCNT	0.015	0.24	44	0.1
$(OH)_2$SiOCPc-MWCNT	0.016	0.16	30	0.038
(OH)GaOCPc-MWCNT	0.016	0.1	28	0.022

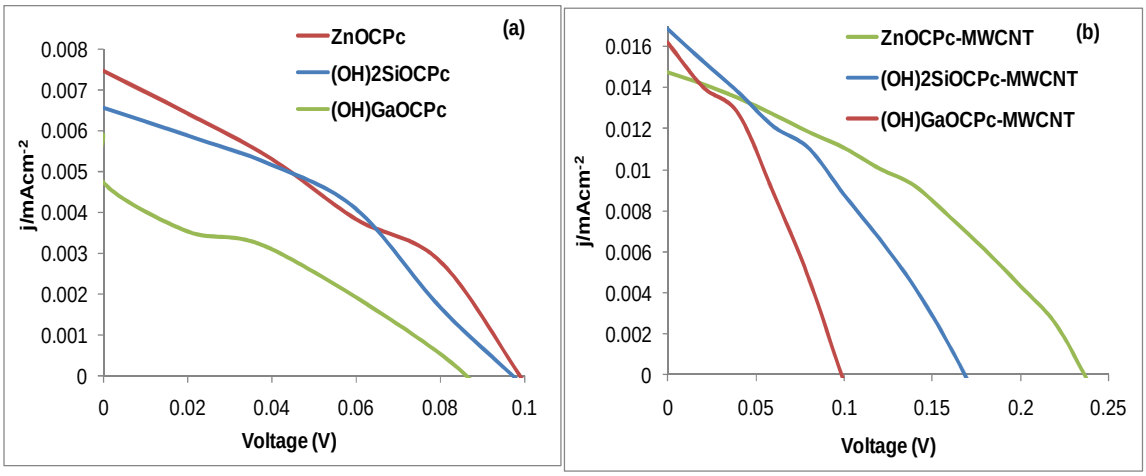

Figure 4.23: Current-Voltage curve of (a) ZnOCPc, SiOCPc and GaOCPc and (b) ZnOCPc-MWCNT, $(OH)_2$SiOCPc-MWCNT and (OH)GaOCPc-MWCNT under 1 sun illumination.

CHAPTER FIVE

5 CONCLUSIONS AND RECOMMENDATIONS

In this study, it has been shown that successful synthesis and satisfactory characterisation of metal octacarboxyphthalocyanines (MOCPc, M = Zn, Si, Ga) using microscopic, spectroscopic and electrochemistry were achieved. The UV/Vis spectroscopic study of all the MOCPc complexes showed the intense absorption band at 690 nm, indicating the Q-band of the metal phthalocyanines. The band originates from the $\pi - \pi^*$ electron transition in the main conjugated system of the metal phthalocyanines macrocycle ring (Shaposhnikov *et al.,* 2005). It is known that the unsubstituted metal phthalocyanines has intense absorption at 660 nm. Therefore, the red shift of the Q-band was an indication of the presence of the octacarboxy groups in the complexes. FTIR spectroscopy also supported the UV/Vis spectra of MOCPc as it confirms the existence of characteristics patterns of carboxylic acid group on the MOCPc complexes.

The MOCPc complexes were modified with amine-functionalised MWCNT and a successful integration was performed. The MOCPc-MWCNT hybrid were characterised using UV/Vis, FTIR, XRDs, EDX, SEM, TEM, solution electrochemistry and EIS spectroscopy. The UV-Vis spectra showed the red shift at the Q-band upon integration with MWCNT. This is an indication of the presence of the electron withdrawing amine-functionalised MWCNT. FTIR spectroscopy confirmed the presence of the amine group in the MWCNT–NH_2 and was used to confirm the existence characteristics patterns of the

integrated material (MOCPc-MWCNT). Therefore, the presence of C=O indicates the -COOH group of the MOCPc and multiple peaks appearing around 2200 cm^{-1} attribute the presence of carbon-carbon double bond of the MWCNTs. It is also a way of showing that these two materials are fully integrated. The existence of the metals (Zn, Ga and Si), carbon and oxygen was corroborated by the EDX profiles. The SEM, TEM and AFM images revealed the change in morphology after MWCNTs were introduced in MOCPc.

The MOCPc and MOCPc-MWCNT and were further characterised by employing solution electrochemistry which showed up to four reduction redox couples and two oxidation redox couples. These redox couples were assigned to the phthalocyanine ring. Electrochemical characterisation of these materials in DSCs (TiO_2/MOCPc-MWCNT and TiO_2/MOCPc) using cyclic voltammetry, linear sweep voltammetry and chronoamperometry were performed. The linear sweep voltammetry showed the same onset potential for both MOCPc and MOCPc-MWCNT and different maximum peak current. The maximum peak current for ZnOCPc and ZnOCPc-MWCNT were higher compared to other materials, indicating the faster movements of electrons to the conduction band of the semiconductor.

The results showed that such a hybrid can act as potential photoelectric conversion material for optoelectronic applications, even under low light illumination. The incorporation of the MWCNTs on the surface of the TiO_2 showed an enhanced electron transfer kinetics but with little or no significant evidence of curbing charge recombination process. Electron transfer

mechanisms are a subject of further experimentation to understand how the DSSC performance (obtained from the photo-chonoamperometric and photo-impedimetric data) decreased as ZnOCPc > $(OH)_2$SiOCPc > (OH)GaOCPc. The chronoamperometric performance of MOCPc-MWCNTs gives promise for easy capturing of solar energy especially in times or areas of poor sunshine conditions, and storing them for future use, for example a DSSC-Supercapacitor device. This type of renewable energy device employing MPc-MWCNTs is currently being explored at our laboratory at the CSIR.

The solar simulator was used to determine the performance and the efficiency of DSCs. It was observed that the ZnOCPc–MWCNT gave better performance and efficiency than SiOCPc-MWCNT and GaOCPc-MWCNT in DSCs even though the overall cell efficiencies were lower than expected with ZnOCPc–MWCNT, SiOCPc–MWCNT and GaOCPc–MWCNT in DSCs. The results can therefore be seen as a very promising first step in the study of these sensitisers in DSCs.

Future work will be needed in order to enhance the performance of this device. Therefore, it is suggested that the cell performance may be improved by integrating MWCNT with MOCPc via covalent bonding instead of non-covalently $\pi - \pi$ stacking. A coupling agent, dicyclohexylcabodiimide (DCC), could be employed to attach the octacaboxylic group from the MOCPc to the amine functionalised group from MWCNTs. It is expected that the interaction that occurs due to the existence of a formal bond between the MOCPc with MWCNTs will be more effective in enhancing the cell performance. A detailed study of the effect of covalently bonded MWCNTs is recommended.

REFERENCES

AGBOOLA, B.O. 2007. Catalytic activities of Metallophthalocyanines towards detection and transformation of pollutants. Ph.D, University of Rhodes.

AGBOOLA, B.O., OZOEMENA, K.I., NYOKONG, T., FUKUDA, T. & KOBAYASHI, N. 2010. Tuning the physico-electrochemical properties of novel cobalt (II) octa [(3, 5-biscarboxylate)-phenoxy] phthalocyanine complex using phenylamine-functionalised SWCNTs. *Carbon*, 48(3): 763-773.

AMIRUDIN, A. & THIERRY, D. 1995. Application of electrochemical impedance spectroscopy to study the degradation of polymer coated metals. *Progress in organic coatings*, 26: 1-28.

BACKUS, 1976. Solar cells. The institute of electrical & electronics engineers. Inc. New York.

BAYIR, Z.A. 2005. Synthesis and characterization of novel soluble octa-cationic phthalocyanines. *Dyes and Pigments*, 65(3): 235-242.

BRAUN, A., TCHERNIAC, J. & Deutsch Ber. 1907. *Chem. Ges*, 40: 2709

BROOKS, M.R. 2006. Dye–Sensitised Solar Cells Based on TiO_2 Nanoparticles [Online]. Available from: www.engr.sjsu.edu/MatE297/Brook_TiO_2_Nanoparticles.doc. [Accessed: 25/03/2011].

BURCZY, A., LOUPY, A., BOGDAL, D. & PETIT, A. 2005. Improvement in the synthesis of metallophthalocyanines using microwave irradiation. *Tetrahedron*, 61(1): 179-188.

CAMPIDELLI, S., BALLESTEROS, B., FILORAMO, A., DÍAZ, D.D., DE LA TORRE, G., TORRES, T., RAHMAN, G.M.A., EHLI, C., KIESSLING, D. & WERNER, F. 2008. Facile decoration of functionalized single-wall carbon nanotubes with phthalocyanines via “Click Chemistry. *Journal of the American Chemical Society, 130(34) : 11503-11509.*

CHANG, C., CHANG, C., LU, H., WU, T. & DIAU, E. 2008. Fabrication and Photovoltaic Characterization of bio-sensitized solar cells using myoglobin-based sensitizers. *Journal of Nanoscience and Nanotechnology*, 8: 1-8.

CHENG, D.L., LIN, C.Y., LIU, C.S., KAO, K.S. & WANG, C.M. 2010. Fabrication of nanocrystalline TiO_2 film by aerosol deposition method for dye–sensitised solar cells. *Materials Science*, 654-656: 2807-2810.

CHIDAWANYIKA, W. & NYOKONG, T. 2010. Characterization of amine-functionalized single-walled carbon nanotube-low symmetry phthalocyanine conjugates. *Carbon*, 48(10): 2831-2838.

CHUNG, I., LEE, B., HE, J., CHANG, R.P.H. & KANATZIDIS, M.G. 2012. All solid state dye sensitized solar cells with high efficiency. *Nature,* 486: 485.

COATES, J. 2000. Interpretation of infrared spectra, a practical approach [Online]. Available from: http://infrared.als.lbl.gov/BLManual/IR_Interpretation.pdf. [Accessed: 27/11/2012].

COLBERT, D. & SMALLEY, R. 2002. Past, present and future of fullerene nanotubes: buckytubes. *Perspectives of Fullerene Nanotechnology*, 3-10.

COLUCCI, J., MONTALVO, V., HERNANDEZ, R. & POULLET, C. 1999, Electrochemical oxidation potential of photocatalyst reducing agents. *Electrochimica Acta*, 44(15): 2507-2514.

CONG, F., NING, B., JI, Y., WANG, X., KE, F., LIU, Y., CUI, X. & CHEN, B. 2008. The facile synthesis and characterization of tetraimido-substituted zinc phthalocyanines. *Dyes and Pigments*, 77(3): 686-690.

DE LA TORRE, G., BOTARRI, G., HAHN, U. & TORRES, T. 2010. Functional phthalocyanines: synthesis, nanostructuration, and electro - optical applications. *Structure and Bond*, 135: 1-44.

DHUNGEL, S.K. & PARK, J.G. 2010. Optimization of paste formulation for TiO2 nanoparticles with wide range of size distribution for its application in dye sensitized solar cells. *Renewable Energy*, 35(12): 2776-2780.

DUNLAP, M. & ADASKAVEG, J. 1997. Introduction to the scanning electron microscope [Online]. Available from: <http://www.sci.sdsu.edu/emfacility/555class/class1.html>. [Accessed: 27/11/2012].

DURMAS, M. & NYOKONG, T. 2007. Synthesis, photophysical and photochemical properties of tetra - and octa - substituted gallium and indium phthalocyanines. *Polyhedron*, 26: 3323-3335.

FEI, B., LU, H., HU, Z. & XIN, J.H. 2006. Solubilization, purification and functionalization of carbon nanotubes using polyoxometalate. *Nanotechnology*, 17: 1589.

FUITZ, B. & HOWE, J., 2007. Transmission electron microscopy and diffractometry of metals. 4th ed. New York: Dordrecht London.

GIRIBABU, L., SINGH, V.K., JELLA, T., SOUJANYA, Y., AMAT, A., DE ANGELIS, F., YELLA, A., GAO, P. & NAZEERUDDIN, M.K. 2013. Sterically demanded unsymmetrical zinc phthalocyanines for dye-sensitized solar cells. *Dye and Pigments*, 98: 518-529.

GRAMRY INSTRUMENTS. Basics of electrochemical impedancespectroscopy [Online]. Available from: http://www.gamry.com/assets/Application-Notes/Basics-of-EIS.pdf. [Accessed: 01/06/ 2012].

GRÄTZEL. M. & McEVOY, A.J. 1994. Principles and applications of dye sensitised nanocrystallined solar cells (DSC). *Solar Energy Material and Solar Cells*, 32: 221.

GRÄTZEL, M. 2000. Perspectives for dye-sensitized nanocrystalline solar cells. *Progress in Photovoltaics: Research and Applications*, 8 (1): 171-185.

GRÄTZEL, M. 2003. Dye-sensitized solar cells. *Journal of Photochemistry and Photobiology C: Photochemistry Reviews*, 4(2): 145-153.

GRÄTZEL, M. 2004. Conversion of sunlight to electric power by nanocrystalline dye-sensitized solar cells. *Journal of Photochemistry and Photobiology A: Chemistry*, 164(1-3): 3-14.

GREENLIEF, 2004. UV-VIS Absorption spectroscopy [Online]. Available from: http://www.chem.missouri.edu/greenlief/courses/4200f04/uv-vis%20lab.pdf. [Accessed: 28/11/ 2011].

HAFNER, B., 2007. Scanning Electron Microscopy Primer [Online]. Available from: <http://www.charfac.umn.edu/sem_primer.pdf>. [Accessed: 27/11/ 2011]

HAGFELDT, A. & GRÄTZEL, M. 2000. Molecular photovoltaics. *Accounts of Chemical Research*, 33(5): 269-277.

HAGFELDT, A., BOSCHLOO, G., SUN, L., KLOO, L. & PETTERSSON, H. 2010. Dye-sensitized solar cells. *Chemical Review*, 110: 6595-6663.

HALME, J., 2002. Dye - sensitized nanostructure and organic photovoltaic cells: technical review and preliminary tests. M.Sc. dissertation, Helsinki University of Technology.

HIRSCH, A., 2002. Functionalization of single-walled nanotubes. Angewandte Chemie International Edition, 41: 1853-1859.

HORIUCHI, T., MIURA, H., SUMIOKA, K. & UCHIDA, S. 2004. High efficiency of dye-sensitized solar cells based on metal-free indoline dyes. *Journal of the American Chemical Society*, 126(39): 12218-12219.

HOSHIKAWA, T., YAMADA, M., KIKUCHI, R. & EGUCHI, K. 2005. Impedance analysis of internal resistance affecting the photoelectrochemical performance of dye-sensitized solar cells. *Journal of the Electrochemical Society*, 152(2): E68-E73.

IDOWU, M., OGUNSIPE, A. & NYOKONG, T. 2007. Excited state dynamics of zinc and aluminum phthalocyanine carboxylates. *Spectrochimica Acta Part A: Molecular and Biomolecular Spectroscopy*, 68(3): 995-999.

IDOWU, M., LOEWENSTEIN, T., HASTALL, A., NYOKONG, T. & SCHLETTWEIN, D. 2010. Photoelectrochemical characterization of electrodeposited ZnO thin films sensitized by octacarboxy metallophthalocyanine derivatives. *Journal of Porphyrins and Phthalocyanines*, 14(2): 142-149.

IIJIMA, S. 2002. Carbon nanotubes: past, present, and future. *Physica B: Condensed Matter*, 323(1-4): 1-5.

JANG, S.R., VITTAL, R. & KIM, K.J. 2004. Incorporation of functionalized single-wall carbon nanotubes in dye-sensitized TiO_2 solar cells. *Langmuir*, 20 (22): 9807-9810.

KALSIS, P.S. 1993. Spectroscopy of organic chemistry. 6th ed. Wiley Eastern Limited, New Dehli: 61: 164.

KALYANASUNDARAM, K. & GRÄTZEL, M. 1998, Applications of functionalised transition metal complexes in photonic & optoelectric devices. *Coordination Chemistry.Review*, 77: 34-414.

KASUMOV, A.Y., BOUCHIAT, H., REULET, B., STEPHAN, O., KHODOS, I., GORBATOV, Y.B. & COLLIEX, C. 1998. Conductivity and atomic structure of isolated multiwalled carbon nanotubes. EPL (Europhysics Letters), 43: 89.

KHELASHVILI, G., BEHRENS, S., WEIDENTHALER, C., VETTER, C., HINSCH, A., KERN, R., SKUPIEN, K., DINJUS, E. & BÖNNEMANN, H. 2006. Catalytic platinum layers for dye solar cells: A comparative study. *Thin Solid Films*, 511-512: 342-348.

KIM, S.S., YUM, J.H. & SUNG, Y.E. 2005. Flexible dye - sensitized solar cells using ZnO coated TiO_2 nanoparticles. *Journal of Photochemistry and Photobiology A: Chemistry*, 171(3):269-273.

KIM, S.H. 2006. Functional dyes. 1st ed. Amsterdam: Netherland.

KNIER, G., 2002. How do photovoltaics work [Online]. Available from : http://science.nasa.gov/science-news/science-at nasa/2002/solarcells/. [Accessed : 17/08/2011].

LAM, H. Performance of UV-Vis spectrophotometers [Online]. Available from: http://www.cvg.ca/images/Performance_UV_Vis.pdf. [Accessed: 16/02/2012].

LASIA, A. 1999. Electrochemical impedance spectroscopy and its applications. *Modern Aspects of Electrochemistry*, 32: 143-248.

LEE, K.M., HU, C.W., CHEN, H.W. & HO, K.C. 2008. Incorporating carbon nanotube in a low-temperature fabrication process for dye-sensitized TiO_2 solar cells. *Solar Energy Materials and Solar Cells*, 92(12): 1628-1633.

LEE, C., LU, H., LAN, C., HUANG, Y., LIANG, Y., YEN, W., LIU, Y., LIN, Y., LIN, Y., DIAU, E. & YEH, C. 2009. Novel Zinc porphyrin sensitizers for dye-sensitized solar cells: synthesis and spectral, electrochemical, and photovoltaic properties. *Journal of Chemistry European*, 15: 1403-1412

LEE, T.Y. & YOO, J. 2005. Adsorption characteristics of Ru(II) dye on carbon nanotubes for organic solar cell. *Diamond and Related Materials*, 14 (11-12): 1888-1890.

LE ROUX, L.J., 2009. The effects of Reverse Bias on the efficiency of dye solar cells. PhD thesis, University of Western Cape, Cape Town.

LEZNOFF, C.C. & LEVER, A.B.P, 1989, Phthalocyanines: Properties and applications, ed, Leznoff, C.C. & Lever, A.B.P. VCH, New York, 1-54.

LI, P., WU, J., LIN, J., HUANG, M., LAN, Z. & LI, Q. 2008. Improvement of performance of dye-sensitized solar cells based on electrodeposited-platinum counter electrode. *Electrochimica Acta*, 53 (12): 4161-4166.

MANSFIELD, E., KAR, A., QUINN, T. & HOOKER, S. 2010. Quick crystal microbalances for microscale thermogravimetric analysis. *Analytical Chemistry*, 82: 24.

MARAIS, E.N., 2007, Removal and photocatalysts of 4 - Nitrophenol using metallophthalocyanines. M.Sc dissertation, University of Rhodes, Grahamstown.

MARTINEAU, D. 2011. Dye solar cells for real, the assembly guide for making your own solar cells. Available from: http://www.solaronix.com/documents/dye_solar_cells_for_real.pdf. [Accessed: 17/08/2012].

MASILELA, N., IDOWU, M. & NYOKONG, T. 2009. Photophysical, photochemical and electrochemical properties of water soluble silicon, titanium and zinc phthalocyanines. *Journal of Photochemistry and Photobiology, A: Chemistry*, 201 (2-3): 91-97.

MASILELA, N., NOMBONA, N., LOEWENSTEINA, T., NYOKONG, T. & SCHLETTWEIN, D. 2010. Symmetrically and unsymmetrically substituted carboxy phthalocyanines as sensitizers for nanoporous ZnO films. *Journal of Porphyrins Phthalocyanines*, 14(11): 985-992.

MCKEOWN, N. 1998. Phthalocyanine materials: Synthesis, structure and function. 1st ed. Cambridge: Cambridge university press.

NAZEERUDDIN, M.K., HUMPHRY-BAKER, R., LISKA, P. & GRÄTZEL, M. 2003. Investigation of sensitizer adsorption and the influence of protons on current and voltage of a dye-sensitized nanocrystalline TiO_2 solar cell. *The Journal of Physical Chemistry B*, 107(34): 8981-8987.

NGUYEN, T., LEE, H. & YANG, O. 2006. The effect of pre-thermal treatment of TiO_2 nano-particles on the performances of dye-sensitized solar cells. *Solar Energy Materials and Solar Cells*, 90(7-8): 967-981.

NONOMURA, K., KOMATSU, D., YOSHIDA, T., MINOURA, H. & SCHLETTWEIN, D. 2007. Dependence of the photoelectrochemical performance of sensitised ZnO on the crystalline orientation in electrodeposited ZnO thin films. *Physical Chemistry Chemical Physics,* 9(15): 1843-1849.

NYOKONG, T. 2007. Effects of substituents on the photochemical and photophysical properties of main group metal phthalocyanines. *Coordination Chemistry Reviews*, 251(13-14): 1707-1722.

O'REGAN, B. & GRÄTZEL, M. 1991. A low cost, high effeciency solar cell based on dye sensitized colloidal TiO_2 films. *Nature*, 737-740.

O'REGAN, B.C., LOPEZ-DUARTE, I., MARTINEZ-DIAZ, M.V., FORNELI, A., ALBERO, J., MORANDEIRA, A., PALOMARES, E., TORRES, T. & DURRANT, J.R. 2008. Catalysis of recombination and its limitation on open circuit voltage for dye sensitized photovoltaic cells using phthalocyanine dyes. *Journal of American Chemical Society*, 130(10): 2906-2907.

OZOEMENA, K.I. & NYOKONG, T. 2003, Electrochemical behaviour of thiol-derivatised zinc (II) phthalocyanine complexes and their self-immobilised films at gold electrodes. *Microchemical Journal*, 75(3): 241-247.

PALISAITIS, J. 2008. Transmission Electron Microscope [Online]. Available from: http://www.fei.com/products/transmission-electron-microscopes/titan.aspx. [Accessed: 27/11/2011].

POLO, A.S., ITOKAZU, M.K. & MURAKAMI IHA, N.Y. 2004. Metal complex sensitizers in dye-sensitized solar cells. *Coordination Chemistry Reviews*, 248(13-14): 134-1361.

RADUSHKEVICH, L. & LUKYANOVICH, V. 1952. The carbon structures formed by thermal decomposition of carbon monoxide on the Iron. *Journal of Physical Chemistry*, 26: 88.

RAMANATHAN, T., FISHER, F., RUOFF, R. & BRINSON, L. 2005. Amino - functionalised carbon nanotubes for binding to polymers and biological systems. *Chemistry of Materials*,17: 1290-1295.

RAPOSO, M., FERREIRA, Q. & RIBEIRO, P.A. 2007. A guide for atomic force microscopy analysis of soft condesed matter [Online]. Available from: http://www.formatex.org/microscopy3/pdf/pp758-769.pdf. [Accessed: 20/03/2013]

REYNAL, A. & PALOMARES, E. 2011. Ruthenium polypyridyl sensitisers in dye solar cells based on mesoporous TiO_2. *Journal of Inorganic Chemistry*, 29: 4509-4526.

SANCHEZ, M., FACHE, E., BONNET, D. & MEUNIER, B. 2001. Synthesis of organo-soluble metallophthalocyanines bearing electron-withdrawing substituents. *Journal of Porphrins and Phthalocyanines*, 5: 867-872.

SAHOO, N.G., RANA, S., CHO, J.W., LI, L. & CHAN, S.H. 2010. Polymer nanocomposites based on functionalized carbon nanotubes. *Progress in Polymer Science*, 35(7): 837-867.

SAKAMOTO, K. & OHNO, E. 1997. Synthesis and electron transfer property of phthalocyanine derivatives. *Progress in Organic Coatings,* 31(1-2): 139-145.

SAKAMOTO, K. & OHNO, E. 1998. Electrochemical characterization of soluble cobalt phthalocyanine derivatives. *Dyes and Pigments*, 37(4): 291-306.

SAKAMOTO, K. & OHNO, E. 1999. Synthesis of octasubstituted cobalt phthalocyanines and their redox properties. *Journal of Porphyrins and Phthalocyanines*, 3(6-7): 634-642.

SAKAMOTO, K. & OHNO, E. 2008. Synthesis of soluble metal phthalocyanine derivatives and their electron transfer properties. *Journal of the Society of Dyers and Colourists,* 112(12): 368-374.

SASTRAWAN, R. 2006. Photovoltaic modules of dye solar cells. PhD. dissertation, University of Freiburg, Breisgau.

SAWATSUK, T., CHINDADUANG, A., SAE-KUNG, C., PRATONTEP, S. & TUMCHARERN, G. 2009. Dye-sensitized solar cells based on TiO2-MWCNTs composite electrodes: Performance improvement and their mechanisms. *Diamond and Related Materials*, 18(2-3): 52-527.

SCOUT, A. 2005. "How solar cells work."How stuff works [Online]."Available from: http://science.howstuffwork.com/solar-cell.html. [Accessed: 17/08/ 2011].

SETTLE, F. 1997. Handbook of instrumental techniques for analytical chemistry. 1st ed. Prentice Hall.

SCHMID, G., SOMMERAUER, M., GEYER, M. & HANACK. M. 1996. Synthesis and Chromatographic Separation of Tetrasubstituted and Unsymmetrically Substituted Phthalocyanines. *Phthalocyanines*, 4: 1-18.

SHAPOSHNIKOV, G.P., MAIZLISH, V.E. & KULINICH, V.P. 2005. Carboxy-substituted phthalocyanine metal complexes. *Russian Journal of General Chemistry*,75 (9): 1480-1488.

SHEN, J., HUANG, W., WU, L., HU, Y. & YE, M. 2007. Study on amino-functionalized multiwalled carbon nanotubes. *Materials Science and Engineering: A*, 464 (1-2): 151-156.

SHIPPY, S. & LU, M. 2007. Cyclic Voltrammetry[Online]. Available from: http://www.chem.uic.edu/chem421/cv.PDF. [Accessed: 29/11/2011].

SISWANA, M.P., OZOEMENA, K.I. & NYOKONG, T. 2006, Electrocatalysis of asulam on cobalt phthalocyanine modified multi-walled carbon nanotubes immobilized on a basal plane pyrolytic graphite electrode. *Electrochimica Acta*, 52 (1): 114-122.

SKOOG, D. AND WEST, D. 1980. Principles of instrumental analysis. 2th ed. Philadelphia: Saunders college.

SPÄTH, M., SOMMELING, P., VAN ROOSMALEN, J., SMIT, H., VAN DER BURG, N., MAHIEU, D., BAKKER, N. & KROON, J. 2003. Reproducible manufacturing of dye sensitized solar cells on a semi automated baseline. *Progress in Photovoltaics: Research and Applications*, 11(3): 207-220.

STILLMAN, M. & NYOKONG, T. 1989, Phthalocyanines: Properties and application, eds. Leznoff, C.C and Lever, A.B.P, VCH publishers, New York, 139-247.

SUN, Y.P., FU, K., LIN, Y. & HUANG, W. 2002. Functionalized carbon nanotubes: properties and applications. *Accounts of Chemical Research*, 35(12): 1096-1104.

TAN, B. & WU, Y. 2006. Dye-sensitized solar cells based on anatase TiO2 nanoparticle/nanowire composites. *The Journal of Physical Chemistry B*, 110(32): 15932-15938.

TAO, M. 2008. Inorganic photovoltaic solar cells: silicon and beyond. *The Electrochemical Society Interface* [Online]. Available from: http://www.electrochem.org/dl/interface/wtr/wtr08/wtr08_p30-35.pdf[Accessed: 26/07/2013].

TORRES, T. 2006. Perspectives in the selective synthesis of phthalocyanines and related compound. *The Journal of Porphrins and Phthalocyanines*, 4: 325-330.

UMEYAMA, T. & IMAHORI, H. 2008. Carbon nanotube-modified electrodes for solar energy conversion. *Energy and Environmental Science*, 1:120-133.

Valcarcel, M., Simonet, B.M., Cardenas, S. & Surrez, B. 2005. Present and future applications of carbon nanotubes to analytical science. *Analytical and Bioanalytical Chemistry*, 382:1783-1790.

VENTURES, M. 2008. The chronoamperometry: The cottrell's equation [Online]. Available from : http://www.menlatech.com/docs/chromatology.pdf. [Accessed: 30/11/ 2011].

VILALTA-CLEMENTE, A. & GLOYSTEIN, K. 2008. Principles of Atomic Force Microscopy (AFM) [Online]. Available from: http://www.mansic.eu/documents/PAM1/Frangis.pdf. [Accessed: 03/12/2012].

VOLLMAN,H. 1971, In chemistry of synthetic dyes. Venkataraman, K. ed. Academic press: New York. 283-311.

WANG, Q., MOSER, JACQUES-E. & GRATZEL, M. 2005. Electrochemical impedance spectroscopic analysis of dye sensitized solar cells. *Journal of Physical Chemistry*. B, 109: 14945-14953.

WEBER, J. & BUSH, D. 1965. Inorganic. *Chemistry*, 4: 469.

WIDMANN, G. 2001. Information for users of METTLER TOLEDO thermal analysis systemes [Online]. Avalaible from: http://us.mt.com/mt_ext_files/Editorial/Generic/3/TA_UserCom13_024092971 0242401_files/tausc13e.pdf. [Accessed: 28/11/2011].

WIEDERKEHR, N.A 1996. The aggregation behaviour of Zinc - tetracarboxyphthalocyanines and its spectral sensitisation on titanium dioxide film. *Journal of Brazillian Chemical Society*, 1: 7-13.

WIKIPEDIA. 2011. Transmission Electron microscopy [Online]. Available from: http://en.wikipedia.org/wiki/Transmission_electron_microscopy. [Accessed: 27/11/ 2011].

WILDGOOSE, G., BANKS, C. & COMPTON, R. 2006. Metal nanoparticles and related materials supported on carbon nanotubes : *Method and applications*. *Review*, 2: 182-193.

WILLIAMS ,R. 1960. Becquerel photovoltaic effect in binary compounds. *Journal of chemical physics*, 32: 1505-1514.

WINTER, G., HECKMANN, H., HAISCH, P., EBERHARDT, W., HANACK, M., LUER, L., EGELHAAF, H.J. & OELKRUG, D. 1998. Study of substituent effects on the photoconductivity of soluble 2,(3)- and 1,(4)-Substituted phthalocyaninato- and naphthalocyaninatotitanium(IV) oxides. *Journal of American Chemical Society*, 120(45): 11663-11673.

WOHRLE, D., SCHNURPFEIL, G., KNOTHE, G. 1992. Efficient synthesis of phthalocyanines and related macrocyclic compounds in the presence of organic bases. *Dye and Pigments*, 18: 91-102.

WU, M., YANG, Z.H., JIANG, Y.H., ZHANG, J.J., LIU, S.Q. & SUN, Y.M. 2010 Improvement of dye-sensitized solar cell performance through electrodepositing a close-packed TiO_2 film. *Journal of Solid State Electrochemistry*, 1-7.

WU, W., MENG, F., LI, J., TENG, X. & HUA, J. 2009. Co-sensitization with near-IR absorbing cyanine dye to improve photoelectric conversion of dye-sensitized solar cells. *Synthetic Metals,* 159 (11): 1028-1033.

Yasuda, A., Kawase, N., Matsui, T., Shimidzu, T., Yamaguchi, C. & Hisaji, M. 1999. Carbyne: eletrochemical preparation and nanotube formation. *Reactive and Functional Polymers*, 41 (1-3): 13-19.

ZHANG, Q. & CAO, G. 2011. Nanostructured photoelectrodes for dye-sensitized solar cells. *Journal of Nano Today,* 6: 91-109.

ZHANG, D., SHI, L., FANG, J., LI, X. & DAI, K. 2005. Preparation and modification of carbon nanotubes. *Materials Letters,* 59(29-30): 4044-4047.

APPENDIX A

FTIR SPECTRA

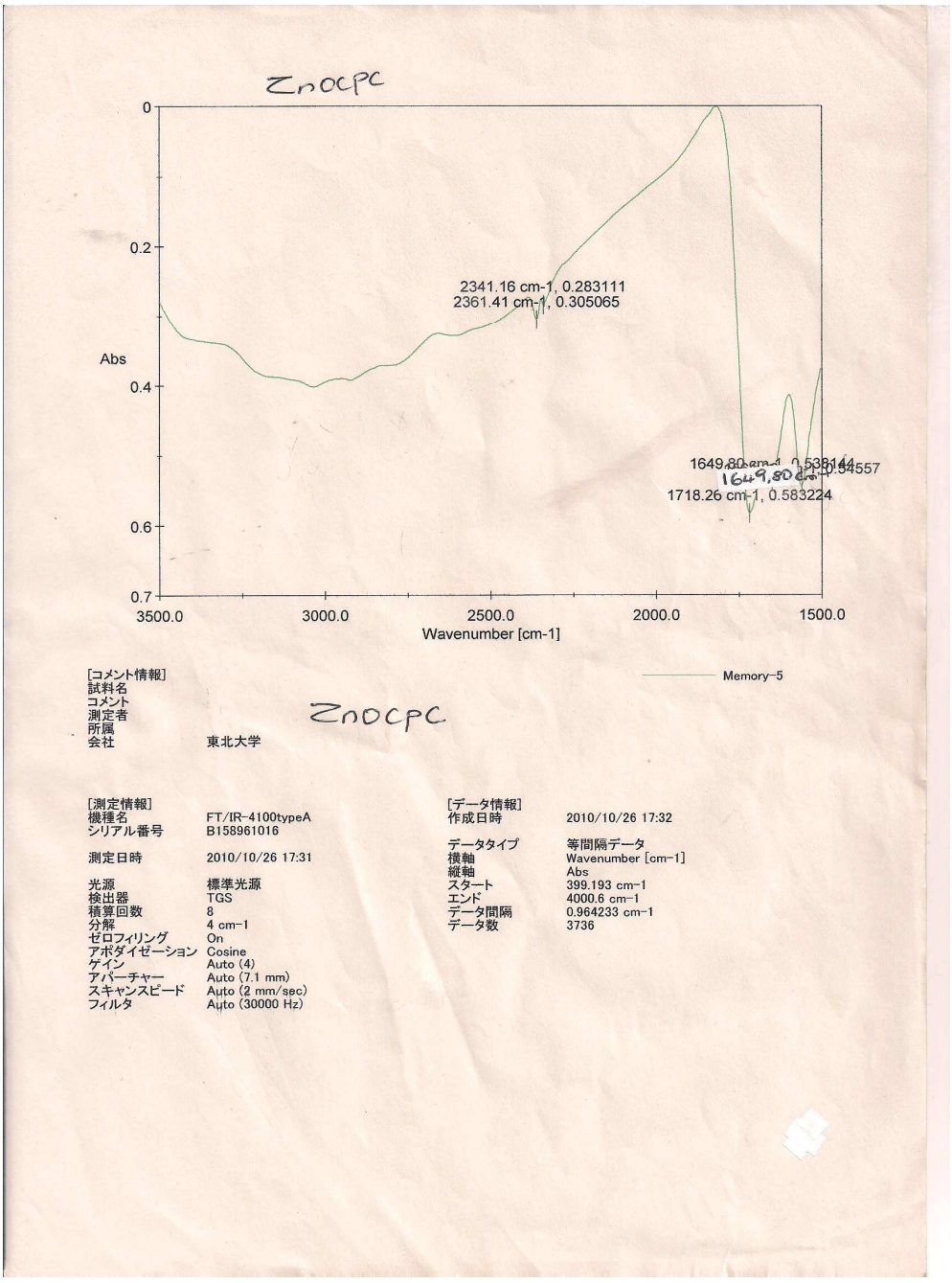

A.1: FTIR spectrum of ZnOCPc

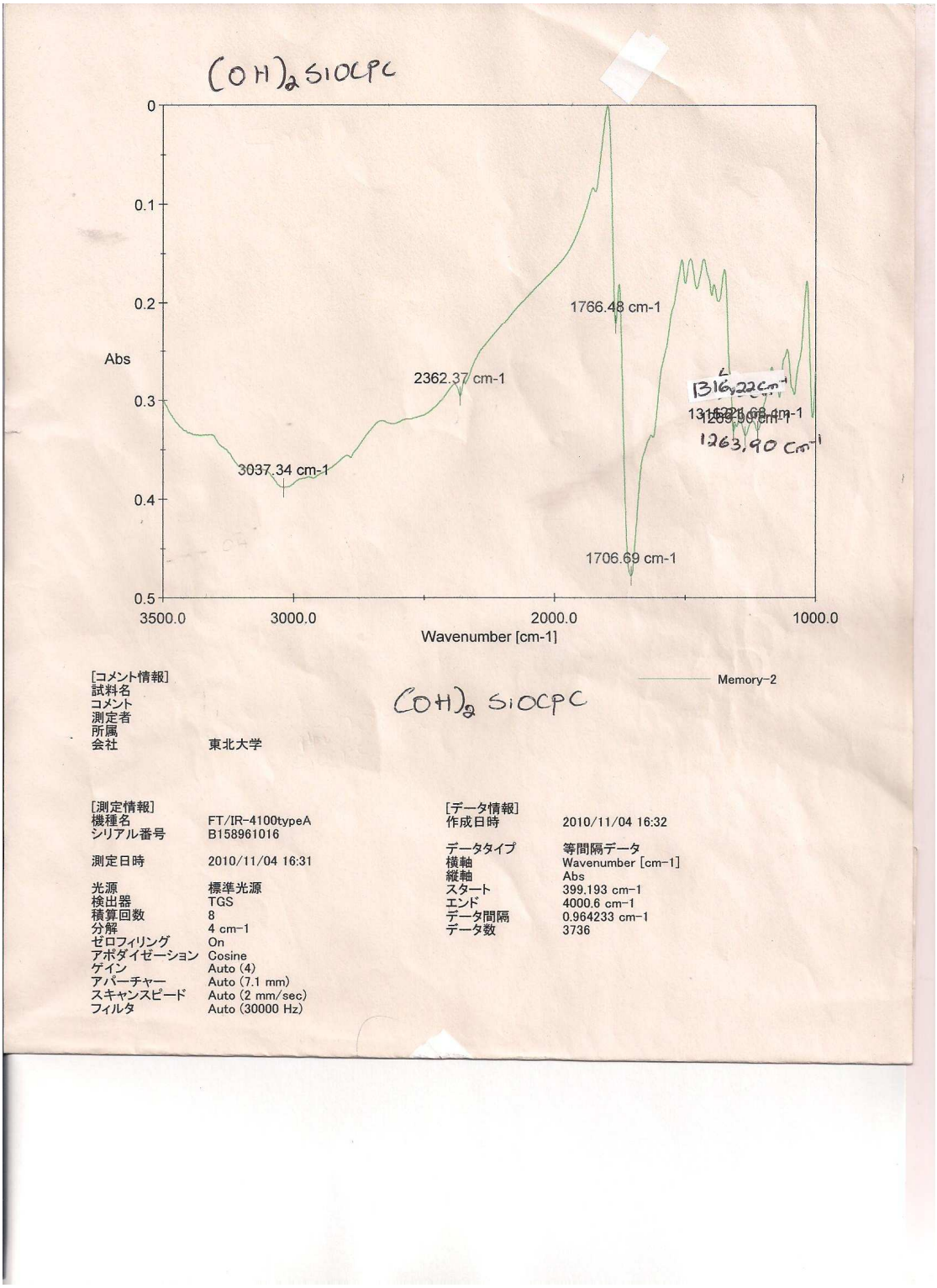

A.2: FTIR spectrum of $(OH)_2OCPc$

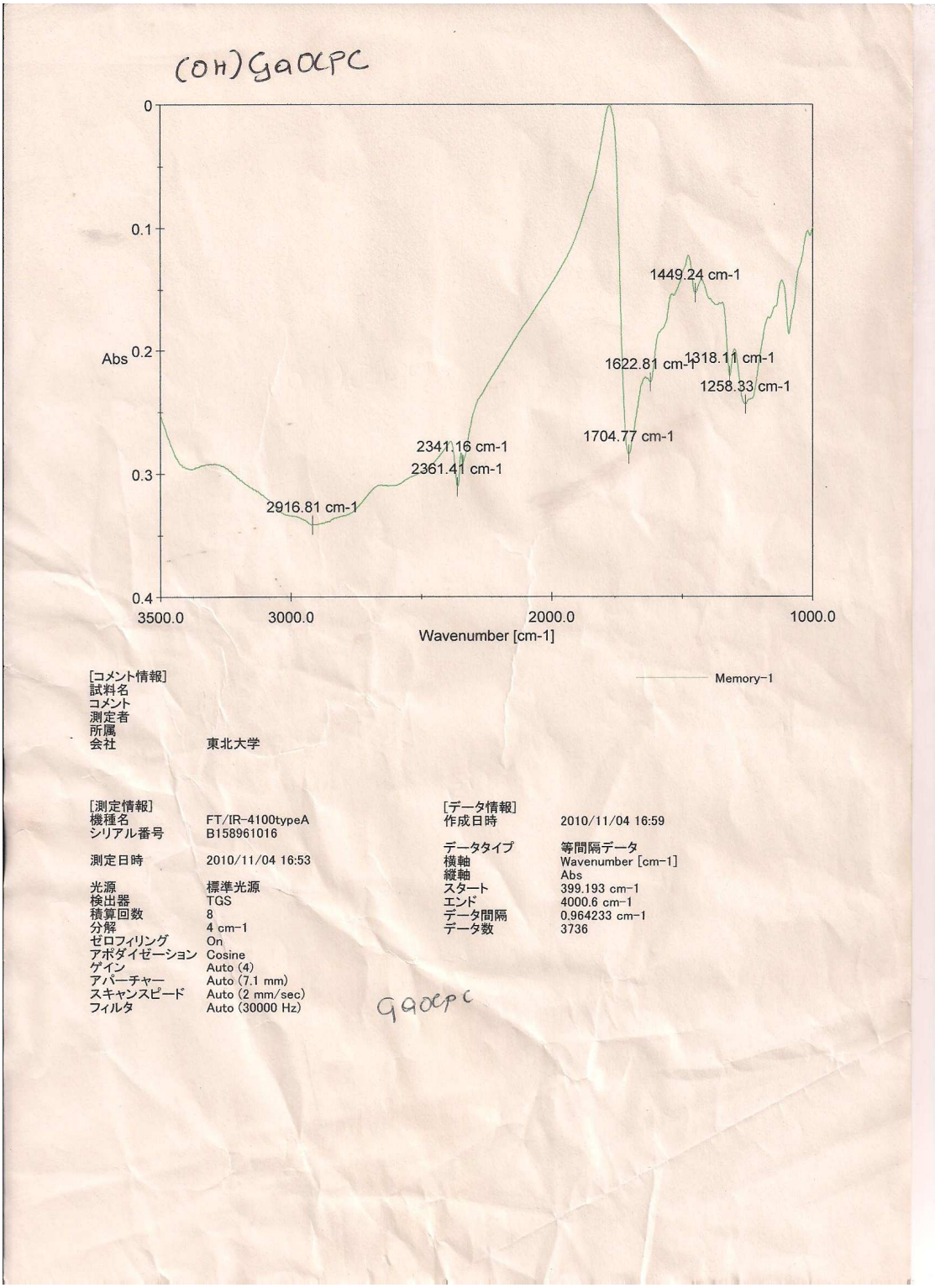

A.3: FTIR spectrum of (OH)GaOCPc

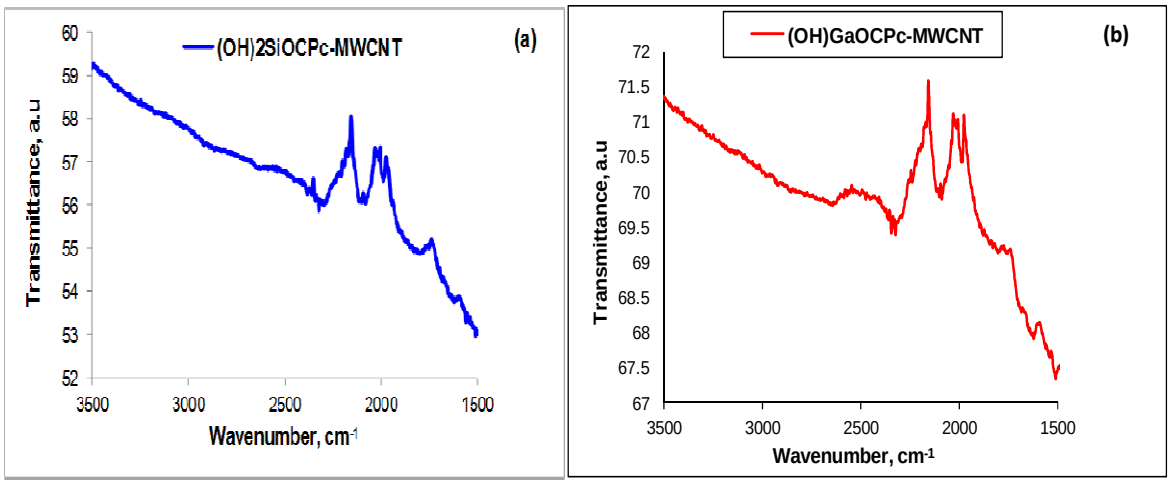

A.4 FTIR spectra of **(a)** $(OH)_2$SiOCPc-MWCNT and **(b)** (OH)GaOCPc-MWCNT

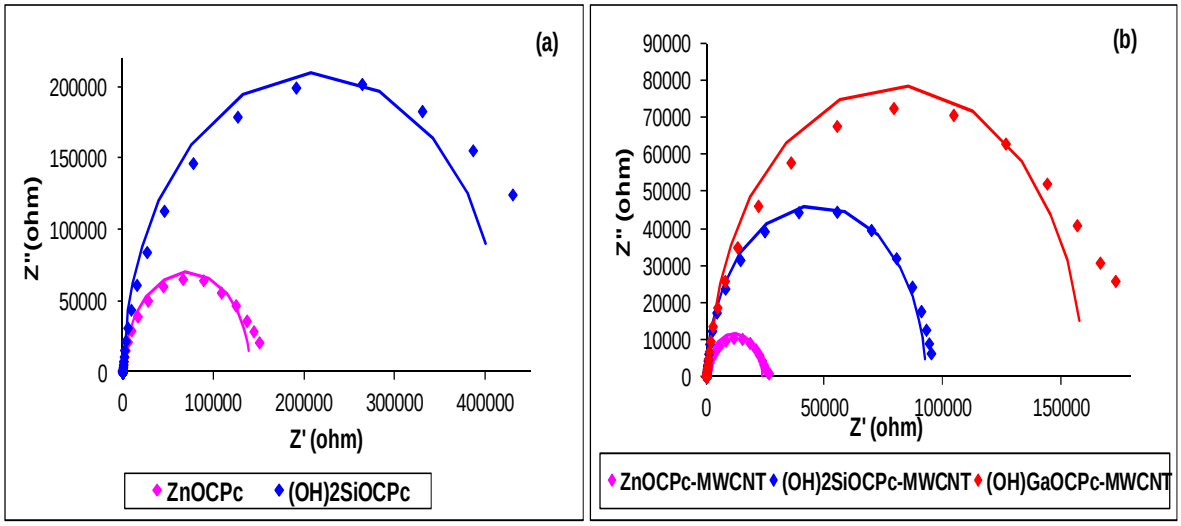

A.5 Nyquist plots of DSCs fabricated with **(a)** TiO_2/ZnOCPc, TiO_2/GaOCPc and TiO_2/$(OH)_2$SiOCPc **(b)** their corresponding MWCNT-integrated hybrid in the dark

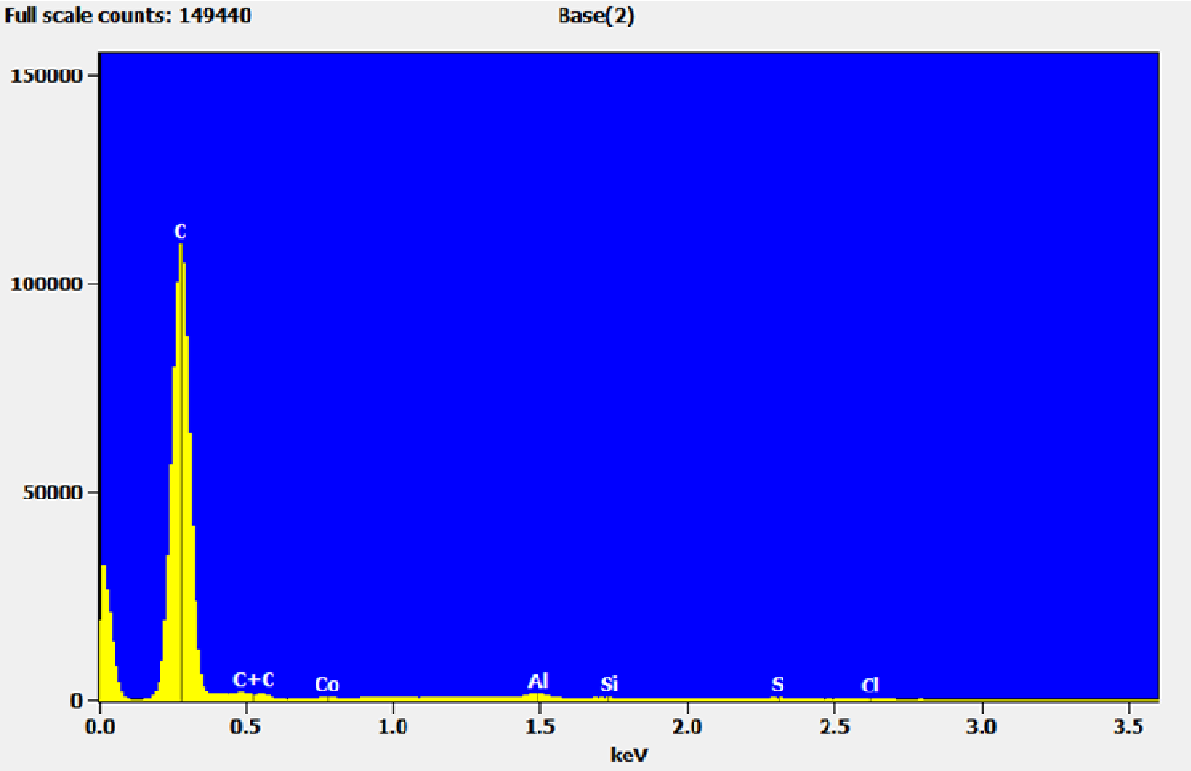

A.6 EDX profile of MWCNT-NH_2

APPENDIX B

RESEARCH OUTPUTS RESULTING FROM THIS THESIS

(A) Manuscript Submitted for Publication

Nonhlanhla E. Mphahlele, Kenneth I. Ozoemena, Lukas J. Le Roux, Charl J. Jafta, Leskey Cele, Mkhulu K. Mathe, Tebello Nyokong, and Nagao Kobayashi, "Carbon Nanotube-Enhanced Photoelectrochemical Properties of Metallo-octacarboxyphthalocyanines for the Development of Dye-Sensitised Solar Cells", (submitted 2012) (see attached).

(B) Conference / Workshop Presentations (4 oral, 2 posters)

1. "*The effect of Multi-walled carbon nanotubes on Metal octacarboxyphthalocyanines for Dye Solar Cells application".* Nonhlanhla Mphahlele*,* Kenneth I. Ozoemena, Lukas le Roux, Leskey Cele, IBSA workshop, Thaba ya Batswana, 15 October **2012** (**ORAL**)

2. *Metallo- octacarboxyphthalocyanines with multiwalled carbon nanotubes hybrid for dye solar cells applications: Synthesis and characterisation"..* Nonhlanhla Mphahlele, Kenneth I. Ozoemena, Lukas le Roux, Leskey Cele, 2nd international symposium on electrochemistry , UWC – Cape Town, South Africa, 18 – 20 July, **2012 (ORAL)**

3. *"Metal octacarboxyphthalocyanines with multiwalled carbon nanotubes for dye solar cells applications: Synthesis and characterisation"..* Nonhlanhla Mphahlele, Kenneth I. Ozoemena, Lukas le Roux, Leskey Cele, 11th

SETMI conference and SA –Japan transport technology forum, Pretoria, South Africa, 23 November, **2011 (ORAL)**

4. *"Zinc octacarboxyphthalocyanines/Multiwalled carbon nanotubes for the development of dye solar cells".* Nonhlanhla Mphahlele, Kenneth I. Ozoemena, Lukas Le roux, Leskey Cele, SA/ Germany Science, research and Technology Cooperation Agreement, Research project period : 2008 – 2010, End of program workshop, 7 – 8 September, Rhodes University, **2010 (ORAL)**
5. *"Metal octacarboxyphthalocyanines/Multiwalled carbon nanotubes hybrid for the development of dye solar cells".* K.N.E Mphahlele, K.I Ozoemena, L.J le Roux and L.M Cele, 11th international conference on frontiers of polymers and advanced materials, Pretoria, South Africa, 22 – 27 May **2011 (Poster).**
6. *"Phototelectrochemistry of metallo – octacarboxyphthalocyanines for the development of dye solar cells".* Nonhlanhla Mphahlele, Kenneth I. Ozoemena, Lukas Le Roux, Mkhulu K. Mathe, Tebello Nyokong, Leskey M. Cele, Shimizu Soji, and Nagao Kobayashi, South Africa – Japan workshop, Stellenbosch, South Africa, 12 – 13 September **2011 (Poster).**